Dispersion and two-phase flow in material from different carbonate pore classes

by Marius Heide

Master thesis
Petroleum technology – reservoir chemistry

Department of Chemistry
University of Bergen
June 2008

Abstract

Carbonate reservoirs are currently estimated to contain more than 50 % of the world's oil reserves. The economical value of improving knowledge on fluid flow in these reservoirs is therefore vast. Carbonate reservoirs are commonly much more heterogeneous than sandstone reservoirs, due to their biological origin and local deposition. Also, diagenetic processes may cause selective dissolution which further increases heterogeneity. On average, carbonate oil reservoirs have lower recovery factors than sandstone oil reservoirs.

Lønøy (2006) recently presented a pore-type classification for carbonate rocks based on sedimentological and diagenetic characteristics. The classification scheme includes 20 pore-type classes, counting interparticle, intercrystalline, intraparticle, moldic and vuggy porosity, as well as mudstone microporosity. Furthermore, the classification also comprises pore sizes and porosity distributions.

In this thesis, dispersion tests in water-saturated state and at residual oil saturation, and water floods were performed on 11 carbonate core samples from three pore classes (as defined by Lønøy, 2006); intercrystalline uniform macropores, moldic macropores and tertiary chalk. The dispersion analysis involved a new approach, calculating tracer (added NaCl) concentration through measurements of conductivity and temperature, and simulating the results using Coats and Smith's (1964) differential capacitance model to estimate dispersivity and amount of dead-end pores. In addition, the effect of flow rate on dispersion was studied for three carbonate core samples. Also, the impact of salinity and ion valency (Na^+ and Ca^{2+}) on absolute permeability was investigated for two carbonate samples.

The new approach to dispersion analysis generated large data sets, making it possible to learn more about the connectivity and heterogeneity of pore structures. Permeability measurements varying ion type and concentration showed that soluble minerals (such as anhydrite) may cause dissolution and lead to significant increase in permeability. Also, the results indicate that the Ca^{2+} content in brine affects permeability; this is consistent with previous studies on clay in sandstones. The flow rate effect study confirmed that velocity should be kept high enough to avoid diffusion-dominated flow. Heterogeneous core samples are more sensitive to velocity due to a higher amount of dead-end pores.

Even though the number of core samples was low, a strong link between flowing fraction and recovery factor was found. Homogeneous samples also showed a more predictable relation between dispersion profiles at the two saturations. Analysing the extension of the pore class concept to fluid flow, there seems to be no direct correlation between the selected pore classes and dispersion characteristics. This study has shown that, apparently, water-flooding performance is more closely linked to flowing fraction, wettability and permeability than pore classes.

Acknowledgements

The results of this thesis rely heavily on laboratory analysis. Therefore, I would first and foremost like to sincerely thank Sverre Hetland, my co-supervisor, who has been ever so helpful on all laboratory matters. He has explained the way all relevant laboratory equipment functions, and also pointed out uncertain factors that need to be addressed. Also, he has taken part in many discussions related to laboratory results, and in that way given good ideas that have sparked my own imagination.

Next, I am grateful to my supervisor Arne Skauge for introducing me to carbonates and dispersion, and for being very cooperative in general… even though his position means he is often busy. Arne has been the most influential person on planning my thesis, and several clarifying status meetings have been arranged in his office. In addition to this, he has administrated a specially designed course for me during the autumn semester of 2007, dealing with diffusion and dispersion. This course definitely improved my knowledge on these topics.

Both Arne and Sverre have been proofreading all chapters in the final spurt, and given me constructive feedback. This has been very much appreciated as well.

As Arve Lønøy's pore-type classification is one of the main topics of this thesis, it seemed somewhat unlikely that Lønøy himself should occur in this section. However, as many questions appeared when the results were discussed, Arne suggested that I consulted him. The concise comments and viewpoints of Arve Lønøy (via e-mail) made the interpretation of the results much easier, and for that I am thankful.

CIPR PhD students Bartek Florczyk Vik and Shahram Pourmohammadi are also thanked for taking an interest in my thesis. Bartek has brought up several interesting issues regarding dispersion, while Shahram has provided information on the previous dispersion analysis methods at CIPR as well as assisting with simulation using UTCHEM.

It seems appropriate to express thanks to CIPR as an organisation; both because they have placed employees at disposal, and because I was permitted to use core samples that are part of the collaboration program with Statoil and Hydro.

Finally, even though it is somewhat of a cliché, I appreciate the moral support I have received from my nearest. My girlfriend Gry Gjerstad has been very supportive, as have my parents.

Marius Heide (Bergen, 2 June, 2008)

List of contents

Chapter 1: Introduction

1.1 Aim of study

The purpose of this thesis is to present laboratory methods and analyses that may help to better understand fluid flow in carbonate reservoirs. The heterogeneity of carbonates makes it difficult to assign mean flow properties for larger sections; consequently prediction of the reservoirs' behaviour during production is often uncertain. Obtaining information of pore types and pore geometry through experimental analysis is therefore an important part of understanding the flow properties of carbonates. A classical approach for acquiring this type of knowledge is *dispersion* analysis; the studies of how effluent concentration changes during a miscible displacement. Dispersion is one of the key topics of this thesis.

Based on previous attempts to classify carbonate pore fabrics, Lønøy (2006) recently identified 20 different pore classes based on a combination of depositional environment and porosity/permeability- relationships. This classification is the basis for studying different pore types in this thesis. Laboratory dispersion tests were run for core samples from selected pore classes (from North Sea and Iranian reservoirs) based on Lønøy's classification, and compared in order to find out whether the classification seems reasonable.

There are many ways of measuring dispersion. The general idea of injecting a tracer that displaces a fluid in a miscible process is widespread; however various combinations of fluids and measurement techniques exist. In this thesis a new dispersion method is presented, based on sodium chloride (NaCl), sea water and electrical conductivity measurements. Documentation and testing of this method is an important part of the thesis.

Several aspects of dispersion are investigated here; (1) dispersion tests for water-saturated core samples, (2) dispersion tests for samples at residual oil saturation, (3) simulation of the laboratory dispersion tests at both saturations using Coats and Smith's (1964) differential capacitance model (with dead-end pores) and (4) the effect of flow rate on dispersion profiles.

Even though dispersion analysis can provide valuable knowledge on its own, a better insight into the flow pattern in the reservoir requires comparison with more realistic production conditions. Water flooding is the most extensive recovery method on the Norwegian continental shelf, and possible to reproduce in core samples at laboratory scale. Dispersion test samples in this thesis will therefore undergo water-flooding experiments as well, with the intention of comparing the water-flooding results with dispersion test results.

Finally, it is also within the scope of this thesis to look into the interactions between brine and carbonate reservoir rocks. For sandstones it is a documented fact that presence of clay combined with low-salinity water leads to fines migration and clogging of pore throats, which in turn will cause an instant decrease in permeability. For carbonates this phenomenon is not recognised, due to lower clay content. However, fresh water tends to set off dissolution of carbonate. These theoretical aspects will be examined through laboratory measurements of absolute permeability for some carbonate cores. If permeability is significantly altered due to brine composition it is desirable to avoid this during dispersion tests, as it can change the flow pattern and the dispersion profile for a given sample. Also, it is definitely an issue that would influence production performance.

1.2 An introduction to CIPR's work

CIPR is an abbreviation for *Centre for Integrated Petroleum Research*. According to their website (10 April, 2008) their main focus is to:

> *"Contribute to extended production by increasing recoverable reserves in existing oil and gas fields".*

The organisation consists of geologists, chemists, physicists and mathematicians; a combination of all these spheres is necessary to better understand and model multiphase flow and recovery mechanisms. Also, many projects are entrusted to UiB master students and PhD students. Their theses add to the knowledge of more experienced scientists and professors.

Heterogeneous reservoirs are a field of particular interest for CIPR. Several projects concerning carbonates have been carried out; first and foremost the purpose of these projects is to systematise flow properties and improve understanding of the mechanisms involved in oil recovery from different types of carbonate rocks. The results from dispersion tests and water floods in this thesis are a part of extensive collaboration projects with the oil companies Statoil and Hydro (now merged to StatoilHydro). A number of core samples are handed over to CIPR for them to perform a series of analyses for each sample. The samples originate from North Sea oil fields such as Ekofisk, Tor and Oseberg, and also from the Barents Sea and the Persian Gulf. Typically the following parameters are studied at CIPR:

- Porosity and absolute permeability.
- Dispersion profiles for (1) water-saturated conditions and (2) at residual oil saturation.
- Drainage and imbibition; production performance during injection of oil (decane) and sea water.
- Relative permeability.
- Capillary pressure.
- Wettability.

Some of these experimental analyses are also simulated using computer software and various models. In recent years the effect of wettability on flow properties has been found to be significant; thus there is a growing demand of laboratory tests regarding wettability. Therefore dispersion tests and water floods are performed both for cleaned cores (presumably water-wet) and for cores that have undergone an ageing process increasing the affinity to oil (restored state cores).

Summing up, dispersion tests and water floods studied in this thesis constitute a small, but yet important part of the collaboration program between CIPR and StatoilHydro. The new method for dispersion analysis was not intentionally a part of the program, but could definitely be of interest.

1.3 Methodology

Laboratory studies are an essential part of this thesis. Due to this fact, the whole of chapter 3 is dedicated to experimental methods and analysis. However, the main methods will be explained briefly here.

There are primarily *three* types of laboratory procedures that are relevant for this thesis; (1) dispersion tests, (2) water-flooding tests and (3) measurements of absolute permeability.

The set up for dispersion is based on elements that are well-established as a general approach when measuring dispersion. However, certain factors are new; the tracer consists of synthetic sea water with an additional (known) amount of sodium chloride, and normalised concentration profiles (dispersion profiles) are obtained by means of conductivity measurements. The method is discussed in detail in chapter 3.2. The experimental data are simulated using UTCHEM, which is a computer program that generates dispersion profiles based on Coats and Smith's (1964) capacitance model. This model is presented in chapter 2.3.2, and the simulation process is described in chapter 3.3.

The procedure of water-flooding experiments will not be discussed in detail in this thesis.

Measurements of absolute permeability using water are often considered straightforward. Certainly reading the pressure drop at multiple injection rates is a simple concept; yet there are many uncertain factors that need to be addressed. In this thesis, the purpose is to detect possibly minor permeability variations when altering water composition. Uncertainty is therefore the key issue when this subject is brought up in chapter 3.4.

Data processing, as well as designing and editing charts, is performed using Microsoft Excel.

1.4 Previous work

As pointed out, carbonates are generally more heterogeneous than sandstones. Consequently it is not easy to classify carbonates and model fluid flow. Nevertheless, carbonates contain much of the world's present oil, and the profit of increasing the knowledge about them is massive. Over the last 50 years there have been a number of studies on carbonate rocks. This has undoubtedly shed light on some interesting issues, yet today many questions still remain. One of the most important topics regarding carbonates is *pore-type classification*. Three classification approaches stand out; these are all introduced in chapter 2.1. The first approach was made by Archie (1952), relating pore-size distributions to permeability, saturation and rock fabrics. Choquette and Pray's (1970) classification is perhaps the most widely used among geologists, as their system is related to depositional setting and diagenesis. Lucia's classification (1983, 1995 and 1999) is, as Archie's, more linked to petrophysical properties, making it more suitable for reservoir engineering approaches. Figures illustrating Choquette and Pray's and Lucia's division of pore classes are found in chapter 2.2.

More recently, Lønøy (2006) developed a pore-type classification consisting of 20 different classes (see chapter 2.2). Pore *type*, pore *size* and *porosity distribution* are the key elements; this can be considered a combination of Choquette and Pray's and Lucia's classifications. Porosity/permeability relationships for Lønøy's classification look promising; still the system has not been thoroughly tested for flow properties such as dispersion characteristics and two-

phase flow. CIPR have concluded several projects on this subject, and the results have been published in a few papers. Low oil recovery from (water floods of) carbonate core samples has been found to be associated with a high fraction of dead-end pores, or even inaccessible pores (Skauge et al., 2005; Skauge et al., 2006). Also, connectivity in secondary porosity systems such as moldic pores has proved important for permeability and recovery performance (Skauge et al, 2005; Pourmohammadi et al., 2007). Moreover, Pourmohammadi et al. (2007) showed through measurements of electrical conductivity and NMR that mixing properties are correlated with tortuosity and pore-size distribution. Although these results are interesting, there is still much research left to do on linking Lønøy's pore-type classification with fluid flow parameters.

Most of the fundamental theory on the subject of dispersion date back to the 1950s and 1960s. For the work performed in this thesis, there are two key publications concerning dispersion; (1) Perkins and Johnston (1963), who investigated the influence of several parameters' influence on dispersion, such as heterogeneity and the presence of an immobile phase; and (2) Coats and Smith (1964), who developed a differential capacitance model to describe mass transfer (diffusion) between the flowing fraction and the so-called dead-end pores. Their model resulted in Eqs. 2.8a and 2.8b. These equations have later been subject to experimental analysis by among others Salter and Mohanty (1982) and Jasti et al. (1988). Although some weak points have been found, the general conception is that Coats and Smith's model is consistent with results from experimental dispersion analysis. Salter and Mohanty also extended the model to apply to two-phase flow. A more detailed approach to diffusion and dispersion theory is found in chapter 2.3.

Experimental dispersion analysis has commonly been performed injecting a miscible tracer and measuring the effluent concentration. In this thesis two previous methods are addressed, namely (1) injection of 4-fluoro benzoic acid (4-FBA) and concentration calculations through UV spectrometry; and (2) injection of potassium iodide (KI) and concentration calculations through measurements of electrical conductivity. The concepts of these methods are briefly explained in chapter 3.2. A key element in this thesis is the introduction of a new method that improves data quality and time-efficiency compared to the two previous methods; an introduction to the NaCl conductivity method is found in chapter 3.2.

The effect of water salinity on absolute permeability (known as water sensitivity) has been examined throughout the 1980s and 1990s, but the studies have been limited almost exclusively to sandstone cores. The fact that low-saline water can cause release of clay particles (fines) which migrate and block pore throats is now universally recognised. Permeability reduction resulting from this (formation damage) has been observed to depend on both ion concentration and ion valency in the formation water (Khilar and Fogler, 1983 and 1984; Kia et al., 1987). Even though hydrodynamic forces may also, in theory, cause fines migration, this mechanism is practically negligible due to the critical velocity required being as high as 1 cm^3/s (Ochi and Vernoux, 1998). There are few examples of water sensitivity studies in carbonate cores, but Dahab et al. (1993) found no permeability variations in limestones flushed with various NaCl concentrations. This is most likely due to the very low clay content in carbonates. Carbonates are, however, susceptible to dissolution if the formation water is sufficiently low-saline; this may instead *increase* permeability.

Based on the above-mentioned studies and chapter 1.1, one finds the following links between this thesis and previous work on related topics:

- Dispersion theory is well-documented; the Coats and Smith model is valid.
- A basic setup for dispersion tests has already been developed, but in this thesis a new combination of tracer and concentration measurements is introduced in order to lessen uncertain factors and improve time-efficiency and data quality.
- A relatively new carbonate pore-type classification has been proposed by Lønøy (2006). This thesis examines the classification's link to flow properties.
- Dispersion results and water-flood results have been compared by Skauge et al. (2006). It is the intention of this thesis to try and confirm the results from their analysis and to possibly find other trends.
- Water sensitivity in carbonate rocks is often neglected, but has not been extensively studied. This thesis aims to determine whether formation damage is in fact occurring in carbonates, and if so, to what extent.

Chapter 2: Carbonates and fluid flow in porous media

2.1 Introduction

Throughout the last 50 years, extensive studies have been performed on the subject of carbonate reservoir rocks. The understanding of different pore structures has improved significantly, and so has the knowledge of fluid flow. The scope of this chapter is to present well-known information on carbonates and single-phase and two-phase fluid flow in porous media. As previous work on these subjects is widespread, the main focus will be directed at issues directly related to this master thesis.

Carbonate pore types will be first on the agenda. The importance of this subject is apparent, as nearly all flow experiments and simulations will be compared according to pore types. Secondly, the topics diffusion and dispersion are considered. This part covers a brief introduction to diffusion, as well as an overview of dispersion models, mechanisms and established experimental methods. A reasonable subject to look at next is two-phase flow. Injecting water and/or oil into a core sample and measuring the effluent phase volumes, provides vital knowledge on fluid flow properties. Also, this thesis focuses on how single-phase dispersion test results can be compared with two-phase flow results and dispersion at residual oil saturation. Finally, there is a need to examine ionic composition of injection water, and its influence on permeability. For sandstones, this is a well documented subject. However, in this thesis *carbonates* are of interest, so an effort is made to adapt some of the existing knowledge.

2.2 Carbonate pore-type classification

Carbonate reservoirs are characterised by extreme geological and petrophysical heterogeneities, an attribute which distinguishes them from siliciclastic reservoirs (Lucia et al., 2003). While porosity/permeability crossplots often show clear trends for sandstone reservoirs, they are commonly dominated by a wide range and a scatter of data for carbonate reservoirs. Permeability, in particular, can seem almost randomly distributed and have large local variations.

Rock fabrics, i.e. geological descriptors that relate pore size to particle size, sorting and pore types, have been shown to be decisive for petrophysical heterogeneities. Rock fabrics are often found more continuous than for example porosity/permeability ratios, and therefore understanding rock fabrics is a major task within carbonate reservoir characterisation. Both depositional setting and the post-deposition process known as diagenesis influence on rock fabrics.

Various classification schemes for carbonates have been suggested; only a few are widely used though. These will now be briefly discussed, followed by an introduction to Lønøy's (2006) recent modification of these classifications.

Previous classifications

Archie (1952) was the first to make an attempt at relating rock fabrics to petrophysical properties in carbonate rocks. Archie recognised that the pore space should be divided into *matrix porosity* and *visible porosity*; different textures indicate different matrix porosities. This classification has been used mostly to estimate porosity. As pointed out by Lucia (1999), Archie's descriptions are difficult to relate to geological models as they are independent of depositional and diagenetic terms. Also, the scheme does not take into account the fact that there are various types of visible porosity, such as moldic porosity and interparticle porosity. Thus, Archie's classification has been subject to extensive modifications. Two main concepts of this model are implemented in later classifications; (1) pore-size distribution controls permeability and saturation; and (2) pore-size distribution is related to rock fabrics.

Choquette and Pray (1970) presented a classification that has been widely used. Their classification is based on *generic* divisions of carbonate pore types, rather than petrophysical divisions. All carbonate pore space is divided into *fabric selective* and *nonfabric selective*; nonfabric selective pores can cut across grains, whereas fabric selective pores cannot. This division is illustrated in Fig. 2.1. The overview is slightly modified from Choquette and Pray, as primary and secondary porosity also are separated clearly.

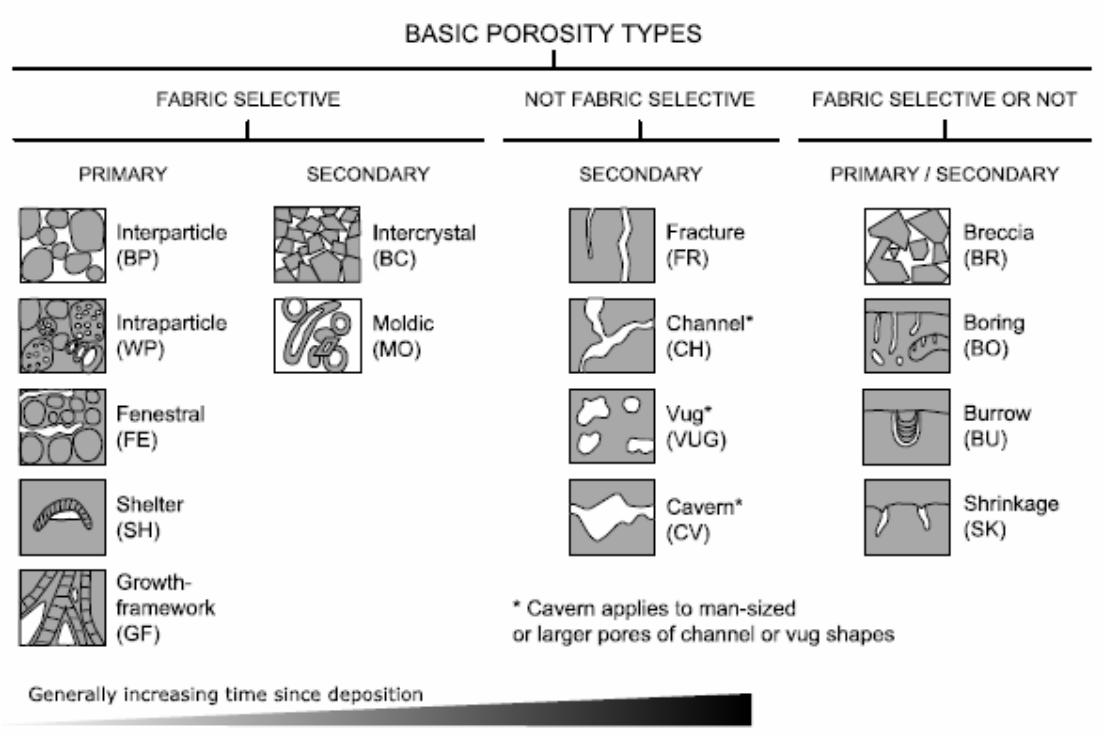

Figure 2.1 – Choquette and Pray's (1970) classification of carbonate pore types, modified by Rafaelsen and Nielsen (2005). Note the main division between fabric selective porosity and nonfabric selective porosity.

Since Choquette and Pray's model is more closely linked to depositional setting and diagenetic processes, it better fits into geological models than Archie's classification.

Lucia (1983, 1995 and 1999) developed the classification that is perhaps the most used among reservoir engineers. Lucia's model is directly linked to pore geometries and flow properties. Two main types of porosity are identified; *interparticle porosity* and *vuggy porosity*. Vuggy porosity, as defined by Lucia (1983), is pore space that is within grains or crystals or that is significantly larger than grains or crystals; that is pore space that is not interparticle. Vugs can either occur as interconnected or *touching vugs* (nonfabric selective) or as *separate vugs* (fabric selective), and are formed by dissolution of grains, matrix and/or cement. Whether touching or separate, vugs can be present as fractures, large cavities or smaller chambers. Vuggy pores are of irregular size and shape. For interparticle porosity Lucia, sharing Archie's view that pore size controls permeability and that pore size is linked to rock fabrics, suggested a pore class division based on grain size (of particles or crystals) and sorting. Fig. 2.2a illustrates the three main interparticle pore classes defined by Lucia (1983, 1995 and 1999), modified by Rafaelsen and Nielsen (2005). The main limestone rock fabrics are grainstone, grain-dominated packstone and mud-dominated fabrics. A similar division can be made for dolostone rock fabrics, however crystal size also influences pore size for dolostones. Fig. 2.2b illustrates the subdivisions of carbonate vuggy pore space, also modified by Rafaelsen and Nielsen.

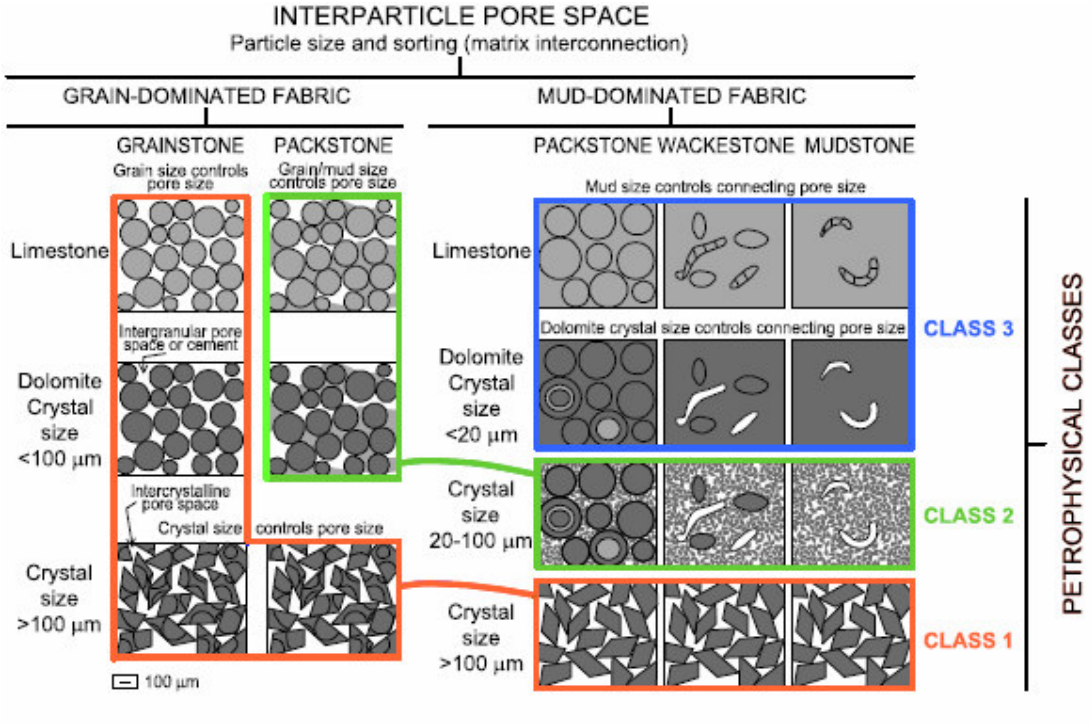

(a) Lucia's classification of carbonate interparticle pore types.

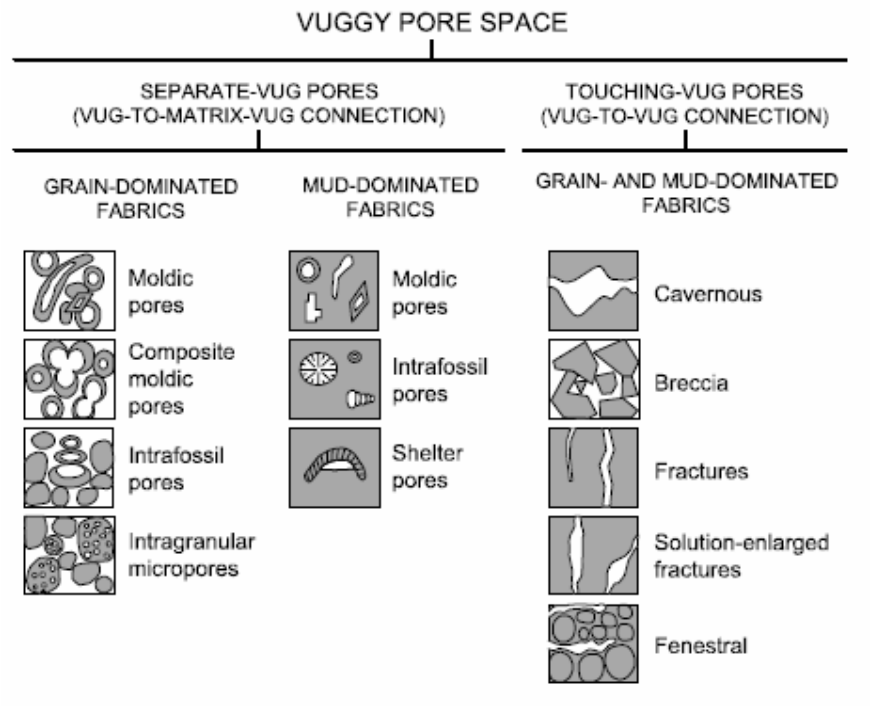

(b) Lucia's classification of carbonate vuggy pore types.

Figure 2.2 – Lucia's (1983, 1995, 1999) classification of carbonate pore types, modified by Rafaelsen and Nielsen (2005). The two main pore types are (a) interparticle pores and (b) vuggy pores; these are further subdivided by studying which rock fabrics are dominant. Vugs can be separate or touching.

Lønøy's classification

Lønøy (2006) aimed to provide a higher degree of correlation between porosity and permeability than what was achieved for previous classifications. Based on R^2 values for porosity/permeability crossplots, a new pore-type system including 20 pore-type classes was developed; the new system shows a much more predictable relation between porosity and permeability. Lønøy's classification combines sedimentological and diagenetic features with flow-related properties, and uses elements of both Choquette and Pray's (1970) classification and Lucia's (1983, 1995 and 1999) classification. Also, several new elements are introduced.

The three main elements in the new pore-type classification are:

- *Pore size*. The influence of pore size on permeability (and consequently rock fabrics) was emphasised by both Archie (1952) and Lucia (1983, 1995 and 1999). However, Lucia used grain size and sorting to separate pore-type classes. But as cements commonly occlude pore space and reduce pore throats, the relation between pore size and grain size is indirect and often incorrect. This may explain the wide range and scatter of data in all of Lucia's pore-class fields. For Lønøy's classification, pore sizes of the different classes vary with pore type and are not based on other published definitions. They are instead visually determined.

- *Pore type*. Six main pore types were defined; (1) interparticle, (2) intercrystalline, (3) vuggy, (4) intraparticle, (5) moldic and (6) mudstone microporosity. The first five pore types are nearly identical to those defined by Choquette and Pray, whereas the last one is new. Note that interparticle pores are separated from intercrystalline pores in Lønøy's classification; this is consistent with Choquette and Pray's model, but disagrees with Lucia's model which groups these two pore types together. This is verified by the fact that there is a significant difference in permeability trends between intercrystalline and interparticle porosity (Lønøy, 2006).

- *Porosity distribution*. The porosity scheme adopted from Choquette and Pray was subdivided into *uniform* and *patchy* subclasses on the basis of visual observations from thin-sections and full plugs. Patchy porosity distributions are observed to yield higher permeability than uniform porosity distributions, due to the porosity being concentrated over a smaller volume and the pore system thus being better connected for patchy porosity distributions (Lønøy 2006). Patchiness is often related to secondary dissolution and/or selective cementing during diagenesis.

Tab. 2.1 illustrates Lønøy's new porosity classification system. The definitions for the six main pore types used mostly agree with Choquette and Pray's definitions.

Interparticle porosity is defined as porosity occurring between grains (intergrain) (Choquette and Pray, 1970; Lønøy, 2006). Interparticle pores are commonly primary in origin, but may also be formed by secondary dissolution of cements or matrix.

Intercrystalline porosity is the porosity between crystals that may be of either primary or secondary origin (Lønøy 2006). If of secondary origin, intercrystalline pores are associated with calcite recrystallisation or dolomitisation. Patchy intercrystalline pore distribution is normally related to patchy cementation controlled by depositional setting; common cement mineralogies are chert, gypsum/anhydrite and calcite.

Vuggy pores are secondary solution pores that are not fabric selective (Choquette and Pray, 1970; Lønøy, 2006). The vuggy pores studied by Lønøy mostly fall into Lucia's (1983, 1995 and 1999) touching-vug pore system, i.e. they are interconnected.

Intraparticle pores are pore spaces occurring within grains, either of primary origin or formed through the decay of organic material in carbonate skeletons (Lønøy 2006).

Moldic pores are secondary pores formed by the selective, complete or partial dissolution and recrystallisation of grains or crystals (Lønøy, 2006). Moldic macropores are commonly formed through dissolution, and their porosity distribution is controlled by both diagenesis and depositional setting.

Mudstone micropores may actually be defined as interparticle or intercrystalline pores, but are not grouped with these pore types due the extremely small pore sizes. The pore structure is variable. Mudstone microporosity includes both true chalks and chalky microporosity. Chalk micropores are primary in origin. Chalky micropores are not related to chalk, but the pore structure is similar.

Table 2.1 – Lønøy's (2006) porosity classification system. A total of 20 pore classes are apparent, based on the six main pore types, pore sizes and patchy or uniform porosity distribution. The pore sizes are determined visually. Note the introduction of mudstone microporosity, with chalks being subdivided according to age.

Lønøy's porosity classification system				
Pore Type	**Pore Size**	**Porosity Distribution**	**Pore Fabric**	**Short form**
Interparticle	Micropores (10-50 μm)	Uniform	Interparticle, uniform micropores	IP-UMi
		Patchy	Interparticle, patchy micropores	IP-PMi
	Mesopores (50-100 μm)	Uniform	Interparticle, uniform mesopores	IP-UMe
		Patchy	Interparticle, patchy mesopores	IP-PMe
	Macropores (>100 μm)	Uniform	Interparticle, uniform macropores	IP-UMa
		Patchy	Interparticle, patchy macropores	IP-PMa
Intercrystalline	Micropores (10-20 μm)	Uniform	Intercrystalline, uniform micropores	IC-UMi
		Patchy	Intercrystalline, patchy micropores	IC-PMi
	Mesopores (20-60 μm)	Uniform	Intercrystalline, uniform mesopores	IC-UMe
		Patchy	Intercrystalline, patchy mesopores	IC-PMe
	Macropores (>60 μm)	Uniform	Intercrystalline, uniform macropores	IC-UMa
		Patchy	Intercrystalline, patchy macropores	IC-PMa
Intraparticle			Intraparticle	
Moldic	Micropores (<10-20 μm)		Moldic micropores	M-Mi
	Macropores (>20-30 μm)		Moldic macropores	M-Ma
Vuggy			Vuggy	
Mudstone microporosity	Micropores (<10 μm)		Tertiary chalk	C-T
			Cretaceous chalk	C-C
		Uniform	Chalky micropores, patchy	
		Patchy	Chalky micropores, uniform	

As can be seen in the porosity/permeability relationships presented by Lønøy (2006), there is still a scatter of data points for the pore classes, even though the R^2 values are much higher than the ones obtained by Lucia (1983, 1995 and 1999). The scatter could be due to other pore types present (than the dominant) or thin-sections that are not representative of the entire plug. Both pore sizes and porosity patchiness have continuous ranges, which makes it difficult to classify samples with several pore sizes present and/or samples with an intermediary degree of patchiness. Also, analytical errors may occur.

SCAL analysis performed by CIPR concerning Lønøy's classification

As described in chapter 1.2, CIPR have collaboration projects with Statoil and Hydro. An important part of these projects is *SCAL* (special core analysis), which entails all the laboratory tests mentioned in chapter 1.2. Since the development of Lønøy's classification, several projects have been performed in order to find connections between pore types and fluid flow properties. The results so far are mixed; some conclusions seem clear and clarifying, but the heterogeneity of carbonates (within pore classes as well) often causes scattered data that are hard to interpret. Interplay between intergrain channels, fractures and secondary (dissolution) porosity types such as moulds or vugs may cause dual porosity systems that cannot be classified as a single pore type; this makes it difficult to predict the influence pore types have on two-phase flow properties and simpler petrophysical parameters such as conductivity and tortuosity.

Dispersion analysis of intercrystalline pore systems have showed that pore sizes affect dispersion (Skauge et al., 2005); macropores, mesopores and micropores have also been found distinguishable through NMR pore-size characterisation (Pourmohammadi et al., 2007). Pourmohammadi et al. (2007) also concluded that high tortuosity increased dispersion (see chapter 2.3.2 for an introduction to dispersion) for most pore types; the interplay between tortuosity and dispersion properties was also found to be dependent on pore size and connectivity for moldic pore types.

2.3 Diffusion and dispersion

2.3.1 Diffusion

Molecular diffusion is the transport of molecules that occurs due to concentration gradients (more correctly gradients of chemical potential). The phenomenon is not associated with bulk flow. In reservoir engineering, molecular diffusion is of interest when considering miscible fluid displacements; it will cause an initially sharp interface between two miscible fluids to gradually develop into a diffuse mixing zone.

The diffusion coefficient D_o (also referred to as diffusivity), is commonly used to describe molecular diffusion in fluids. There is a significant difference between D_o, which is the coefficient in absence of porous media, and D, which is the effective diffusion coefficient. D recognises the fact that pore fluids flow with an interstitial velocity $v = q/(\varphi A)$. Here, q is volumetric flow rate, φ formation porosity and A cross-sectional area.

Even though the diffusion coefficient depends on several factors, such as temperature and concentration, it can in most reservoir engineering applications be treated as a constant.

For unsteady-state, one-dimensional diffusion, Fick's second law describes the concentration of the two miscible fluid's components in the mixing zone;

$$\frac{\partial C}{\partial t} = D_o \frac{\partial^2 C}{\partial x^2}, \tag{2.1}$$

where C is concentration, t time, and x distance. This is a well-known equation, often referred to simply as the *diffusion equation*. Note that this equation is valid only for non-moving fluids, as the diffusivity D_o is used.

Molecular diffusion is comparable to electrical conductivity (Klinkenberg, 1951). The formation resistivity factor F is defined empirically in terms of Archie's law as the ratio of conductivity of the fluid phase, to the conductivity of a saturated porous medium. Perkins and Johnston (1963) presented a correlation between the formation factor and the diffusion coefficients;

$$\frac{D}{D_o} = \frac{1}{F\phi}. \tag{2.2}$$

The term $F\varphi$ is sometimes replaced with a tortuosity factor τ. This factor depends on the texture of the medium, and is reported to range from 1.25 to 1.65 (Perkins and Johnston, 1963). Consequently, D has a lower value than D_o.

Fluid properties and flow velocity are believed to be the factors that decide the importance of molecular diffusion in reservoirs. For miscible fluids with very differing mobilities, channels and fingers are likely to develop; hence, the interfacial area between the fluids will be large, and diffusion will be important. For a piston-like displacement, however, diffusion will be of limited significance. Molecular diffusion is the dominating mixing mechanism at low velocities (or more correctly at low Reynolds numbers), whilst other mechanisms will be

superior when velocity is increased sufficiently. The term *dispersion* is used when on the subject of mixing that generally is present during bulk flow.

2.3.2 Dispersion

Dispersion is a phenomenon associated with all types of mixing in a porous medium. The term *dispersivity* is also commonly used, especially when considering measurements. Dispersion is traditionally considered to arise as a combined effect of molecular diffusion and convection-induced mixing. However, the terms *mixing* and *dispersion* are often confused, and the dispersion-term is extended, because: (1) capacitive mixing can also occur due to mass transfer to/from locally stagnant regions; and (2) flux-induced mixing is likely to be important on a larger scale due to channels and/or viscous fingers. In this thesis, dispersion can be caused by all the above-mentioned mechanisms.

Various models have been suggested to describe dispersion, and theories to explain the mechanisms are a much-discussed subject. Instead of reeling off all the different approaches in detail, this section will focus on one specific model; this model will be used throughout the thesis. However, a general understanding of dispersion is required to better recognise the model's strengths and weaknesses. The approach will be mostly non-mathematical, concentrating on understanding mechanisms.

Frequently, dispersion is categorised based on dimensions; microscopic (pore scale), macroscopic (core scale) and megascopic (field scale). The mechanisms which control dispersion are dependent on the scale; large scale heterogeneities such as stratification, impermeable formations and high-permeable channels are unlikely to be reproduced accurately in laboratory experiments. At microscopic level, molecular diffusion dominates.

Dispersion in the direction of mean flow is termed *longitudinal dispersion*. This topic should ideally be discussed separately from dispersion perpendicular to the direction of flow, *transversal dispersion* (occasionally referred to as lateral dispersion). The reasons for this are: (1) the mechanisms which control dispersion in the two directions are different; (2) their contributions to total dispersion have different magnitudes; and (3) the interplay between convective mixing and molecular diffusion has different correlations with parameters like velocity in the two directions.

Microscopic dispersion

On a microscopic level, dispersion is analogous to the molecular diffusion process. Einstein's diffusion model (Gudmundsson, 1992) is therefore used as a basis for most dispersion equations. The model is similar to Fick's laws mentioned in chapter 2.1, and leads to an equation known as Einstein's relationship;

$$D_{oi} = \frac{\bar{x}^2}{2\bar{\tau}}, \qquad (2.3)$$

where D_{oi} is the bulk phase coefficient of component i, $\bar{x}$ the characteristic length from the interface between the two miscible fluids, and $\bar{\tau}$ the corresponding time.

Fig. 2.3a illustrates a simplified model for longitudinal dispersion. Fluid accelerates through narrow ports, and is retarded when entering voids; consequently mixing takes place.

Modifying the regularly packed model shown in Fig. 2.3a, the *stream splitting* mechanism can be depicted as in Fig 2.3b. Here, the fluid flow occasionally splits in two due to collisions with packing. This results in lateral dispersion.

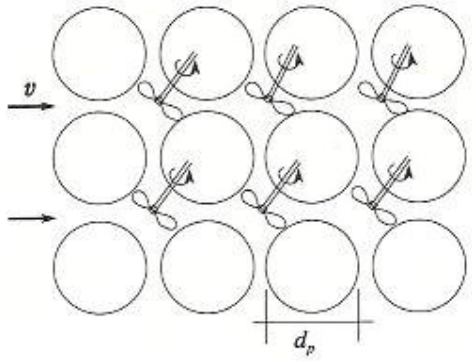

(a) Idealisation of longitudinal mechanical mixing (mixing cells).

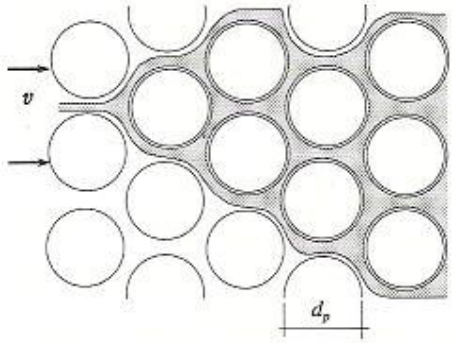

(b) Idealisation of transversal dispersion by stream splitting.

Figure 2.3 – Models for mixing in porous media (Holt, 1992).

Other convective mixing mechanisms than mixing cells and stream splitting can also appear. Fig. 2.4 demonstrates longitudinal dispersion in liquids in a capillary tube. For laminar flow, the velocity at the walls of the tube is zero; this will cause liquid B to penetrate into liquid A. A mixing zone will develop at a more rapid rate than would be obtained from diffusion alone. Taylor (1953) demonstrated that if diffusion can dampen out radial concentration gradients, the mixing zone created by this mechanism will be symmetrical and have a speed equal to the injected fluid. Aris and Amundson (1957) also reached this conclusion, even though their model was based on mixing cells in series.

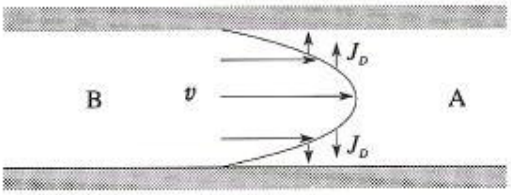

Figure 2.4 – Longitudinal dispersion in a capillary tube (Holt, 1992). Liquid B will penetrate into liquid A due to the velocity variations for laminar flow.

Dispersion may also be due to pore structure, namely: (1) incomplete connectivity, obstructions and/or recirculation of fluid; or (2) *dead-end pores* and/or adsorption. Coats and Smith (1964) have developed a differential capacitance model to better describe mass transfer between flowing fluid volume and stagnant fluid in dead-end pores. This model is the starting point for all dispersion analysis in this thesis, and will be discussed later in a separate section.

Eq. 2.3 and the models depicted in Fig. 2.3 and Fig. 2.4 constitute the basis of equations known as *standard convection-diffusion equations*. Although different symbols and forms exist, the concepts are essentially the same. Eq. 2.4 is reported by Holt (1992);

$$\frac{K_k}{D_o} = \frac{1}{\tau} + A_k \left(\frac{v d_p \sigma}{D_o} \right)^{m_k}, \tag{2.4}$$

where K_k is the effective dispersion coefficient (k is ℓ for longitudinal or t for transversal), τ the tortuosity factor (explained in connection to Eq. 2.2), A_k and m_k constants, and σ a packing or inhomogeneity factor. The first term is a diffusion term (based on Fick's law), while all contributions (based on Einstein's relationship) to convective mixing are added into the second term. The inhomogeneity factor is in the range 1 to 10.

When introducing Eq. 2.4 the question arises; under which conditions is this equation valid? And which of the two terms contributes more to dispersion? Perkins and Johnston (1963) investigated the effects of several parameters on dispersion; these were particle size and shape, heterogeneities, mobility ratio, density differences, turbulence and the presence of an immobile phase. They found that all parameters affected dispersivity; for example dispersion increases with increasing heterogeneity and also if the particle size distribution is wide. In this thesis equal densities and viscosities and laminar flow are always assumed. The effect of an immobile phase (oil) will be discussed as a separate topic later in this section.

To better understand the interplay between diffusion and convective mixing, it is necessary to be familiar with a couple of terms; the Peclet number and the Reynolds number. The Peclet number, N_{Pe}, is defined as (Lake, 1989)

$$N_{Pe} = \frac{uL}{\phi D}, \tag{2.5}$$

where u is velocity, L length, φ porosity and D the diffusion coefficient. The Peclet number expresses the ratio of convective to diffusive transport, and should not be confused with the *Bodenstein number* (Salter and Mohanty, 1982), where the diffusion coefficient is replaced with the longitudinal dispersion coefficient. The length L can in some matters be interpreted

as a characteristic pore size; however L in Eq. 2.5 is the length of the entire porous medium. The Reynolds number is the ratio of inertial forces to viscous forces, and is defined as

$$N_{\mathrm{Re}} = \frac{\rho u L}{\phi \mu}, \tag{2.6}$$

where ρ is density and μ viscosity (other parameters are the same as in Eq. 2.5). In reservoir engineering, this number is used to identify flow regimes; laminar and turbulent flow are very different when it comes to flow patterns and as to which physical laws that are valid. For laminar flow (low Reynolds numbers) viscous forces dominate and the fluid flow is smooth. Turbulent flow (high Reynolds numbers), however, tends to create fluctuations and leave parts of the fluid stagnant. The transition between laminar and turbulent flow is not sharp, but has been reported to be in the region of 10 to 1,000 (Perkins and Johnston, 1963).

Fig. 2.5 illustrates Peclet numbers for both longitudinal and transverse dispersion, as a function of Reynolds numbers. Dispersion for gases is not further discussed in this thesis.

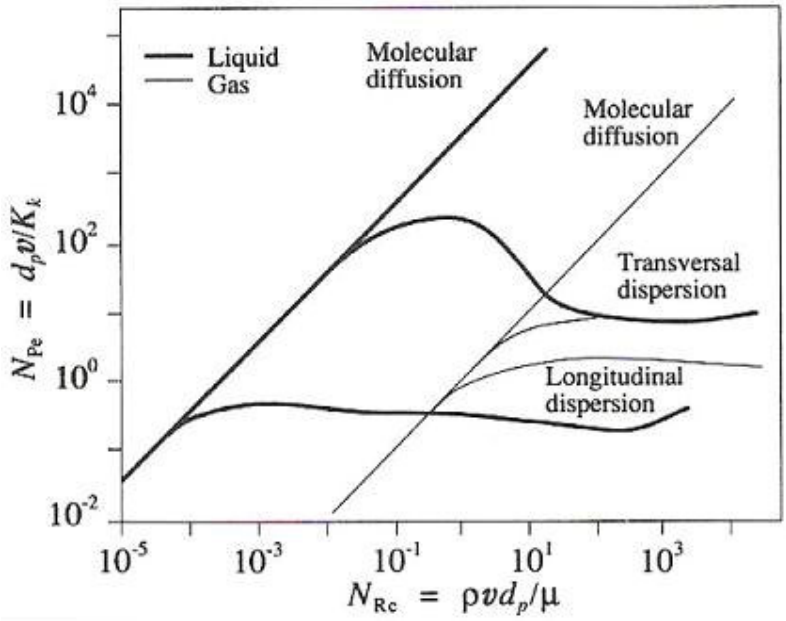

Figure 2.5 – Wilhelm's display of longitudinal and transversal dispersion, as presented by Carberry (1976; referred by Holt, 1992). With the definition of Reynolds number used, the transition from laminar to turbulent flow occurs around $N_{Re} = 40$.

For liquids it is seen that convective flow dominates both longitudinal and transversal dispersion for $N_{Re} > 10^{-2}$. As for Eq. 2.4, this suggests that the first term (diffusion term) is negligible for all Reynolds numbers higher than this. Blackwell (1962) argued that transversal dispersion coefficients were only about 1/24th those in the longitudinal direction; this indicates that longitudinal dispersion dominates, and that convective mixing might control total dispersion for Reynolds numbers as low as 10^{-4} (see Fig. 2.5). According to Lake (1989), the mechanical dispersion term dominates the molecular diffusion for interstitial velocities above 3 cm/day, or approximately 3.5×10^{-5} cm/s. For a core sample with diameter 3.8 cm, this corresponds to a volumetric rate in the region of 0.02 ml/min.

In Eq. 2.4, the value of the constant m_ℓ (also known as β) is a target for discussion. Deans (1963) formed a model consisting of well-stirred tanks in series (diffusion was neglected); this yielded a dispersion coefficient proportional to velocity, thus $m_\ell = 1$. In Taylor's (1953) model, which included transversal diffusion and longitudinal velocity variations, the dispersion coefficient was found proportional to velocity squared, thus $m_\ell = 2$. Perkins and Johnston (1963) observed factors in the range 1 to 1.25 experimentally. Hence, Deans' local mixing interpretation seems more fitting. If this is accepted, along with neglecting the diffusion term, Eq. 2.4 for longitudinal dispersion can be written as (Lake, 1989)

$$K_\ell = \frac{D_o}{\tau} + A_\ell \left(\frac{v d_p \sigma}{D_o} \right)^{m_\ell} D_o \cong \alpha_\ell |v| . \qquad (2.7)$$

α_ℓ is the *longitudinal dispersivity*, a measure of the local heterogeneity scale. The dimensionless mixing zone is directly related to the longitudinal dispersivity.

Megascopic dispersion

For field-scale displacements, it is difficult to categorise mixing exclusively as flux-induced, capacitive or dispersive (Arya et al., 1988). Here, dispersive mixing is associated with the traditional convection-diffusion equation. These three simplified mechanisms do however make it easier to understand and study aspects of megascopic dispersion.

The growth of the mixing zone will be different for the three mixing processes; therefore it is desirable to settle which one is the more important. A dispersive process is only valid when both the heterogeneity factor and the length/width ratio are low (Arya et al., 1988). This is not the case for field-scale displacements, thus inhomogeneities are expected to be the controlling factors for megascopic dispersion.

Arya et al. (1988) also showed that dispersivity increases with measurement distance, as shown in Fig. 2.6. This can be explained by the fact that dispersivity increases with increasing heterogeneity; larger scale is equivalent to larger heterogeneity scale.

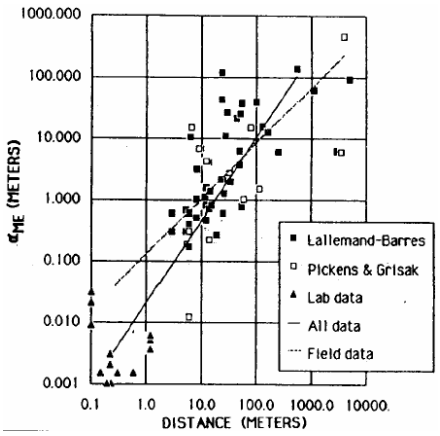

Figure 2.6 – Log-log plot of dispersivity as function of measurement distance (Arya et al., 1988). Dispersivity increases with distance due to increased heterogeneity.

Experimental methods

Studying dispersion in porous media can be performed in various ways. However, as pointed out, the scope of this thesis is to study dispersion when the two fluids are fully miscible and of equal viscosity and density. Moreover, the flow should be strictly laminar. When these conditions apply, a common approach is to inject a tracer solution with known concentration of certain ions (horisontally with constant flow rate) into a core sample consisting of only water (or another pure liquid); the composition of the initial water is also known. As the tracer solution flows through the core, there are several methods of evaluating the dispersivity, including:

- X-ray imaging of the core, to obtain the in-situ tracer distribution.
- Optical measurements of coloured tracers.
- Analysis of effluent tracer concentration based on titration.
- Analysis of effluent tracer concentration based on measuring electrical conductivity.

Common tracers include KaI, KCl and NaCl. Regardless of which tracer is used, it is important to make sure that ion exchange and/or adsorption does not take place inside the core. Adsorption of tracer molecules will cause a delay in effluent tracer concentration.

If 100 % tracer concentration does not equal 1, which may be caused by inaccurate calibration, the effluent concentration should be normalised in order to fulfil this criterion. As shown by Taylor (1953), the mixing zone travels with the same speed as the injection rate. This fact leads to the conclusion that the 50 % concentration breakthrough should occur at exactly one pore volume injected tracer (corrected for all "non-core" volume), if the medium is homogeneous and no adsorption or ion exchange exists. However, for heterogeneous samples, this is often not so, as will be discussed later. Analysis of the concentration profiles can give information on both dispersivity and pore structure; the standard convection-diffusion theory is only one of the models available for this purpose.

The Coats and Smith model

The concept of dead-end pockets was first presented by Turner (1959). The intention of introducing these pore structures was to represent microscopic heterogeneity mechanisms; certain pores are presumably bypassed by flow. As suggested by Deans (1963), this behaviour is better described by a capacitance model than by the standard convection-diffusion equation. Deans' model was further developed by Coats and Smith (1964). Their differential capacitance model is described by the following equations;

$$K\frac{\partial^2 C}{\partial x^2} - u\frac{\partial C}{\partial x} = f\frac{\partial C}{\partial t} + (1-f)\frac{\partial C^+}{\partial t}, \tag{2.8a}$$

$$(1-f)\frac{\partial C^+}{\partial t} = M\left(C - C^+\right), \tag{2.8b}$$

where u, K and C are interstitial velocity, dispersion coefficient and concentration *in pores occupied by the fluid*. M is the mass transfer coefficient between the stagnant (also called dendritic) regions and the flowing fluid, while f is the flowing fraction (dimensionless) of accessible fluid. C^+ is the concentration in the stagnant fraction, x is distance and t time. It should be noted that the symbols are not exactly the same as presented originally by Coats

and Smith, but this notation is widely used, for example by Salter and Mohanty (1982) and by Skauge et al. (2006). Three terms have other symbols here compared to the original model: (1) the dispersion coefficient (D); (2) the mass transfer coefficient (K); and (3) the concentration in the stagnant fraction (C^*). The reason for choosing the notation given here is evident; D is already associated with diffusion coefficients and K with dispersion coefficients. Eq. 2.8a is a standard convection-diffusion equation for the flowing fraction, where the diffusion term is neglected. Eq. 2.8b is a mass balance equation for the stagnant regions; the mass transfer between flowing fraction and stagnant regions is thought to occur only as molecular diffusion (confirmed by Jasti et al., 1988). For low velocities, M is large and the mass transfer will consequently be effectively instantaneous, yielding symmetric dispersion profiles; hence, the standard convection-diffusion equation is adequate. For high velocities, M is small, and convective mixing overshadows dead-end-pore diffusion; a high-velocity profile is therefore likely to be very effective (steep), until it reaches a concentration where there is a need to "wait" for the dead-end-pore mass transfer. Also, it is evident that if f is unity, the equations reduce to the standard convection-diffusion equation. As the standard convection-diffusion equation is expected to produce symmetrical S-shaped effluent concentration profiles (around 1 PV), it is presumably suitable for low velocities. However, for intermediate velocities, profiles that exhibit asymmetry are more likely to occur (if dead-end pores are present); this is better described by the differential capacitance model in Eqs. 2.8a and 2.8b.

The validity of Eqs. 2.8a and 2.8b is discussed by several authors. Coats and Smith (1964) themselves recognised the facts that: (1) the capacitance effects may be exaggerated in laboratory experiments, due to higher velocities and different M than in field-scale displacements; and that (2) sufficiently high velocities will cause turbulence, which would result in an earlier breakthrough (than the model predicts) for lower effluent concentrations. The Coats and Smith model was also studied by Salter and Mohanty (1982) in association with their two-phase tracer displacements. They found difficulties fitting floods where the flowing fraction (f) was either very low or near unity. Low values of f were difficult due to the model only using *one* mass transfer coefficient; since dead-end pores are of varying size, ideally this should be described by a *series* of mass transfer coefficients. This problem is more clarified when the stagnant fraction is large. At high values of f, the model tends to produce multiple solutions; this is because the mass transfer diffusion term also produces S-shaped solutions. The effects of f, the Bodenstein number and M are illustrated in Figs. 2.7, 2.8 and 2.9.

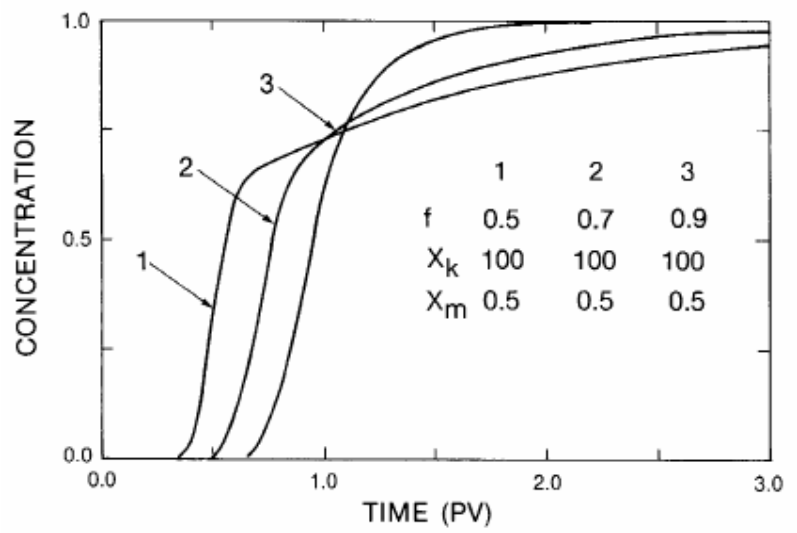

Figure 2.7 – The effects of flowing fraction on effluent profiles (Salter and Mohanty, 1982). X_k *is the Bodenstein number and* X_m = ML/u *is a rate group. As f decreases, breakthrough is earlier and the tail is longer.*

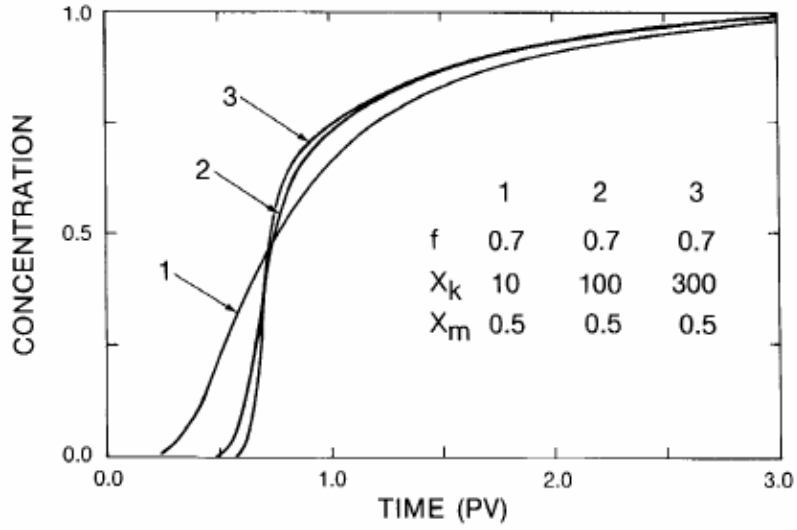

Figure 2.8 – The effects of Bodenstein number on effluent profiles (Salter and Mohanty, 1982). As the Bodenstein number decreases effluent concentration gets more dispersed.

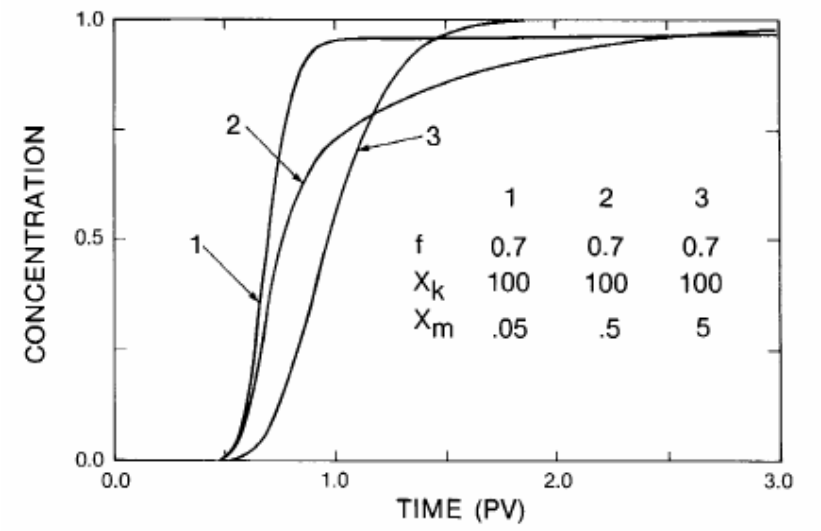

Figure 2.9 – The effects of mass transfer coefficient on effluent profiles (Salter and Mohanty, 1982). At low values of M *the stagnant regions will behave like isolated fluid, increasing the efficiency.*

The effects that are seen on Figs. 2.7, 2.8 and 2.9 can be explained rationally by considering the distribution of fluid into flowing, dendritic and isolated fractions in each case. Fig. 2.7 indicates earlier breakthrough as *f* decreases; this is because an increased amount of dead-end pores causes increased heterogeneity, which in turn results in earlier breakthrough. With this early breakthrough, more tailing is evidently observed. From Fig. 2.8 it is seen that lower values of the Bodenstein number leads to a more dispersed concentration profile; this effect can be predicted directly from the definition of the Bodenstein number, as commented regarding Eq. 2.5. A lower value of or X_k yields an increased dispersion coefficient. Finally, Fig. 2.9 shows that low *M* values produce a piston-like displacement; the dead-end pores will act as though they were completely isolated because the mass transfer takes place so slowly. For higher *M* values the concentration profile looks symmetrical due to nearly instantaneous mass transfer (as commented to Eqs. 2.8a and 2.8b).

Jasti et al. (1988) also investigated Coats and Smith's model. They claimed that the mass transfer coefficient was independent of interstitial velocity, as long as $N_{Pe} < 100$. In similar fashion to Salter and Mohanty, they also found that an increase in *M* gave rise to an increase in *skewness* for effluent concentration profiles; if *M* is sufficiently large, stagnant regions will function as flowing fraction, due to practically instantaneous mass transfer. The question of up-scaling Coats and Smith's model was also brought up by Jasti et al.; replacing laboratory length with field lengths for dimensionless parameters may not produce correct field-scale solutions, due to the fact that large velocity variations and large variations in diffusion-limited zones are likely to come about in reservoirs.

According to Fourar et al. (2005) large variations in local permeability cast doubt on the use of Coats and Smith's model in heterogeneous reservoirs (such as carbonate reservoirs). The permeability variations cause the dispersion coefficient to depend on space location, and thus the average dispersion coefficient found in all standard approaches is no longer applicable. Still, the models may be perfectly suitable for small core plugs, where these large-scale heterogeneities are not found.

Influence of immobile phase on dispersion

It can be argued that this subject should be a part of the "Two-phase flow properties" section; however it is the *dispersion* phenomenon that is of interest here. The immobile phase is here represented by oil and the mobile phase by water. Since water and oil are immiscible, no interphase mass transfer can occur.

Salter and Mohanty (1982) showed that Coats and Smith's model could be extended to two-phase flow, if K, u and f are based on the *recoverable* fraction of the phase in question. The meaning of dendritic fluid needs to be revised, though. When oil is present, dendritic water could also occur due to water or oil being snapped off by the other phase. The extent of dendritic water caused by this mechanism is dependent on the phase distributions, which in turn are strongly linked to wettability. At the endpoint saturations, the flowing fraction of water may be high due to film flow; film flow is a term used to describe fluid flow in nooks and crannies caused by phase distributions and saturation. Highly connected water films are likely to occur if the oil phase is either continuous (S_{wi}) or completely discontinuous (S_{or}) (Salter and Mohanty, 1982). Flowing fraction for water at S_{or} is clearly linked to phase distributions, but high flowing fraction at S_{or} can arise both due to local oil affinity leading to oil being situated in dead-end pores, or film flow. For the oil phase, if the system is water-wet, an *isolated* fraction must also be implemented; this is outside the scope of this thesis though, as only water-phase dispersion is considered.

Thomas et al. (1963) pointed out that dispersion is a function of saturation, and cannot be predicted from dispersion theory developed for single-phase miscible displacements. As the saturation decreases, the flow path becomes more and more tortuous, and thus an increase in dispersivity is to be expected (this was shown by Salter and Mohanty, 1982). To which extent the dispersivity is increased, depends on the phase distributions, which in turn is dependent on wettability.

To sum up, it is in fact possible to investigate the distribution of residual oil by comparing experimental dispersion test results for water-saturated samples with results for samples at residual oil saturation. However, one should be aware of the presence of film flow, as it might increase the flowing fraction; wettability data may help to discover whether high flowing fractions at S_{or} are caused by oil-wetness or film flow.

2.4 Two-phase flow properties

Water flooding as primary recovery technique is widespread on the Norwegian continental shelf. The injected water effectively displaces the oil to production well(s) in an immiscible process, and at the same time maintains the reservoir pressure. The recovery efficiency of conventional water floods is commonly recognised to be mainly influenced by: (1) mobility ratio or in effect oil viscosity; (2) large scale heterogeneities causing permeability variations; (3) wettability; (4) dip angle in direction of flow; and (5) pore-size distribution.

North Sea reservoirs commonly have properties that are favourable for water flooding. All Norwegian oil reservoirs are in the range strongly water-wet to intermediate wet. The viscosity of North Sea oils is generally low, preventing instability phenomena such as viscous fingering (on a microscopic level, fingering can arise due to large-scale heterogeneities as well), and giving rice to a sharp interface between water and oil. The *mobility ratio* is crucial when discussing recovery efficiency; a low mobility ratio (less than 1) will increase both the microscopic displacement efficiency (due to lower average oil saturation) and the volumetric efficiency. The effect of mobility ratio on saturation fronts is shown in Fig. 2.10; high mobility ratios cause earlier water breakthrough and a longer tail production, whilst low mobility ratios produce piston-like displacement processes and higher recovery efficiency. The mobility ratio is dependent on the relative permeabilities, and is therefore a function of saturation. However, *endpoint* mobility ratios are frequently used when roughly classifying a displacement process. For water/oil- systems they are defined as:

$$M_{wo} = \frac{k_{rw,ro} \cdot \mu_o}{k_{ro,iw} \cdot \mu_w}, \tag{2.9}$$

where $k_{rw,ro}$ is the relative permeability of water at residual oil saturation and $k_{ro,iw}$ is the relative permeability of oil at irreducible water saturation.

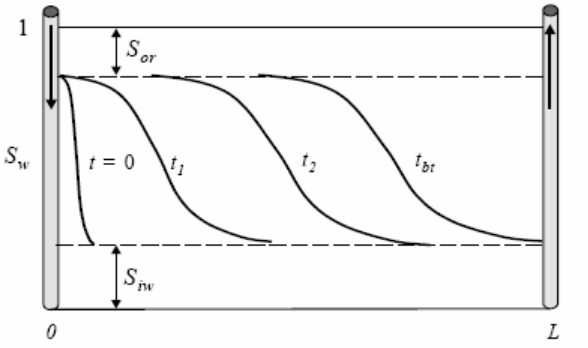

(a) Water displacing oil; saturation front when M_{wo} *>> 1.*

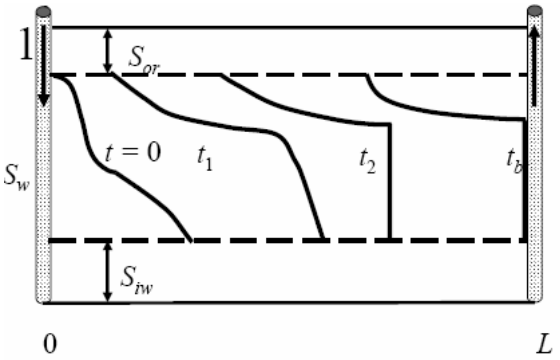

(b) Water displacing oil; saturation front when $M_{wo} \approx 1$.

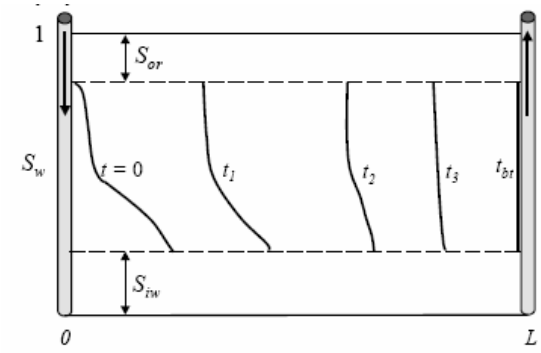

(c) Water displacing oil; saturation front when $M_{wo} < 1$.

Figure 2.10 – Influence of mobility ratio on the saturation front (Lien, 2007). It can be seen that low mobility ratios produce stable fronts; this is desirable as it improves recovery.

Water flooding core samples may give a better understanding on recovery mechanisms and recovery efficiency in real reservoirs. However, several uncertain factors exist; the preservation of reservoir conditions and the use of simpler fluids in laboratory tests are the key issues. As a result of the radical pressure and temperature drop when taking samples to surface conditions, the composition of reservoir fluids will change. The original wettability of the rock is also likely to be altered, especially if cores are exposed to drilling muds. Often samples are cleaned, in order to perform laboratory tests at (presumably) water-wet conditions. The same tests are then repeated after the samples have undergone an ageing process that increases oil affinity; these tests are known as *restored state* test. If the purpose allows, the relevant tests are carried out using simplified fluids, and also often at atmospheric conditions (temperature and pressure). Reservoir oil is often replaced with compositionally simpler and cheaper oil, such as decane. Using oil with well-known properties (density, viscosity, etc.) reduces uncertain factors when interpreting results. Evidently, the densities and viscosities for laboratory oils are not necessary equal to the relevant reservoir oil, making the displacement process for laboratory water floods slightly different. Water viscosity may also be significantly higher at atmospheric conditions. The compositional differences of laboratory fluids and reservoir fluids should also be considered regarding restored state tests, as the wettability is dependent on fluid composition.

For petrophysical properties such as permeability and porosity, it is often difficult to decide whether laboratory results are relevant for the reservoir; this issue also emerges when

considering water floods. In addition to the different properties of laboratory fluids and reservoir fluids, large-scale heterogeneities can lead to low volumetric recovery efficiency and a low overall recovery factor. Carbonate reservoir rocks are often fractured, such as the chalk on Ekofisk. The fractures undeniably affect fluid flow patterns, as fracture permeability often exceeds matrix permeability by up to several orders of magnitude. It is difficult to reproduce large-scale fractures on a laboratory scale, and they are therefore often ignored. It is clear that this simplification may lead to laboratory results that are not necessarily representative for real carbonate reservoirs. Also, the flow regime for laboratory water floods needs to be the same as the actual reservoir flow regime; normally the main issues are keeping the flow laminar (i.e. avoiding turbulence) and avoiding capillary end effects which can arise due to water-wetness and the lower length scale.

Recovery efficiency is normally the main result of laboratory water floods. Both the maximum recovery efficiency and the development through time are of interest. Dimensionless time is often used in order to normalise time; the standard time unit is *injected pore volumes of water*, expressed as

$$t_D = \frac{Q \cdot t}{V_p}, \tag{2.10}$$

where Q is the injection rate of water, t time and V_p the pore volume of the sample. Recovery efficiency can be measured either as fraction of pore volume or as fraction of original oil in place (*OOIP*);

$$E_R = \frac{V_{o,prod}}{V_p}, \tag{2.11a}$$

$$E_R = \frac{V_{o,prod}}{OOIP} = \frac{V_{o,prod}}{(1 - S_{wi}) \cdot V_p}. \tag{2.11b}$$

$V_{o,prod}$ is the produced volume of oil, *OOIP* the initial volume of oil and S_{wi} the initial water saturation. For water-wet samples the recovery efficiency as fraction of *OOIP* will always be higher due to the presence of initial water. Water saturation as a function of time is also commonly seen plotted for laboratory water floods.

Strongly water-wet samples are expected to generate sharp water-cuts, i.e. the amount of oil produced after water breakthrough is negligible. This is illustrated in Fig. 2.11. The remaining oil in the sample when water breaks through is capillary trapped as oil globules with virtually no possibility of forming a continuous flowing phase (if the interfacial tension between oil and water is not lowered). This residual oil saturation after water flooding is termed S_{orw}.

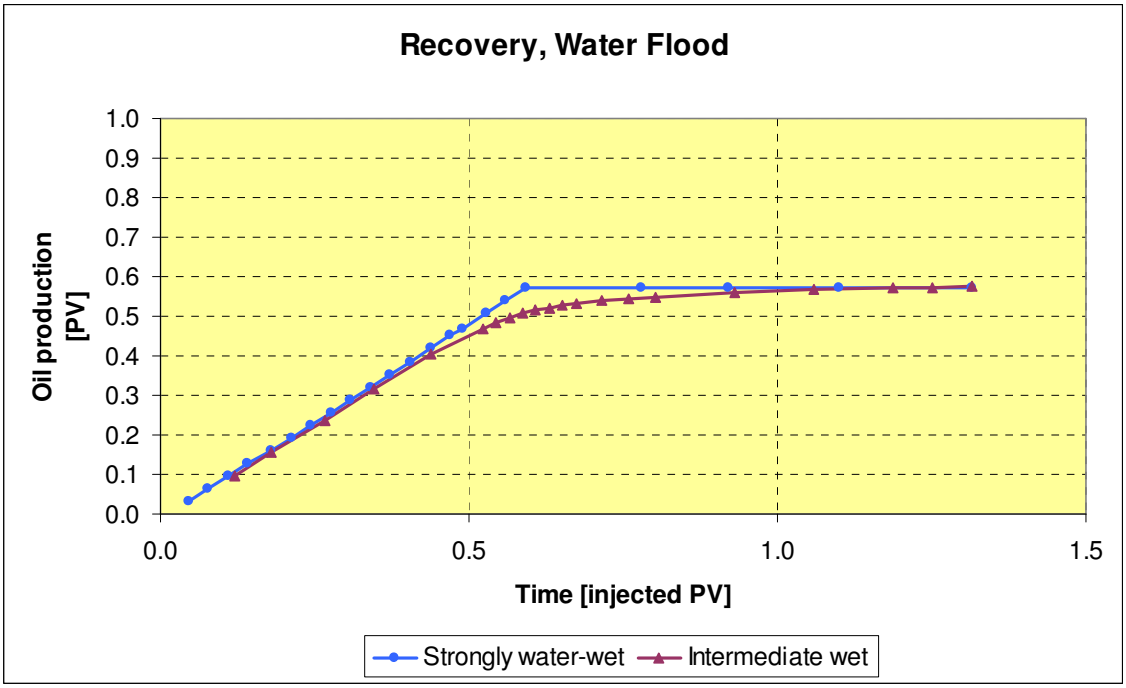

Figure 2.11 – Influence of wettability on water-cut. A sharp water-cut is seen for strongly water-wet samples, while there is a transition zone for intermediate wet samples. The data set is not based on a real water flood, and is only meant to demonstrate the effect of wettability on production profiles after water breakthrough. In reality, wettability can also affect the maximum recovery efficiency. This is not considered here.

Homogeneous samples with well-connected, simple pore structures are expected to have low dispersivity and a low fraction of dead-end pores, as remarked in chapter 2.3.2 (Coats and Smith's model). For water floods, such homogeneous samples should have higher recovery efficiency than heterogeneous (highly dispersive) samples, due to lower average tortuosity and consequently less resistance to form a stable displacement front. However, other parameters such as wettability, endpoint saturations (S_{wi} and S_{orw}), mobility ratio and fluid densities (if the displacement is not horisontal) may also strongly influence recovery efficiency in laboratory water floods.

2.5 Effect of salinity on permeability

Formation damage in sandstones

Reduction of permeability, often termed *formation damage*, can be critical for a reservoir's flow properties, and should be avoided. In sandstone reservoirs, formation damage can occur when the ionic composition of injection water is altered and/or when velocity is high. These topics have been widely discussed over the last decades, and the mechanisms causing permeability decrease in sandstones are now more or less commonly accepted.

Most studies on sandstone permeability have been performed in Berea sandstone plugs. Berea sandstone is widely used as a standard testing material in the petroleum industry, due to its homogeneous properties in terms of porosity and permeability (Ochi and Vernoux, 1998). Clay is frequently detected in sandstones; the main constituent of clay in Berea sandstones is *kaolinite*. Interactions between ions present in the injection water and clay particles on the pore surfaces can lead to clay particles being released, causing them to migrate until they end up blocking pore throats due to interceptions, straining or sedimentation. This phenomenon is illustrated in Fig. 2.12; it is evident that the migration of clay particles can reduce permeability considerably.

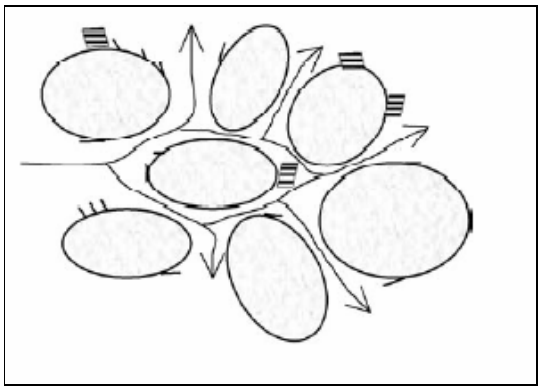

(a) Flow pattern in original sandstone.

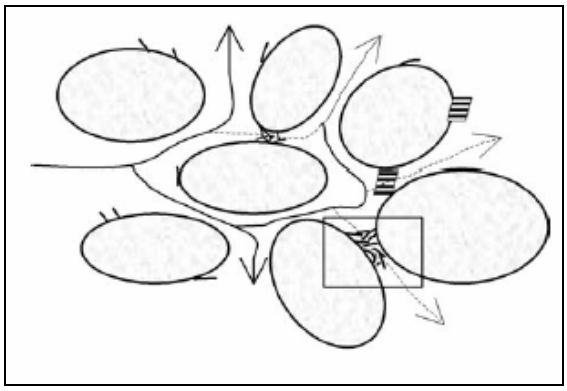

(b) Flow pattern in "damaged" sandstone.

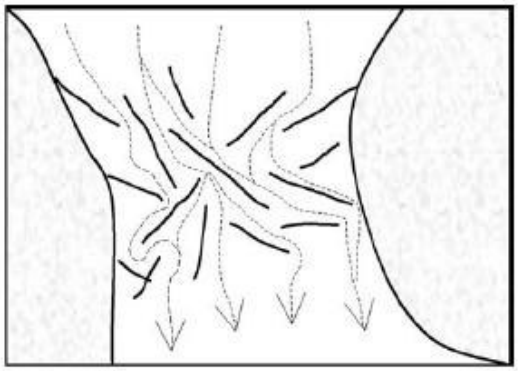

(c)Flow pattern in a plugged pore throat.

Figure 2.12 – Formation damage in sandstones due to clay migration (Tchistiakov, 2000). The illustrations do not reflect the real ratio between sizes of clay and sand particles.

Whether formation damage caused by clay migration, as shown in Fig. 2.12, can take place, depends on the particles' size compared to pore-throat sizes, and on their concentration in the fluid. Release of particles only takes place if the salt concentration (in water) is below a *critical salt concentration, CSC* (Khilar and Fogler, 1983). This occurs when repulsive forces between the electric double-layers of the particles overcome the attractive van der Waals forces; this will cause all clay particles to loosen more or less simultaneously leading to an abrupt permeability reduction.

The *CSC* has been found strongly dependent on the nature of solution cations and on temperature. Khilar and Fogler (1984) observed different degrees of permeability reduction with different monovalent cations (Cs^+ and Na^+) present in the formation before fresh-water flooding. They obtained a reduction of more than 95 % with sodium salt pretreatment, but significantly less reduction when the cations were divalent (Ca^{2+} or Mg^{2+}). According to Kia et al. (1987), no reduction at all is observed when more than 75 % of pore surfaces are covered by calcium ions. Below this critical concentration, the permeability reduction increases with decreasing calcium concentration. Sodium ions, calcium ions and magnesium ions are all commonly present in brine, thus the results are of great relevance.

When the chemical effect is minimised by using high-saline water (above *CSC*), the *hydrodynamic* effect becomes the fundamental mechanism of permeability reduction. This effect has been less studied than the double-layer theory, due to the limited range of flow rates applied in the petroleum industry. Even though the hydrodynamic effect can reduce permeability by more than 50 % (Ochi and Vernoux, 1998), it is in practice less severe than the chemical effect. There are two reasons for this:

- Ochi and Vernoux (1998) proved that a *critical flow rate* must be exceeded for the permeability to decrease due to hydrodynamic release. This critical rate was observed to increase with salinity. For Berea sandstones the critical flow rates were in the region of 1 – 8 cm^3/s, which corresponds to a volumetric injection rate of about 300 – 2500 ml/h for typical laboratory core samples. Such high flow rates would normally generate high Reynolds numbers and consequently turbulent flow, and are for that reason avoided.
- Clay particles are only released from pores where the fluid velocity is higher than the critical velocity. This suggests that, rather than an abrupt permeability decrease, one should expect hydrodynamic release to lead to a gradual reduction; this was in fact what was obtained by Ochi and Vernoux (1998).

Permeability reduction due to fines (clay) migration might not only be harmful. Tang and Morrow (1999) suggested that mobilisation of clay would result in exposure of underlying surfaces, which would increase the water-wetness of the system. The originally mixed-wet clay particles could mobilise previously retained oil droplets attached to them as they detach. This would lead to an increase in oil recovery. And indeed, increased oil recovery associated with low salinity water has been reported by BP in several reservoirs offshore Alaska (Lager et al., 2006). However, no fines migration or significant permeability reductions have been observed. Lager et al. (2006) also proved that the improved recovery is not related to increased pH, but rather *Multicomponent Ionic Exchange (MIE).* This involves the competition of all the ions in pore water for the mineral matrix exchange sites; organic polar compounds are removed from the pore surface and replaced with cations such as Ca^{2+} and Mg^{2+}. Thus, cation exchange capacity is a key element for the effect of low salinity water injection.

Formation damage in carbonates

Due to the much lower clay content, formation damage in carbonates (caused by the mechanisms described for sandstones) is generally not considered a problem. The chemical reactions that release fines from the clay surfaces is expected to be scarce and the ion-exchange capacity low. Dahab et al. (1993) showed that this was indeed the case for some Saudi limestones when the NaCl content of the injection water spanned from 5 to 20 weight-percent.

A more common problem associated with carbonate core samples is an *increase* in permeability due to dissolution of calcite, dolomite, halite, anhydrite or gypsum (T.A. Svanå and A. Waldum, Pers.com.). The dissolution reactions are relatively slow, and dependent on the amount of carbonate material present in the rock (Lager et al., 2006). The following reactions are likely to occur:

- $CaCO_3 \leftrightarrow Ca^{2+} + CO_3^{2-}$
- $CO_3^{2-} + H_2O \leftrightarrow HCO_3^{-} + OH^{-}$

If the injected water is rich in ions (high-saline) these reactions will not be as dominant as for fresh water. On a large scale, karst structures could arise due to fresh-water dissolution of carbonates. On a laboratory scale, fresh water can dissolute carbonate fines and conceivably increase permeability. Another possible scenario is that these fines get trapped in narrow pore throats and thereby *reduces* permeability. The cleaning process of carbonate cores is also challenging for this reason; methanol and toluene are dissolution agents that may free water-wet or oil-wet (respectively) components from pore surfaces.

Chapter 3: Experimental methods and analysis

3.1 Introduction

Chapter 2 has now provided necessary theoretical knowledge on carbonates and fluid flow to better understand the experimental approach in this thesis. In this chapter experimental methods are introduced, as well as the models and tools that are used to interpret the results.

As discussed in chapter 2.3.2, dispersion characteristics for samples are commonly obtained by studying effluent concentration changes when a *tracer* displaces brine in a miscible displacement process. An important aspect of this thesis is the introduction of a new approach to dispersion analysis; this experimental approach will be discussed in detail in this chapter. The process of simulating the experimental results is considered next, emphasising input and output parameters, as well as the actual simulation process and the software used. It is also essential to understand the concepts on which simulation is based on. Finally, the spotlight is directed at measurements of absolute permeability. Although both apparatus and methods are well-known for these measurements, special care needs to taken when altering brine concentration and when detecting potentially small permeability variations. Consequently, the main focus in this part will be on accuracy and uncertain factors.

3.2 A new method for dispersion analysis

Previous methods used at CIPR

Dispersion analysis is a simple way of getting hold of pore structure information and miscible displacement properties. Most test schemes are low-cost and not very time-consuming. Still, a number of different approaches are used, and no standard dispersion test procedure exists. At CIPR, two different methods have been going; (1) UV spectrometry after injection of 4-fluoro benzoic acid (4-FBA) and (2) conductivity measurements after injection of potassium iodide (KaI) solutions.

The main concept of UV spectrometry is to analyse the level of absorption through effluent samples. 4-FBA contains fluoride ions (F^-) which absorbs light. As the injection process progresses the concentration of F^- in the effluent increases; consequently the absorption is expected to increase as well. Effluent samples are taken at different points of time and diluted before absorption is measured. Absorption can be converted to concentration through calibration with known concentrations. As one might expect, this method is rather time-consuming; one single dispersion test analysis could take up to four days of work (S. Pourmohammadi, Pers.com.). Also, the dispersion profiles attained gave rise to suspicion that adsorption was taking place, due to the fact that the normalised concentration at 1 PV was far below 0.5. If this is true, the adsorption could occur when the negatively charged fluoride ions adsorb onto positively charged carbonate pore surfaces in ion exchange processes.

Measuring electrical conductivity of water is a less comprehensive method than UV spectrometry. As the concentration of ions increases, it is evident that the conductivity increases as well. However, the relation between the two parameters could be complex, as conductivity is also a function of temperature (even though it is often referred to at a standard

temperature, such as 20 °C, and thus is considered characteristic for a material). If a calibration that relates concentration to conductivity and temperature is feasible, this method could reduce both testing and analysis time compared to UV spectrometry. In addition, conductivity and temperature are variables that are measurable more or less continuously, so that the amount of data is increased significantly. Potassium iodide is intuitively well-suited for this purpose; it is an uncomplexed salt that is soluble in water:

$$KI \overset{aq.}{\leftrightarrow} K^+ + I^-$$

The main reason for not being fully satisfied with KI as tracer, is that neither of the ions are a natural part of the rock/water system. Thus, it takes more time to obtain equilibrium. Also, the injection of unfamiliar ions may cause unwanted chemical reactions.

A new approach

Based on the results of the two previous methods, there was need of a new method that satisfied the following criteria:

- A time-effective analysis method of the effluent tracer concentration.
- A tracer containing only ions that are already present, either on rock surfaces or as a part of the brine. Fulfilling this also diminishes any chance of adsorption occurring.

At this point, it should be emphasised that describing the method as "new" might be misleading; calculating dispersion profiles based on electrical conductivity measurements is already a recognised method. However, the elements of experimental setup and calibration of ion strength vs. conductivity range to obtain sufficient concentration differences are exclusive. Also, the method is new at CIPR. Thus, using the word "new" seems tolerable.

The conductivity measurements (using KI as tracer) seemed promising compared to UV spectrometry. The only apparent obstacle was the calibration part, and finding a suiting way of measuring conductivity and temperature experimentally. Also, a tracer containing only the acceptable ions had to be found.

Sodium chloride, NaCl, is a salt already present in brine. It is, in similar fashion to KI, an uncomplexed salt, and dissolves into Na^+ and Cl^-- ions. However, carbonate cores already need to be flooded with sea water (containing NaCl) rather than fresh water to avoid dissolution. Thus, the tracer should be synthetic sea water (SSW, see Appendix 1) with a certain amount of NaCl added to it. This amount can be decided by estimating how large conductivity differences it is experimentally convenient to study.

Next to consider is the flooding procedure itself. Fig. 3.1 is a fundamental sketch of the apparatus needed. For practical reasons a bypass opportunity should always be included. Back pressure is also necessary, to avoid air bubbles. The tubing system should be connected to a pump system where valves control whether sea water or tracer is injected. This also permits the exchange of liquids to be computer-controlled. To make sure that the dispersion profile (when the composition changes from sea water to tracer) is in fact correct, it is recommended to reverse the process by injecting SSW after equilibrium is reached (the normalised concentration equals 1.).

As illustrated in Fig. 3.1 temperature and electrical resistance (inverse of conductance) are both measured in the tubing system *behind* the producing end of the core sample. At this point

the difference between *conductance* and *conductivity* should be pointed out; *conductivity is conductance pr. length unit times the cross-sectional area*. However, if the length between the measurement points and the cross-sectional area are constant, conductance is proportional to conductivity; a change in conductance can occur if, and only if there is a change in conductivity. This fact should be kept in mind when studying the calibration procedures, as the unit used is Ω^{-1}, while the method is referred to as a conductivity method.

Temperature is measured by means of a simple termistor. Readings of the two parameters are connected to a computer that continuously makes graphical profiles of the concentration, based on an equation obtained through calibration (see next paragraph). The logging interval can be set manually, but in general it is possible to calculate a very large number of concentrations for a given time period.

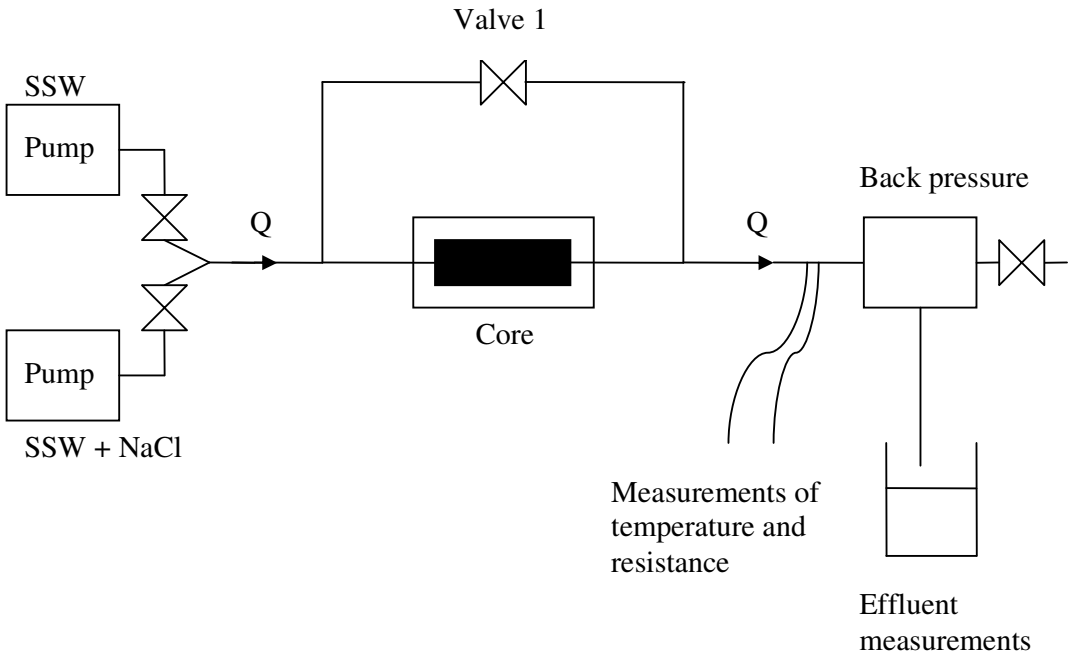

Figure 3.1 – Sketch of apparatus used to obtain dispersion profiles. SSW is an abbreviation for synthetic sea water, for which the composition is given in Appendix 1. Temperature and electrical resistance are measured at short time intervals and logged to a computer. Valves are used to change between sea water and the tracer, which consists of sea water and an additional amount of NaCl. Back pressure reduces the possibility of air in the system.

Calibration and verification of the new method

The purpose of this calibration is to determine the experimental relation between concentration, electrical resistance and temperature. A reasonable concentration unit is *normalised added weight- % of tracer, i.e. 100 % tracer equals 1 and 100 % SSW equals 0*. To obtain an equation of the form $C(R, T)$, the following procedure is applicable:

1. Make a tracer solution of requested strength. Based on the dispersion tests performed in this thesis, 1 % added NaCl (to SSW) should produce adequate resistance differences. In any case, tracer concentration (added weight- % NaCl) should be noted.

2. Prepare at least five different mixed samples of SSW and tracer. In this thesis, five concentrations were utilised; 0 %, 25 %, 50 %, 75 % and 100 % SSW.
3. Measure electrical resistance for each of the five samples at different temperatures. The chosen temperature range should agree with the expected temperature range for the dispersion tests; in this thesis eight temperatures were selected ranging from 18 °C to 47 °C.
4. The practical part is now completed. As first part of the analysis, temperature- and resistance fluctuations should be eliminated by calculating average values of the two parameters, for each solution. This makes it possible to plot resistance as a function of concentration for all the selected temperatures (isotherms). To make the mathematical tasks easier it is possible to normalise the resistance; 100 % SSW yields $R = 1$. However, this is optional.
5. The equations for the isotherms need to be on the same form, for example $C(R) = aR^2 + bR + c$. All the coefficients (here a, b and c) may now be plotted as a function of temperature. The expressions for the coefficients should then be inserted into the general equation, and the final equation is on the form C (R, T).
6. As for all calibrations, the result should be tested properly before accepted. This involves comparison with previous methods and testing it for real core samples.

The following part sums up the six-step procedure for this thesis. As calibrations should be performed afresh for all experimental setups, emphasis should be put on the procedure rather than the actual coefficients that are found here. Qualitatively, the calibration results do however indicate measurement uncertainty as well as testifying the influence of temperature.

Tab. 3.1 shows the tracer concentration and the chosen mixtures of tracer and SSW.

Table 3.1 – An overview of the samples used for calibration. Originally there were only five different mixtures of tracer and SSW, but the calibration procedure was then repeated and the three mixtures representing 25 %, 50 % and 75 % tracer were slightly altered.

Calibration samples		
Concentration of 100 % tracer [added weight- % NaCl]	1.3422	
Sample #	**Tracer concentration [frac.]**	**NaCl added to SSW [weight- %]**
1	0	0
2	0.2483	0.3333
3	0.2499	0.3355
4	0.4999	0.6710
5	0.5009	0.6722
6	0.7493	1.0057
7	0.7541	1.0121
8	1	1.3422

Fig. 3.2 is a plot of the average *conductance* as function of concentration at the eight temperatures. The reason for using conductance as the unit here is to demonstrate that a linear trend best describes the data set. A water bath was used to keep the temperature constant; based on standard deviation considerations of raw data this came off well with an uncertainty

of 0.03 °C at the most. At this point it should be stressed that the temperature unit was °C in all measurements and calculations. The relative uncertainty was never above 0.1 % and was thus negligible. This was also the case for the electrical resistance, where the relative uncertainty was 0.1 % at the most. The concentration is observed to be inversely proportional to the electrical resistance. The trendlines found (through linear regression) to match the data set are given under Fig. 3.2, in Tab. 3.2. R^2 values for the trendlines are 0.997 or higher, so the match is more or less ideal for all data series.

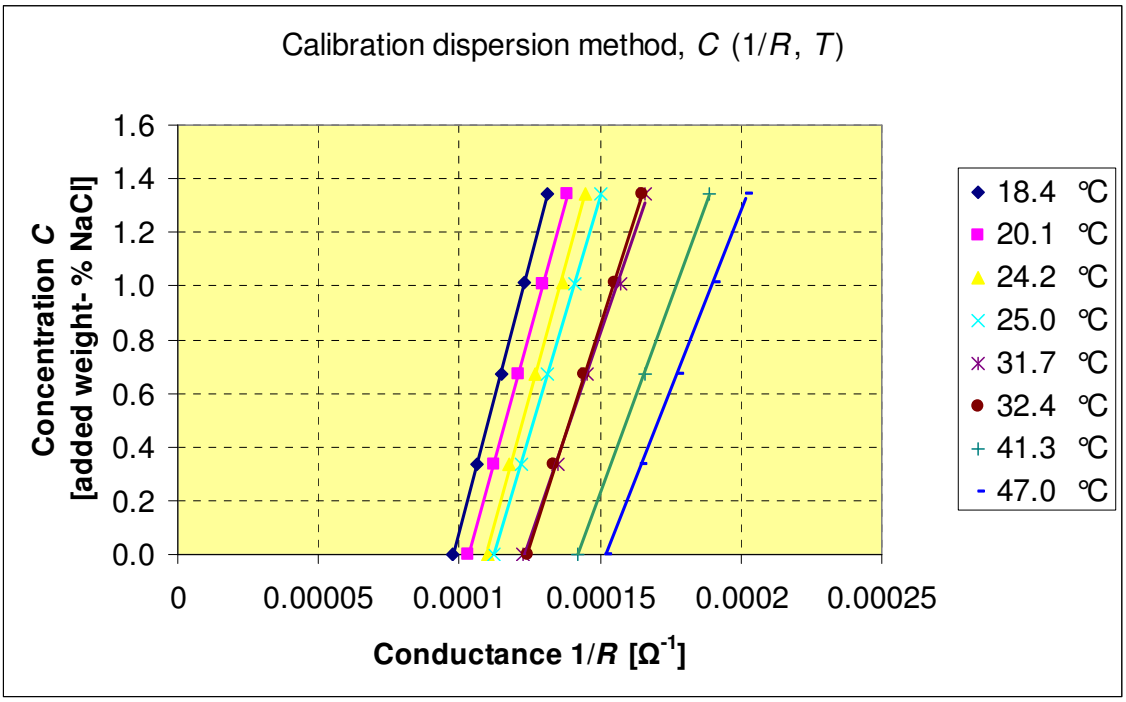

Figure 3.2 – Average conductance measurements for the samples in Tab. 3.1 at eight different temperatures. Linear trendlines have been added to obtain equations on the form $C(R,T) = a \cdot \left(\frac{1}{R}\right) + b$, *where* a *and* b *are temperature-dependent coefficients.*

Table 3.2 – Equations for the trendlines obtained through linear regression in Fig. 3.2.

Trendlines for *C* (*R*, *T*)		
Temperature *T* [°C]	**Trendline equation *C* = *a* · (1/*R*) + *b***	**R^2**
18.44	$C = 40189 \cdot (1/R) - 3.9370$	0.9998
20.10	$C = 38210 \cdot (1/R) - 3.9426$	0.9997
24.19	$C = 38224 \cdot (1/R) - 4.1946$	0.9988
25.04	$C = 35680 \cdot (1/R) - 4.0126$	0.9999
31.68	$C = 30733 \cdot (1/R) - 3.7923$	0.9970
32.36	$C = 32576 \cdot (1/R) - 4.0331$	0.9997
41.33	$C = 28991 \cdot (1/R) - 4.1293$	1.0000
47.04	$C = 26634 \cdot (1/R) - 4.0439$	0.9995

Fig. 3.3 shows the coefficients' dependence on temperature. Even though it is possible to obtain slightly higher R^2 values for high-degree polynomial trendlines for both coefficients, it is simpler and perhaps also more realistic to seek linear solutions. The linear regression for *a* generated $R^2 = 0.94$, which is a rather good match. For *b* the scatter is evident, and this leads to a very low value of R^2, 0.054. As a matter of fact, there are no good arguments that advise against choosing a constant value of *b* instead; however, a linear solution is chosen here.

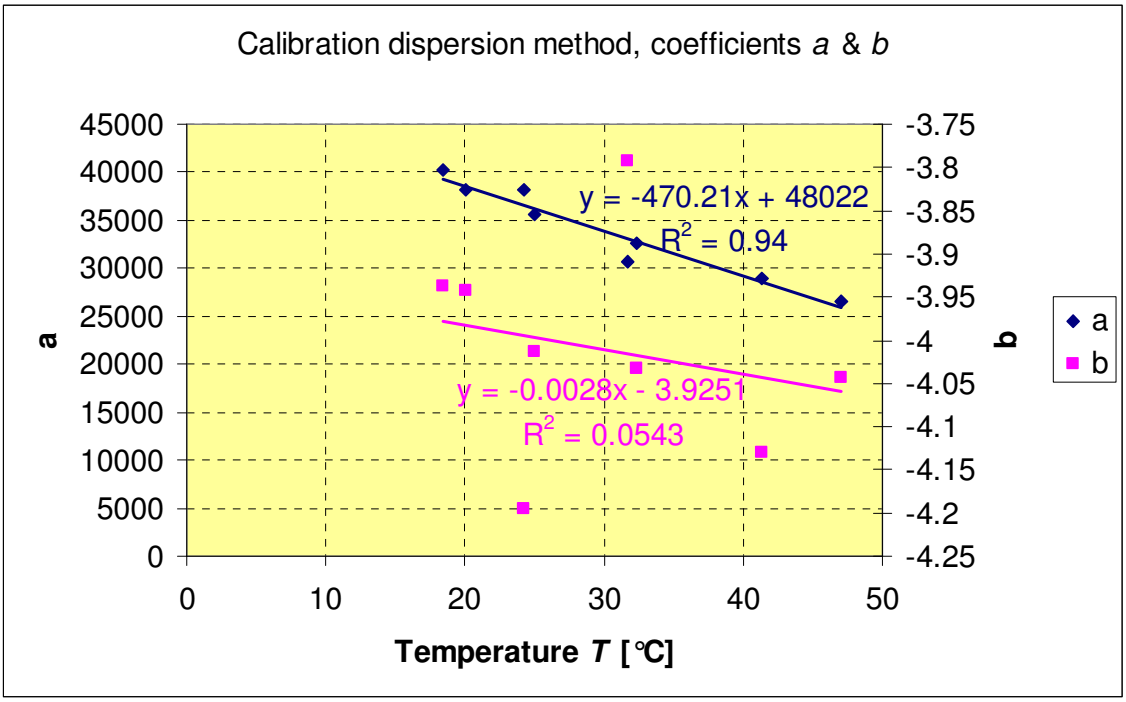

Figure 3.3 – The coefficients found through Fig. 3.2 and Tab. 3.2 plotted as a function of temperature. a *decreases with increasing temperature and linear regression gives a good match. It is difficult to find a trend for the* b *coefficient, since the data are scattered.*

Inserting the two temperature trendlines found (see Fig. 3.3) for the coefficients into the general equation, the final result is:

$$C(R,T) = \frac{(-470.21 \cdot T + 48022)}{R} - 0.0028 \cdot T - 3.9251, \qquad (3.1)$$

where *C* is measured in added weight- % of NaCl to sea water and *R* is measured in Ω. The temperature unit is °C.

Once again, it is important to emphasise that Eq. 3.1 not is a universal solution for calibrations of this kind. Fig. 3.3 shows that conductivity is indeed temperature-dependent, and that it therefore is necessary to measure temperature in order to calculate concentration. If temperature was to be neglected, systematic errors may have occurred due to lower temperature by night than at daytime. Even though this type of error is possible to reduce through comparing tracer injection and the reversed process (i.e. sea water injection, see Fig. 3.4), it is still recommended to always measure temperature.

The uncertainty of concentration calculations based on Eq. 3.1 is hard to determine. Each data point obtained does not only have uncertainty in the measured resistance and temperature; the coefficients in Eq. 3.1 are also uncertain. If concentration, temperature and resistance uncertainties *during calibration* are neglected (as mentioned, these are very small), it is possible to estimate the total concentration uncertainty based on the *least squares method* (see chapter 4.2, Eqs. 4.1a and 4.2a). All the equations given in Tab. 3.2 and in Fig. 3.3 are uncertain, due to the data points not perfectly fitting a linear trendline. Combining this with measurement uncertainty (assumed 0.1 °C and 10 Ω), the total concentration uncertainty for *one data point only* is in the range of 0.05 – 0.06. The uncertainty is somewhat higher for high concentrations, because the electrical resistance is lower (and thus the importance of resistance uncertainty increases).

However, this uncertainty estimation is not adequate for a dispersion profile. Firstly, there is also a time uncertainty, due to pore-volume measurements (discussed later). But more importantly, the shape of a typical dispersion profile affects uncertainty. The following assumptions seem reasonable:

- Categorising the uncertainty as purely ± (0.05) is incorrect; due to the physical laws governing the dispersion process, the concentration of a data point cannot be lower than the concentration point preceding it. The data points are thus not independent.
- Increasing the number of data points reduces the uncertainty of drawing a line through the points. This can be demonstrated by using linear regression for a number of data points; adding more data points reduces uncertainty of the estimated slope (given that R^2 remains constant).
- The uncertainty is most likely *higher* for intermediate concentrations, due to the facts that: (1) the number of data points in this region *pr. concentration* is lower at this steep part of the profile; and (2) the steepness makes the profile less predictable, reducing the dependency between data points. For concentrations near zero or unity the neighbouring data points have very similar concentration values and the uncertainty is consequently lower.

Now that the concentration is expressed through electrical resistance and temperature, it is reasonable to test the equation on some real core samples. The first question that may be asked is whether the injection of tracer is a reversible process when considering concentration changes. This can be checked by injecting SSW when the normalised concentration is 1, i.e. when the electrical resistance equals that of 100 % tracer. Fig. 3.4a illustrates both these processes. To compare the two parts of the profile, the injection of SSW needs to be normalised the opposite way of the tracer injection, so that 100 % SSW equals 1. The two parts can then be plotted on the same time scale and compared as shown in Fig. 3.4b.

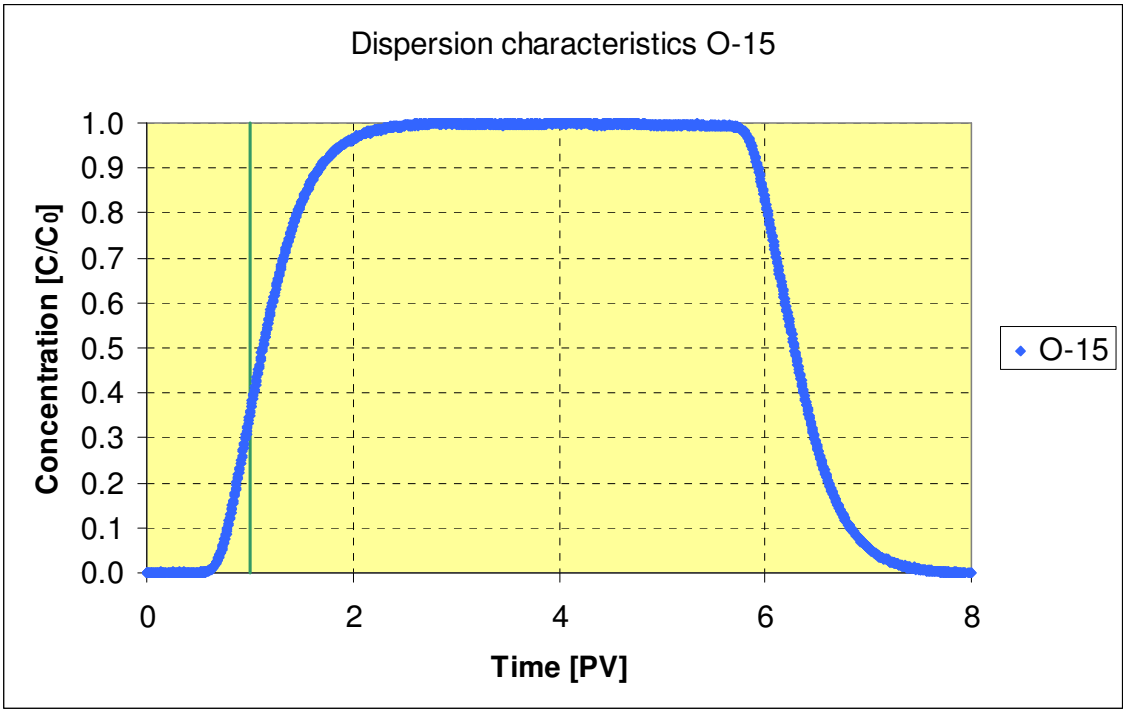

Figure 3.4a – Dispersion test for the core sample O-15 with NaCl (added to SSW) as tracer. Firstly, tracer is injected until C/C_0 *equals 1. Secondly, SSW is injected until* C/C_0 *equals 0.*

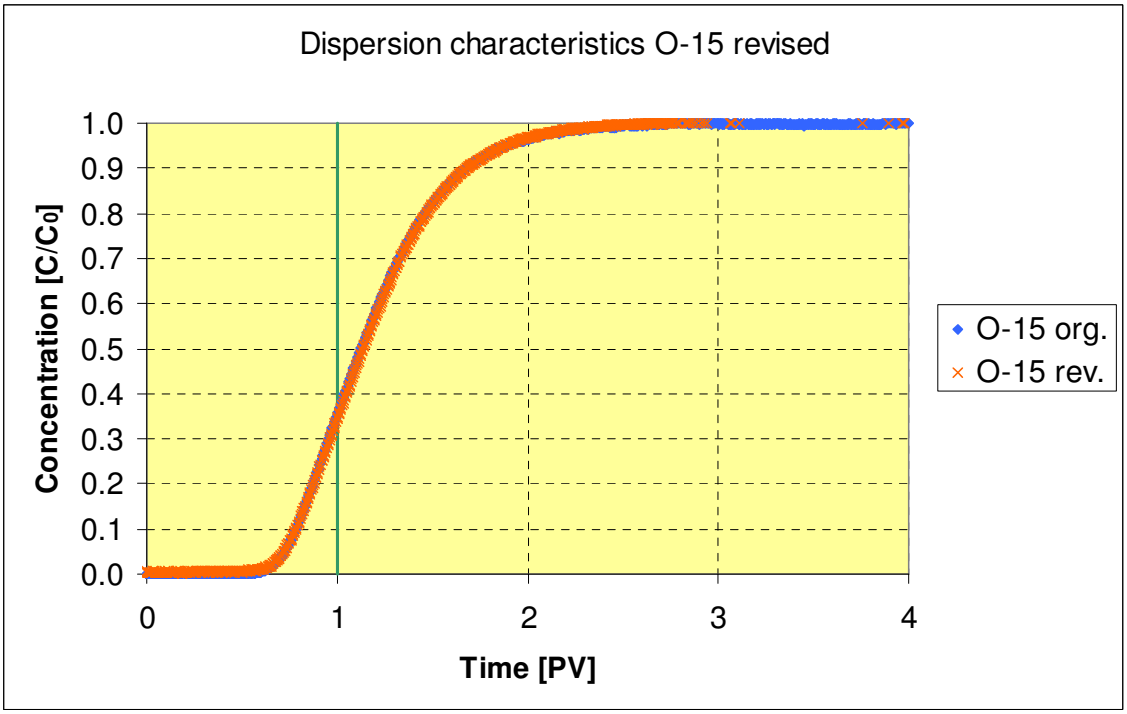

Figure 3.4b – Dispersion test for the core sample O-15. This is the same test as 3.4a, but the SSW injection (represented by orange colour) has been reversely normalised, and is thus comparable to the tracer injection. The two parts overlap completely.

As is apparent from Fig. 3.4b, the tracer injection is a reversible process in terms of concentration profiles. The same procedure was performed for a number of other samples, with the same result. As a result of this, all coming dispersion profiles will only contain the first part of the profile (tracer injection). However, one should bear in mind that *all* tests have undergone this procedure to make sure that the dispersion profile obtained is in fact correct.

Another question that arises is whether this new method is comparable to the two previous methods. Figs. 3.5a and 3.5b show dispersion tests run with the three methods for a low-dispersive core sample (HT-2) and a sample with a more complex pore structure (OS-2).

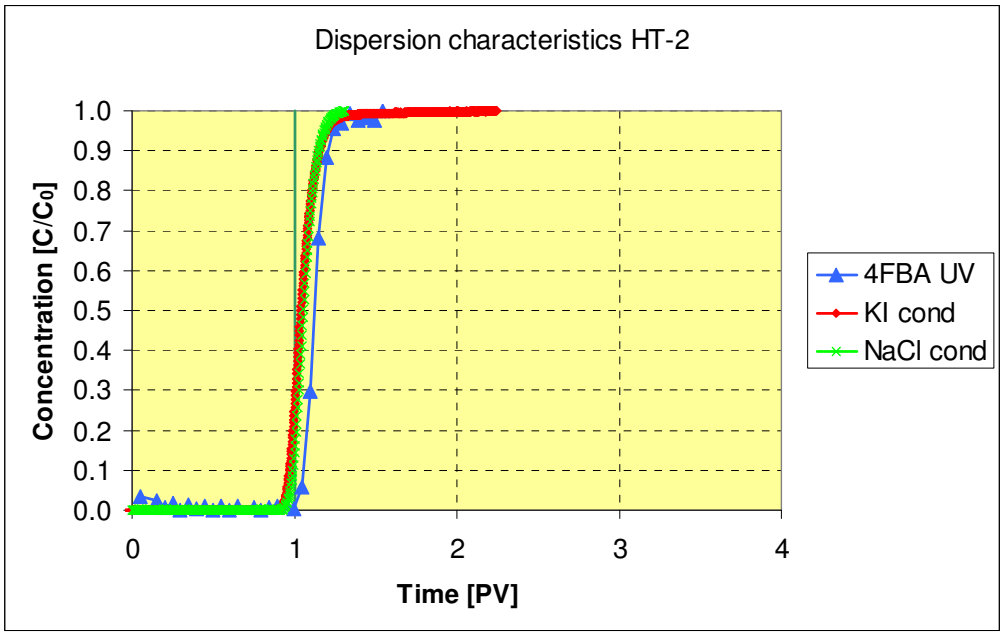

Figure 3.5a – Dispersion tests for HT-2 (Lønøy carbonate pore-type class C-C).

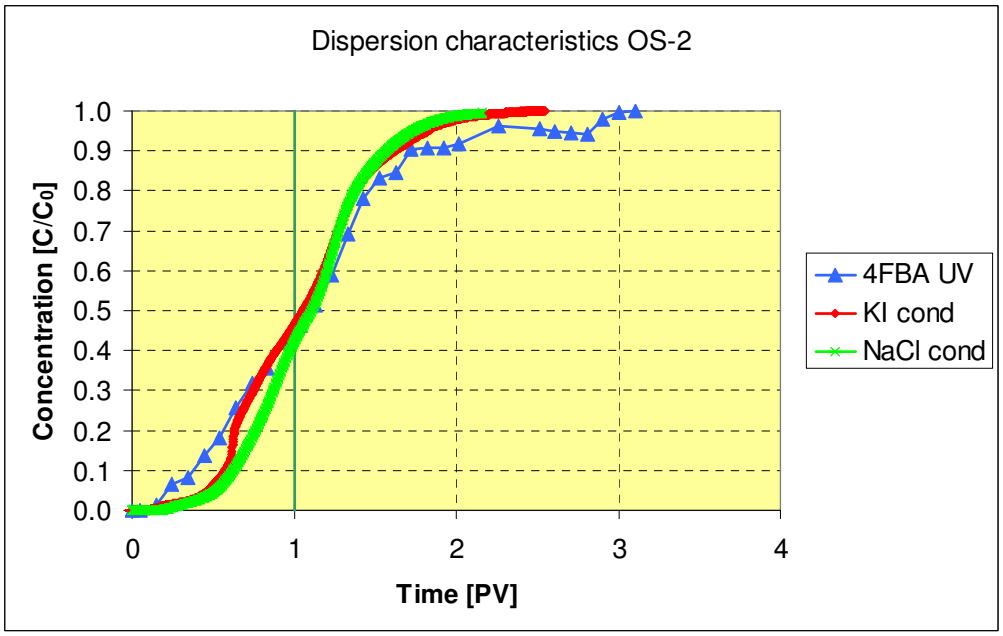

Figure 3.5b – Dispersion tests for OS-2 (C-C).

Starting with HT-2, the conductivity methods overlap completely. As suspected, the 4-FBA UV-spectrometry method is shifted to the right of the other two, indicating that adsorption is taking place. This result was also seen for a couple of other samples.

For OS-2 the adsorption trend is at best dubious. This sample better illustrates another main difference between the methods; as the amount of data is increased significantly for the conductivity methods, they are better suited to describe pore-structure details. The UV-spectrometry profiles often seem jagged and are difficult to interpret, especially for highly dispersive samples.

Even though the NaCl conductivity method looks promising, there is still an unsolved problem that can be seen on Figs. 3.4 and 3.5; a normalised concentration of 0.5 corresponds to a pore volume *greater* than 1. Physically, this is hard to explain (see chapter 2.3.2) if there is no adsorption, which surely does not happen for the NaCl tracer. Hence the explanation is likely to be related to pore-volume measurements; if the pore volume that is measured is too low this will cause the dispersion profile to shift to the right. The reason could also be erroneous measurements of tubing, valves, etc. As these unphysical profiles have no mathematical simulation solution, they will have to be shifted towards the left prior to simulation. This is not a straightforward process, and will be discussed in more detail in chapter 3.3.

A subject that has been left undiscussed is the influence of the flow rate. There are several issues that are of interest:

1. As the velocity decreases, diffusion will become more and more dominant, serving the same purpose as an increased M. The effect this has on the dispersion profile can be studied in Fig. 2.9.
2. If the velocity is sufficiently high, turbulent flow will dominate. The different flow pattern will almost certainly affect dispersion. The transition from laminar flow to turbulent flow is related to the Reynolds number, as discussed in chapter 2.3.2.

In order to minimise these problems, the same interstitial velocity was used for all core samples that underwent dispersion tests. This also makes the results more comparable. An exception was made for very low-permeable samples in order to avoid high pressure drops. Still, all Reynolds numbers were in the region of 0 – 1. This is high enough to avoid diffusion-dominated flow; as discussed in chapter 2.3.2 this limit corresponded to a Reynolds number in the region of 10^{-2} to 10^{-4} or a flow rate of $3.5 \cdot 10^{-5}$ cm/s. It is also well below the transition zone from laminar to turbulent flow, which has been reported to be at $N_{Re} = 10$ at the lowest. The flow rate effect is an interesting topic that definitely affects dispersion analysis; this is why the phenomenon has been separately studied on a selection of core samples in this thesis. The results are discussed in chapters 5.1 and 6.

3.3 Simulation of dispersion tests

The simulation tool used for dispersion tests in this thesis is the program UTCHEM (v. 9.0). The software is developed at the University of Texas at Austin (Texas, USA), and is a three-dimensional chemical flood simulator. UTCHEM is a powerful simulator which covers a wide range of topics, such as surfactant systems and polymer systems. Ample physical and chemical phenomena are also examinable, for instance relative permeability, capillary pressure, interfacial tension, ion exchange and phase behaviour, as well as diffusion and dispersion. The scope here, however, will be only that of one-dimensional (longitudinal) dispersion in a porous medium fully saturated with only one fluid.

The underlying model for the simulation software is a generalised version of Coats and Smith's model presented in chapter 2.3.2. The porous media is divided into N cells with fixed length and cross-sectional area; these input parameters are simply calculated from the measured length and diameter of the core sample in question. Mixing throughout the cells is then mathematically solved in a numerical approach, resulting in normalised concentration profiles as shown in Figs. 2.7 – 2.9. Entering the correct porosity value for the sample makes it possible to calculate the pore volume, and use this as the time unit (see Eq. 2.10).

The general objective of the simulation is to find a combination of dispersivity (α), flowing fraction (f) and mass transfer coefficient (M) that matches the experimental dispersion profile in the best possible way. This is not always straightforward; as discussed in chapter 2.3.2, the model has a tendency of generating multiple solutions when f is high. In addition to this, some pore systems have dead-end pores that barely contribute to fluid flow, and even to diffusion. These pores can be considered *inaccessible*, and will cause a leftwards shift in the dispersion profile. This shift can be applied manually *after* the simulation process. It is important to distinguish between isolated pores that arise due to completely disconnected pores and inaccessible pores that occur due to fluid flow (which is the matter here); in this case the pores are possible to saturate with water or gas during porosity measurements, and thus they will contribute to the pore volume. The transition between dead-end pores and inaccessible pores should be considered gradual rather than sharp. Therefore shifting the profile should be performed with care. If adsorption and/or inaccurate pore volume is suspected, this will also cause the profile to shift; hence, the inaccessible fraction applied to match the profile is in fact a combination of all these factors, and should be treated with an amount of scepticism.

There are several practical approaches for obtaining a good match between simulated data and experimental data. The best way of illustrating the procedure is perhaps by using an example; the following steps are performed when simulating the core sample O-38. Note that all data series are represented as lines rather than data points when plotted; this is justifiable because the data points are so close to each other.

- Step 1: Study the experimental profile and determine the degree of dispersivity.

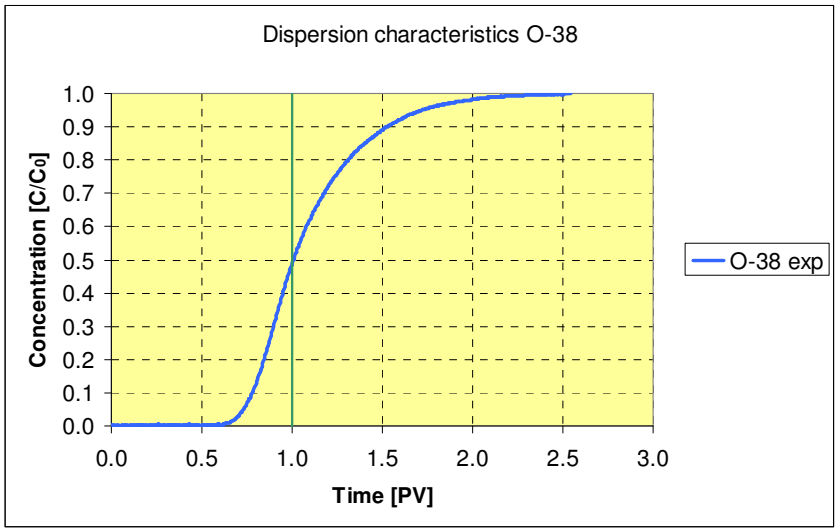

Figure 3.6a – Experimental dispersion profile, O-38.

Fig. 3.6a indicates that this is an intermediate dispersive sample. Dispersive behaviour can be either due to high dispersivity or due to a high fraction of dead-end pores. The concentration at 1 PV is close to 0.5, so a low amount of inaccessible pores is likely.

- Step 2: Try a set of parameters that, based on experience from previous samples, might fit the experimental profile.

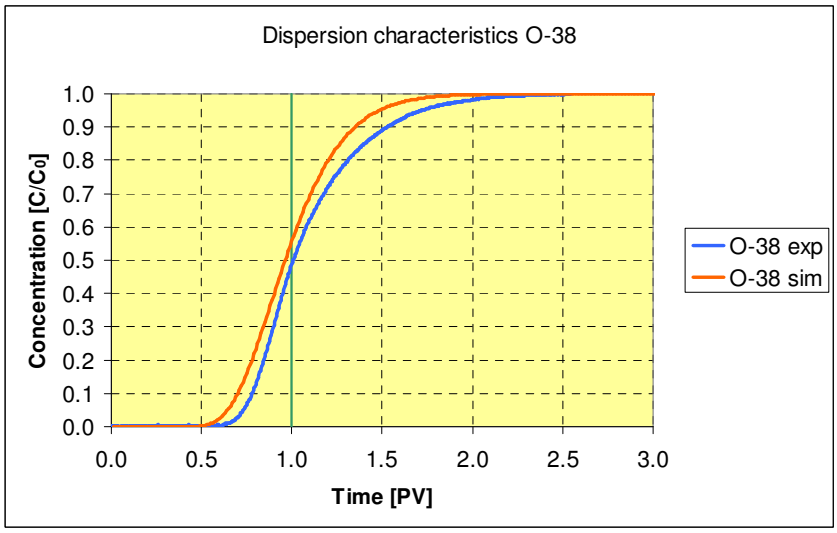

Figure 3.6b – Simulation run , O-38. M = *0.0005* s^{-1}, f = *0.8,* α = *0.10 cm and the fraction of inaccessible pores is* $\varphi_I/\varphi_t = 0$.

The experimental profile has a higher degree of asymmetry than the simulated profile. A better match may be obtained by increasing the amount of dead-end pores as well as lowering the dispersivity to match the first part of the profile better.

❖ Step 3: Emphasise matching the degree of asymmetry; try to use the values of *f* and *α* to make the simulated profile agree with the experimental profile.

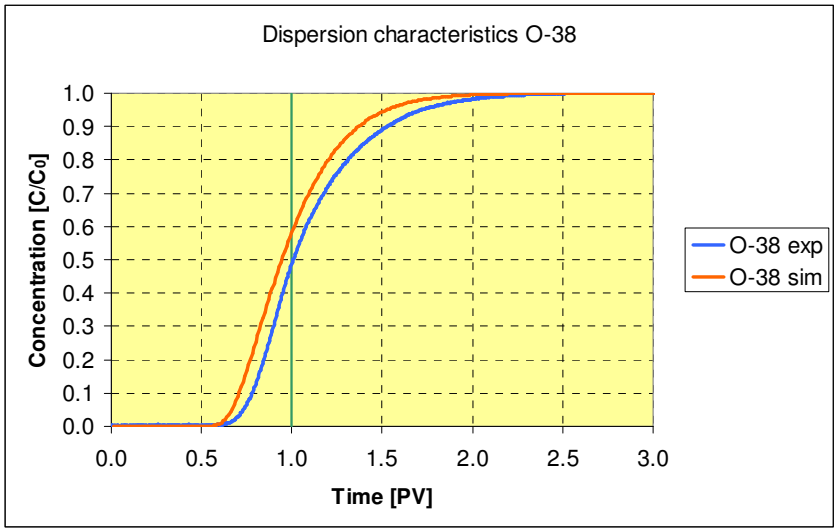

Figure 3.6c – Simulation run 2 for O-38. M = *0.0005* s^{-1}, f = *0.72,* α = *0.03 cm and* φ_I/φ_t = *0.*

The asymmetry of the profiles is now more or less equal. However, the simulated profile is still shifted to the left of the experimental profile, indicating erroneous pore volume or adsorption present in the experimental dispersion test.

❖ Step 4: Shift the simulated profile left or right to overlap the experimental profile.

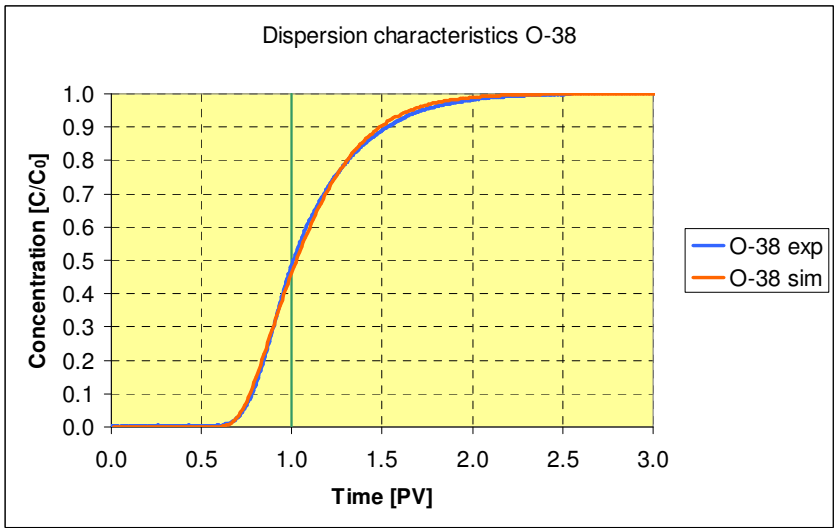

Figure 3.6d – Simulation run 3 for O-38. M = *0.0005* s^{-1}, f = *0.72,* α = *0.03 cm and* φ_I/φ_t = *-0.085. This is the best match obtainable within reason.*

The profiles now nearly overlap completely. As discussed earlier, the fraction of inaccessible pores obtained from simulation is often physically incorrect. In the case of O-38 the inaccessible fraction is negative, which is certainly impossible. The result here instead indicates that the measured pore volume is too low or that adsorption has taken place. For samples that have a significant amount of inaccessible pores, step 4 will more likely comprise shifting the simulated profile to the *left*.

There are mainly two parameters that complicate the simulation process with UTCHEM. The mass transfer coefficient is perhaps the most important. As discussed in chapter 2.3.2, M clearly affects the dispersion profile (see Fig. 2.9). Thus, varying this constant during simulations should be equally important as varying flowing fraction, inaccessible fraction and dispersivity. However, it is very difficult to estimate the value of the constant due to its dependence on pore geometry. Therefore it is often considered more or less constant (as the results show) and less emphasised than the other parameters. Still, it is necessary to adjust the M value for a small number of core samples; these are heterogeneous samples that are practically impossible to match using only f and α. In addition to the dependence on pore geometry, Jasti et al. (1988) suggested that the mass transfer coefficient was only independent of velocity if $N_{Pe} < 100$ (i.e. when diffusion is noteworthy). Peclet numbers for all samples that have gone through dispersion tests in the thesis are given in Appendix 2; most Peclet numbers are *above* 100, which indicate that velocity affects the mass transfer coefficient to some degree.

The other parameter that causes difficulties during simulation is the number of cells. Due to the numerical dispersion phenomenon dispersion profiles may shift significantly if the number is altered; this also influences the dispersivity. For all samples inn this thesis a cell number of 100 was chosen, but there is no guarantee that this number is the most appropriate to use.

3.4 Measuring absolute permeability

Absolute permeability is perhaps the most important parameter in relation to fluid flow in reservoirs. It is a rock property describing the ease of fluid flow through the porous media, and depends mostly on pore-throat size, tortuosity and porosity. Even though absolute permeability is in fact a tensor, it is often treated as a one-dimensional parameter when measured in laboratory experiments. Darcy's law is the fundamental equation for fluid flow in porous media;

$$Q = -\frac{KA}{\mu}\frac{dp}{dx}, \tag{3.2a}$$

where Q is flow rate, K absolute permeability, A cross-sectional area, μ viscosity and dp/dx the pressure gradient. If dp/dx is considered constant over a core sample, Eq. 3.2a can be rewritten as

$$Q = \frac{KA}{\mu}\frac{\Delta p}{L}, \tag{3.2b}$$

where Δp is the pressure drop across the core sample and L its length. This form of Darcy's

law is applied in laboratory measurements; A and L are found through core geometry measurements and μ is known (or can be measured); hence K is obtained when pressure drop and flow rate are measured. Darcy's law is only valid under the following conditions:

1. Laminar flow. When the flow is laminar, fluid layers will slide on top of each other and no turbulence is observed. As described in chapter 2.3.2, the Reynolds number defines the existing flow regime. The flow should also be time-independent.
2. The pore volume must be 100 % saturated with only one fluid.
3. No reactions can occur between fluid and rock. Common reactions include clay hydration, mineral dissolution and fines migration.
4. The flow direction (dip angle) cannot be altered; this would cause gravity forces to change (gravity is neglected in Eqs. 3.2a and 3.2b).
5. Incompressible fluid.

Both gases and non-reactive liquids are widely used to measure absolute permeability. When using gases, however, Darcy's law needs to be modified due to the different flow pattern and compressibility of gases. Fig. 3.7 illustrates the apparatus used for laboratory absolute permeability measurements, where only watery solutions are considered.

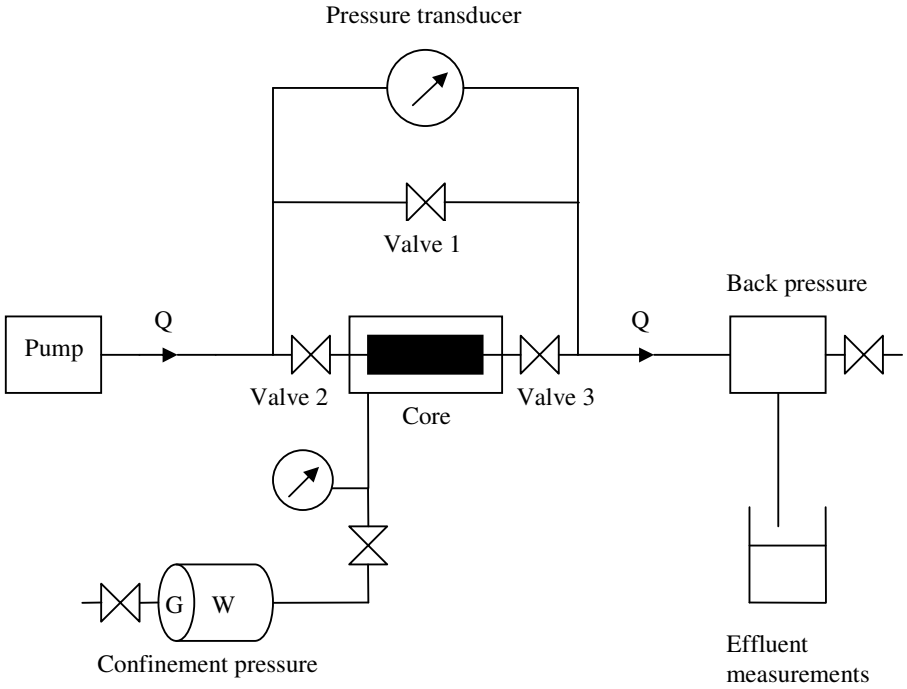

Figure 3.7 – Sketch of apparatus used to measure absolute permeability. Pay special attention to the confinement pressure mechanism, the valve system and the back pressure, all which are incorporated to diminish uncertainty.

The pump should always deliver a steady flow rate, so that the pressure drop is constant when steady-state flow has developed. Even though all pumps allow a fixed flow rate to be set, one should always verify the rate by measuring effluent mass difference. After all, it is a very simple procedure when the liquid density is known at the given temperature.

Confinement pressure can to some extent influence the permeability measurements, especially for core samples that have not previously been exposed to high pressure. Sufficiently high confinement pressure could squeeze the core, leading to tighter pore throats and consequently lower absolute permeability. For this reason, a constant confinement pressure is preferable. This can be obtained by the apparatus illustrated in Fig. 3.7; the expanding nature of the gas will ensure that water is kept in the core holder at a constant pressure.

Another uncertain factor which might arise is the presence of air in the tubing system. This will cause a discontinuity in the liquid phase, and thus influence the measured pressure drop. The possibility of air bubbles is reduced when applying a back pressure as shown in Fig. 3.7.

When investigating the effect of ion concentration and composition on absolute permeability, it is necessary to exchange the injection water frequently. Due to the formation of concentration gradients, diffusion is likely to occur. Hence, it is important to displace the previous solution completely with the new solution. This is where the valve system and the bypass possibility come in handy; the following steps are used to minimise diffusion effects:

1. Close valve 2 and valve 3 (see Fig. 3.7) to preserve the core.
2. Disconnect the pump and change the solvent used. This procedure should be repeated once, to ensure that the pump solvent is of the concentration and composition that is wanted.
3. Connect the pump and open valve 1 (see Fig. 3.7). Displacing the previous solution in the bypass system is necessary to avoid diffusion from this area later on.
4. Close valve 1 and open valves 2 and 3. Pre-flood the core for a number of pore volumes that is ample to displace all leftovers of previous solutions. For high-dispersive samples this amount could be as high as 5 – 6 pore volumes. This operation is performed in order to obtain equilibrium with the new solution, and also makes sure that the effluent density is correct when measuring the flow rate.

Even if all the above precautions are recognised, the permeability measurements are still not necessarily accurate. Although pressure transducers should be calibrated on beforehand, there is still the possibility of an offset (zero flow rate does not generate zero pressure drop) in the pressure measurements. Therefore, it is common practice to carry out a series of permeability measurements, applying four or five different flow rates rather than a single rate. The average absolute permeability is then found by means of linear regression in a plot of pressure drop vs. flow rate. The R^2 value gives an indication of the accuracy of the regression.

The final and leading uncertain factor is the temperature. Density of liquids is only slightly dependent on temperature, if the variations are within range of normal room temperature. Consequently, its influence on flow rates measured by mass differences is small. However, liquid viscosity is more noticeably dependent on temperature. Fig. 3.8 shows viscosity of clean water as a function of temperatures between 15 °C and 30 °C. It is seen that a room temperature increase of about 1 °C leads to a decrease in water viscosity by a factor of 1.02 to 1.03; this can be significant when detecting only small permeability variations.

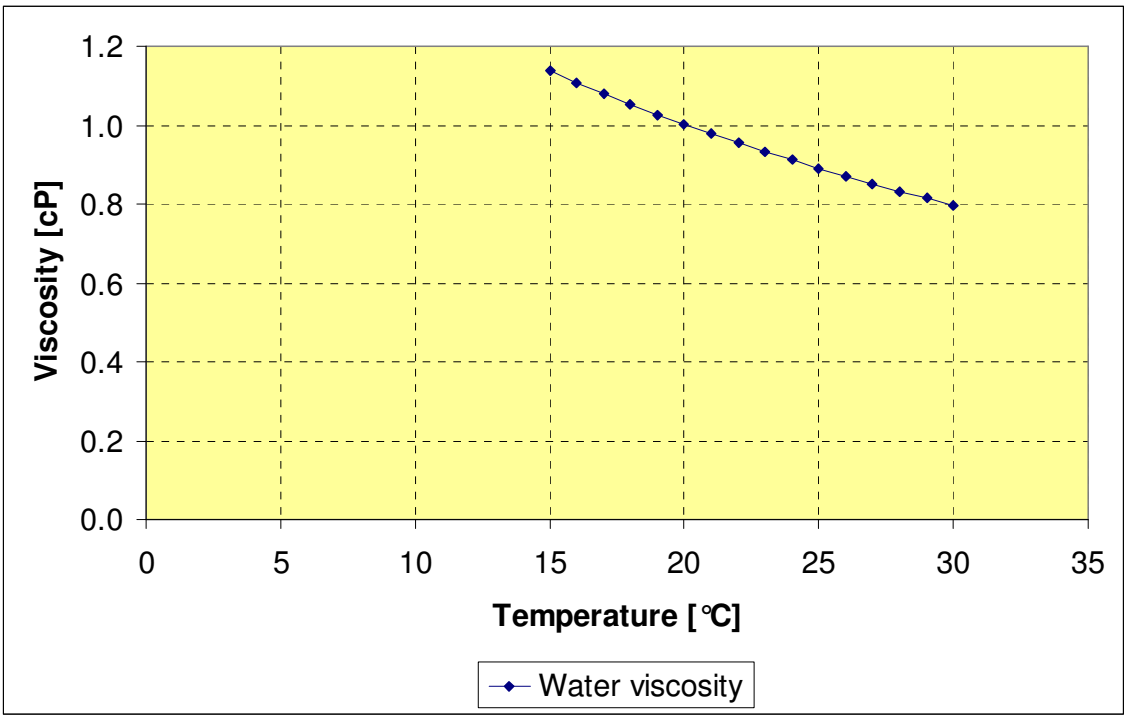

Figure 3.8 – Water viscosity as a function of temperature in a sweeping range of room temperatures. The change in viscosity when temperature fluctuates with 1 – 2 °C should clearly be taken into account when permeability variations amount to only a few percent.

Chapter 4: Salinity vs. permeability in carbonates

4.1 Procedure and uncertain factors

This chapter brings up the issue discussed in chapter 2.5; does brine salinity affect absolute permeability in carbonates in any way? To examine this, two carbonate core samples have undergone a specially designed program where both ion concentration and ion type are varied. One of these cores, *O-14*, was a reservoir sample from the Barents Sea identified as intercrystalline mesopores with a patchy porosity distribution; the other, *D-1*, was a Dania outcrop core sample. Dania samples originate from an open-cast mine close to Aalborg, Denmark, and are commonly recognised as pure dolomite material ($CaCO_3$).

Absolute permeability was measured using Darcy's law and the experimental setup illustrated in Fig. 3.7. Maximum Reynolds numbers were approximately 11 for O-14 and 0.3 for D-1, so the condition of laminar flow was fulfilled. Both cores were cleaned and dried, prior to a standard water saturation process (release of water into vacuum). To ensure that no air was present in the cores, they were also flooded thoroughly; this should fulfil the condition of 100 % saturation of a single fluid. The flow was horisontal, as showed in Fig. 3.7.

The concerns raised in chapter 3.4 are all taken into account for the laboratory tests:

- Flow rate is measured by means of effluent weight.
- Confinement pressure is kept constant as illustrated in Fig. 3.7.
- Back pressure (5 bar) is applied to avoid air bubbles (see Fig. 3.7).
- The four-step procedure described in chapter 3.4 is followed when exchanging injection water. As pre-flush treatment, approximately 5 PV's was injected into O-14; based on dispersion characteristics this should be more than enough to eliminate any concentration gradients. D-1 was pre-flushed with roughly 2.5 PV's.
- Viscosity and density were both calculated (based on correlations) for all solutions used. The pre-flush treatment ensures that these parameters are always correct.

Temperature measurements were not available for the data series. However, temperature was measured over a period of two days, and found to vary between 20.5 °C and 21.5 °C. This is taken into account when estimating viscosity uncertainty (based on Fig. 3.8).

Tab. 4.1 shows the program both cores underwent. The separate parts were performed in the same order for both cores; firstly the $CaCl_2$ solutions, followed by distilled water; next the mixtures of $CaCl_2$ and NaCl and subsequently the NaCl solutions. Finally the permeability was measured using distilled water again. The two measurements using no salt were meant to examine (1) if the shock effect (permeability drops abruptly for sandstones when injecting fresh water with certain ion types present) is applicable for carbonates as well, and (2) if possible dissolution is affected by ion type. For each part (such as the part using $CaCl_2$ solutions) the measurements were performed in a loop concentration-wise; concentration was first decreased until the lowest concentration, and then increased again. In Tab. 4.1, the starting concentrations are marked 1; 5 indicates the lowest concentration. For the mixtures of NaCl and $CaCl_2$, the total concentration was kept constant at 5 weight- %.

Table 4.1 – Program for absolute permeability measurements for the two carbonate core samples O-14 and D-1. Ca^{2+} represents divalent ions, while Na^{+} represents monovalent ions. Measurements with fresh water are added to check whether possible permeability changes are dependent on the ion type already present in the pore system. Each main part starts and ends at the highest concentration (1). Concentration is measured in weight- %, i.e. the starting concentration for Ca^{2+} is 5 weight- % $CaCl_2$. For the mixtures of Ca^{2+} and Na^{+}, the total concentration is always 5 weight- % salt; the values given in the table are instead the $CaCl_2$-to-NaCl ratio.

Permeability program					
Ions present in water	**Hysteresis program [weight- %]**				
	1	**2**	**3**	**4**	**5**
Ca^{2+} [$CaCl_2$]	5.0	4.0	2.0	1.0	0.5
None [fresh water]			N.A.		
Ca^{2+} and Na^{+} [$CaCl_2$: NaCl]	1:0	5:1	1:1	1:5	0:1
Na^{+} [NaCl]	5.0	4.0	2.0	1.0	0.5
None [fresh water]			N.A.		

Relevant core data are given in Tab. 4.2. One should take notice of the porosity measurements before the first- and after the last permeability measurement; the porosity for O-14 has increased significantly, a trend that is not as clearly seen for D-1. This fact will be discussed more in chapters 4.2 and 6.

Table 4.2 – Core data for the samples O-14 and D-1. Four flow rates are used to calculate absolute permeability (see chapter 3.4 for discussion on this topic). Since D-1 has a much lower permeability the flow rates are also lower, to avoid too high pressure drops. Measurements of dry- and saturated weights are included to demonstrate that these data indeed change during such a long series of measurements. Viscosity and density data for all solutions given in Tab. 4.1 are calculated using correlations.

Core data		
Parameter	**O-14**	**D-1**
Absolute permeability K [mD] [earlier measurement]	2.77	N.A.
Length L [cm]	4.84	4.92
Cross-sectional area A [cm^2]	11.16	11.34
Flow rates Q [cm^3/h]	160, 120, 80, 40	8, 6, 4, 2
Before first measurement [5 % $CaCl_2$]:		
Dry weight [g]	127.63	102.81
Saturated weight [g]	136.52	120.01
Porosity φ	0.158	0.296
After last measurement [fresh water]:		
Dry weight [g]	121.30	102.13
Saturated weight [g]	133.19	119.40
Porosity φ	0.220	0.310

4.2 Results

Quantifiable uncertainty factors during the absolute permeability measurements include core length and diameter, flow rate and pressure drop. However, viscosity is probably the leading factor, as it varies with room temperature fluctuations. Fig. 3.8 provides data sufficient for a rough estimation of viscosity uncertainty; if the room temperature ranges from 20 °C to 22 °C water viscosity can be expected to vary between 1.00 cP and 0.95 cP. Hence, it is reasonable to assume that viscosity uncertainty is 0.05 cP at the most. The linear regression type used for each data set (four measurements of pressure drops at different flow rates) is a modification of the well-known *least squares method*; normally this method does not allow for each data point to have an individual uncertainty. A brief evaluation of uncertain factors shows that flow rate uncertainty is neglectable. Therefore it is sufficient to include pressure drop (*y* direction) uncertainty; this is not a very complicated adaptation. It can be shown that the estimated slope ($\hat{a}$) and its standard deviation ($s_{\hat{a}}$) are then given by the following equations:

$$\hat{a} = \frac{\sum_{i=1}^{n} \frac{1}{(\Delta dp_i)^2} \cdot \sum_{i=1}^{n} \frac{Q_i dp_i}{(\Delta dp_i)^2} - \sum_{i=1}^{n} \frac{Q_i}{(\Delta dp_i)^2} \cdot \sum_{i=1}^{n} \frac{dp_i}{(\Delta dp_i)^2}}{\sum_{i=1}^{n} \frac{1}{(\Delta dp_i)^2} \cdot \sum_{i=1}^{n} \frac{(Q_i)^2}{(\Delta dp_i)^2} - \left(\sum_{i=1}^{n} \frac{Q_i}{(\Delta dp_i)^2} \right)^2}, \tag{4.1a}$$

$$s_{\hat{a}} = \sqrt{\frac{\sum_{i=1}^{n} \frac{1}{(\Delta dp_i)^2}}{\sum_{i=1}^{n} \frac{1}{(\Delta dp_i)^2} \cdot \sum_{i=1}^{n} \frac{(Q_i)^2}{(\Delta dp_i)^2} - \left(\sum_{i=1}^{n} \frac{Q_i}{(\Delta dp_i)^2} \right)^2}}. \tag{4.1b}$$

Q_i and dp_i denote flow rate and pressure drop, respectively, for an *individual* measurement. Pressure drop uncertainty is termed Δdp_i and n denotes the number of individual measurements in a sequence (in this case four).

The estimated slope is inserted into Darcy's law (see Eq. 3.2b) in order to calculate the permeability;

$$K = \frac{\mu \cdot L}{\hat{a} \cdot A}. \tag{4.2}$$

Since all the uncorrelated parameters needed to calculate the permeability for a series are of first order, and are written as a product, the total uncertainty for the permeability is

$$\frac{\Delta K}{K} = \sqrt{\left(\frac{\Delta \mu}{\mu}\right)^2 + \left(\frac{\Delta L}{L}\right)^2 + \left(\frac{s_{\hat{a}}}{\hat{a}}\right)^2 + \left(\frac{\Delta A}{A}\right)^2}. \tag{4.3}$$

Using Eqs. 4.1 – 4.3, the estimated permeability uncertainty for D-1 is ca. 0.0007 mD (more or less constant). For O-14, permeability increase leads to an increase in uncertainty; the lowest uncertainty value is ca. 0.02 mD and the highest 0.4 mD.

Figs. 4.1a, 4.1b and 4.1c show the results for O-14, the reservoir core sample. Uncertainty intervals based on Eqs. 4.1 – 4.3 are also included, but for most data points (Figs. 4.1a and 4.1b) they are actually too small to be visible.

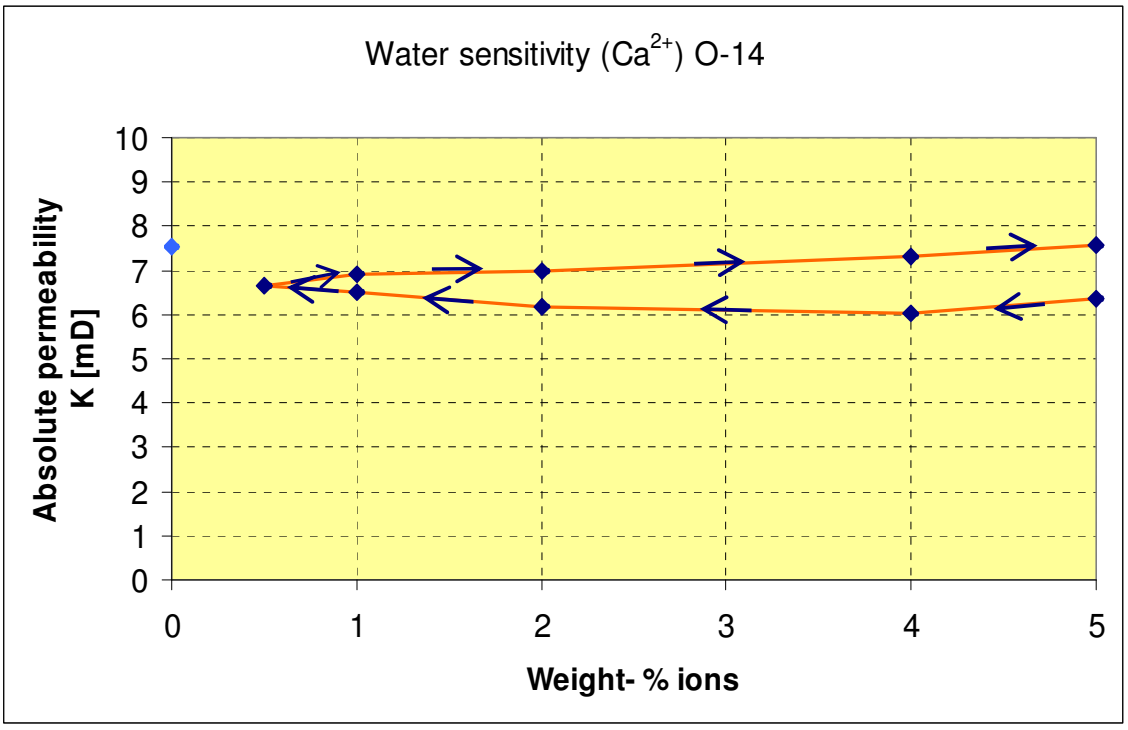

(a) Absolute permeability of O-14, as function of Ca^{2+} content.

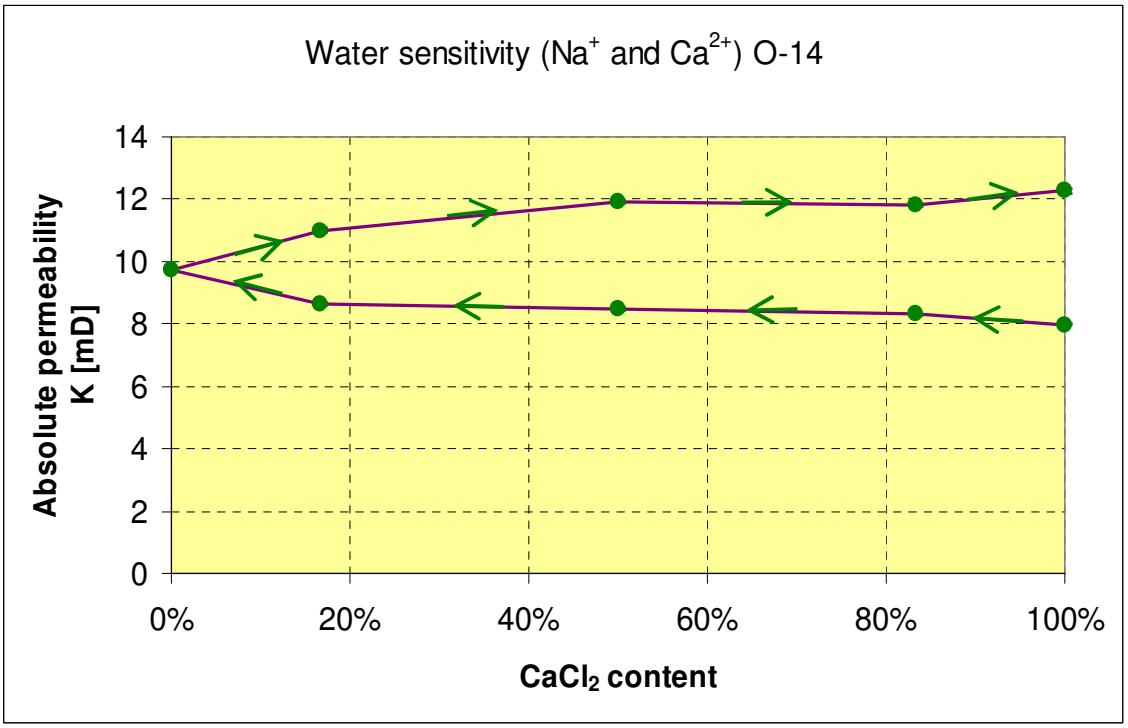

(b) Absolute permeability of O-14, as function of Na^{+} and Ca^{2+} content.

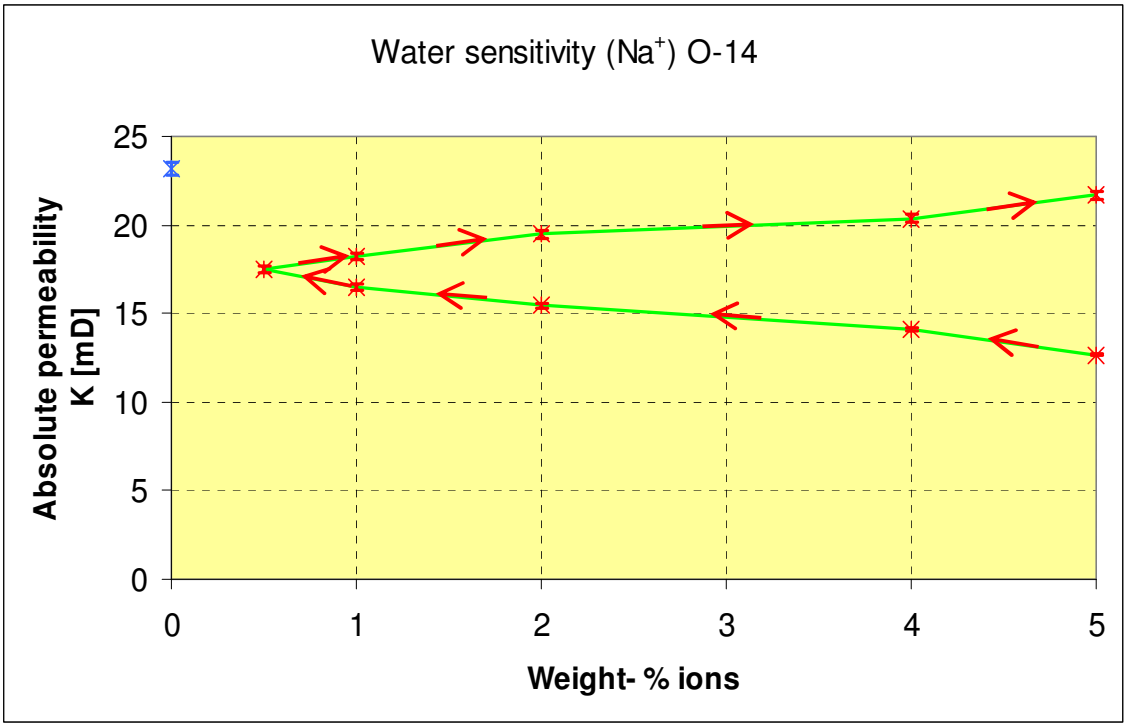

(c) Absolute permeability of O-14, as function of Na^+ content.

Figure 4.1 – The effect of salinity and ion type on absolute permeability for the reservoir core sample O-14. The light blue marks in (a) and (c) indicate fresh-water measurements run after the initial concentration loop. A continuous increase in permeability is observed, irrespective of concentration and ion type. However, the increase is higher for Na^+ than for Ca^{2+}.

Figs. 4.2a, 4.2b and 4.2c show the results for D-1. As for O-14, the uncertainty intervals are too small to be visible on the charts. For practical purposes they are neglectable.

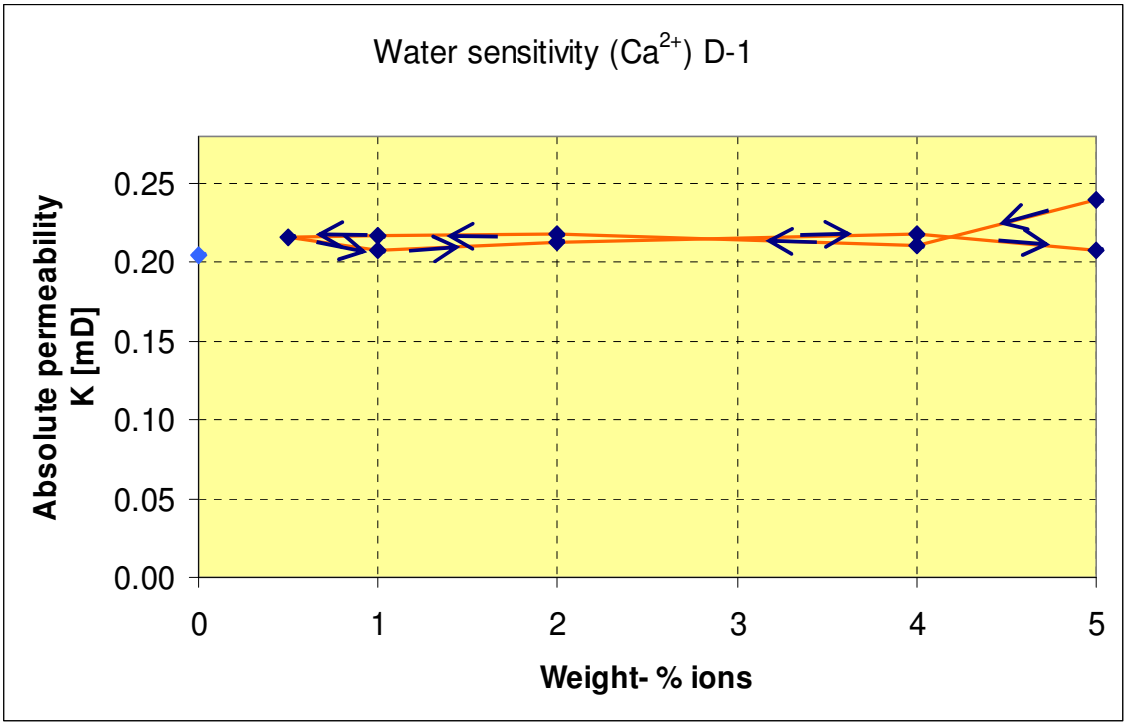

(a) Absolute permeability of D-1, as function of Ca^{2+} content.

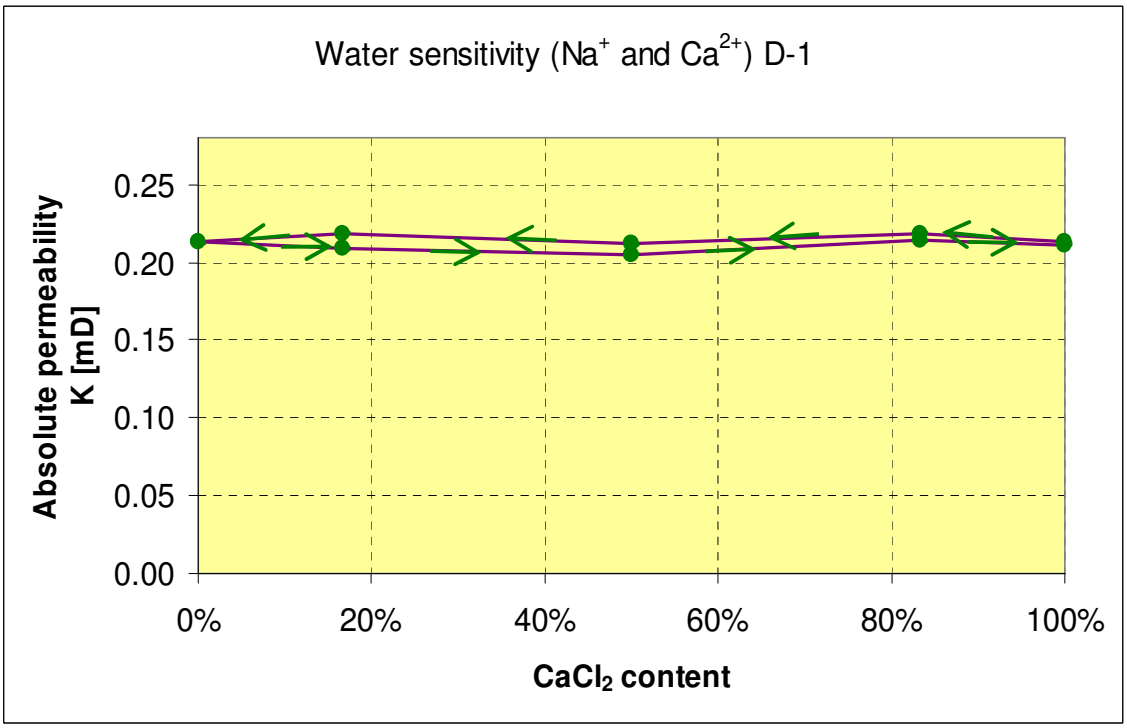

(b) Absolute permeability of D-1, as function of Na^{+} and Ca^{2+} content.

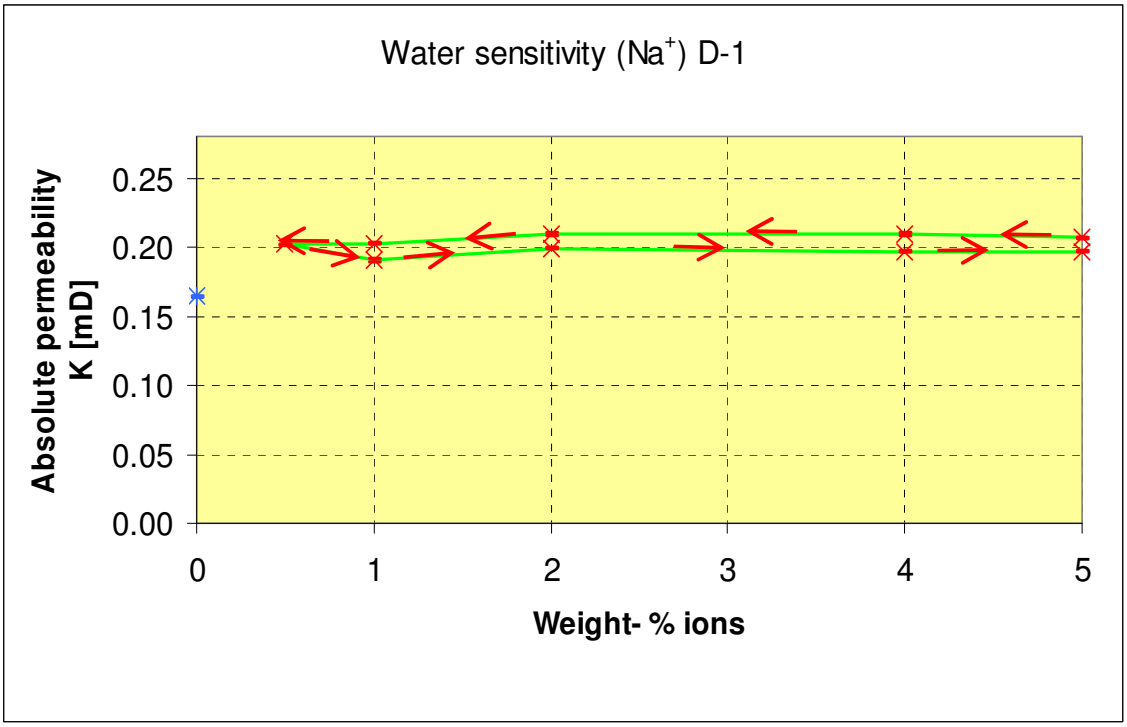

(c) Absolute permeability of D-1, as function of Na^+ content.

Figure 4.2 – The effect of salinity and ion type on absolute permeability for D-1. The light blue marks in (a) and (c) indicate fresh water-measurements run after the initial concentration loop. It is difficult to notice clear trends, but generally the permeability seems to be slightly higher when concentration (or $CaCl_2$ content in (b)) is decreasing.

The results seen in Figs. 4.1 and 4.2 and Tab. 4.2 will be thoroughly interpreted in chapter 6. A glance at these figures reveals that the broad outlines are rather easily found;

- The permeability of O-14 is continuously increasing. Dry weight measurements prior to- and after the measurement series suggest that the cause is dissolution. Even though this is evident, the results should still be analysed in detail. Several issues are of interest; (1) why is there apparently a more significant increase in permeability for Na^+ than for Ca^{2+}? (2) What effect does fresh water have on the increase?
- The permeability of D-1 is more or less constant. Even so, the permeability is observed to be somewhat higher for *decreasing* concentration than for increasing concentration. This trend is also seen for the combination of Na^+ and Ca^{2+}.
- The introduction of fresh water seems to have no immediate effect on the permeability of O-14. For D-1, the permeability decreases a little when Ca^{2+} was present in the core sample. This decrease is also observed when the brine contained Na^+; in fact the permeability drop is over ten times the drop observed for Ca^{2+}. Could this be the same effect that has been found for sandstones (see chapter 2.5)?

Chapter 5: Dispersion and water floods in carbonates

5.1 Effect of flow rate

Since the interplay between diffusion and dispersion is dependent on velocity, it is evident that the flow rate affects dispersion characteristics. As discussed in chapter 2.3.2 (see Fig. 2.9) the skewness of the dispersion profile is expected to increase when the *rate group* (X_m) increases. Also, turbulent flow will occur at sufficiently high flow rates, altering the dispersive behaviour of the core sample. These two issues (raised in chapter 3.2 concerning flow rates) motivate a study of flow rate effects; the question is whether changes on dispersion profiles can be observed within a reasonable range of laboratory flow rates.

To test this out, three carbonate core samples from different pore classes were selected. In addition to the standard interstitial velocity (used for nearly all samples), dispersion tests were performed using a higher flow rate and a lower flow rate. The dispersion profiles were obtained as described in chapter 3.2. The flow rates for the respective samples are presented in Tab. 5.1. Reynolds numbers (N_{Re}) are also given for all rates.

Table 5.1 – Flow rate program for three selected carbonate core samples. Note that the Reynolds numbers are above diffusion-dominated flow (see Fig. 2.5), and also below (or in the very lower part of) the transition zone from laminar to turbulent flow.

Flow rate program							
Sample	**Pore class**	**High flow rate**		**Intermediate flow rate**		**Low flow rate**	
		***Q* [ml/min]**	**N_{Re}**	***Q* [ml/min]**	**N_{Re}**	***Q* [ml/min]**	**N_{Re}**
S-783	IC-UMa	5.000	17.0	0.156	0.53	0.030	0.10
S-889	M-Ma	5.000	13.6	0.169	0.46	0.030	0.08
HE-3	C-T	1.000	2.27	0.273	0.62	0.030	0.07

Results for the three samples are shown in Fig. 5.1. The trends that are seen will be discussed in more detail in chapter 6, but it is clear from these profiles that flow rate effects should be considered dependent on pore structure of the core sample in question.

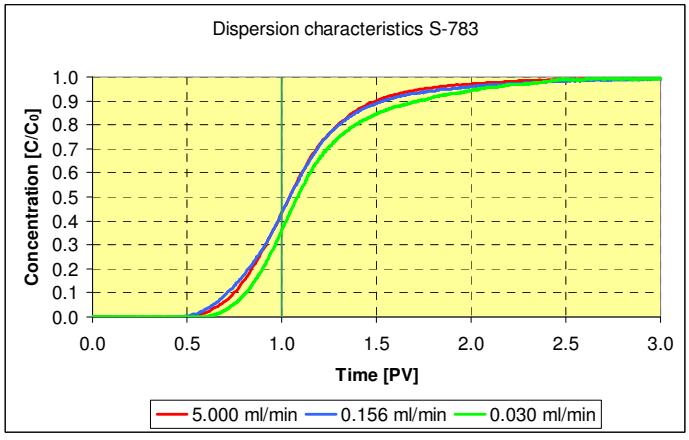

(a) S-783.

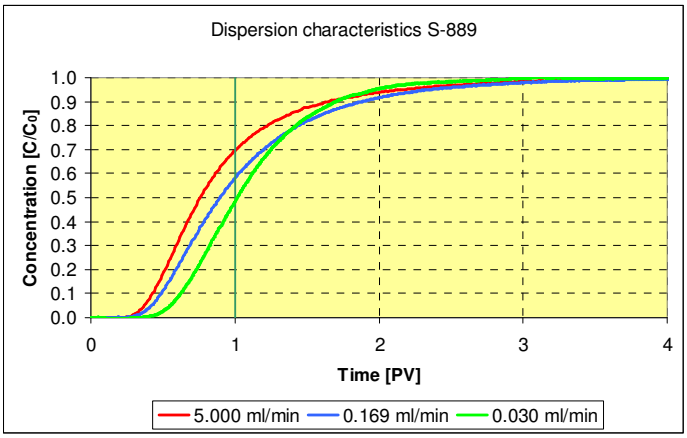

(b) S-889.

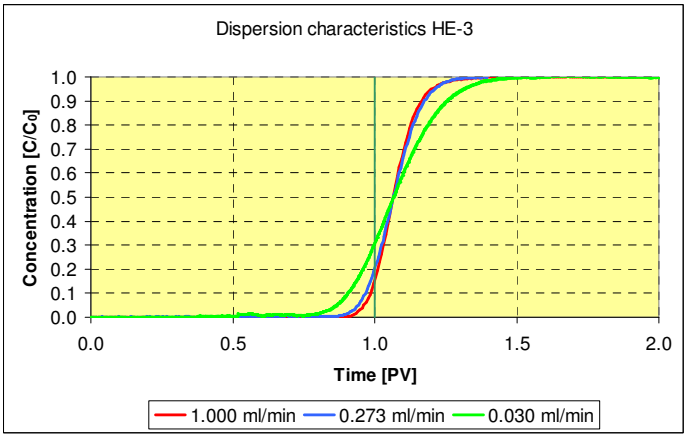

(c) HE-3.

Figure 5.1 – Flow rate effects on dispersion characteristics for three carbonate core samples. Apparently, the effect for the low-dispersive HE-3 (pore class C-T) is not the same as for the more dispersive samples S-783 (IC-UMa) and S-889 (M-Ma).

5.2 Dispersion tests

The main purposes of performing laboratory dispersion tests in this thesis are to:

- Verify that the new dispersion method is valid, i.e. that the dispersion profiles are possible to simulate using Coats and Smith's (1964) model.
- Compare different carbonate pore classes; are the results consistent with Lønøy's (2006) pore-type classification?
- Try to find relations between dispersion characteristics and two-phase flow properties during water floods.
- Examine how the presence of an immobile phase (oil) affects dispersion characteristics, and explain the mechanisms responsible for the results.

5.2.1 Core-plug selection

In order to achieve these goals, 11 core samples were selected; three recognised as having *intercrystalline, uniform macropores (IC-UMa)*, four as having *moldic macropores (M-Ma)*, and the last four were composed of *tertiary chalk (C-T)*. One of the moldic samples (S-929) also consisted partly of interparticle, uniform macropores. The pore type of these samples had been determined visually by Statoil and Hydro prior to them being delivered to CIPR for further analysis. Fig. 5.2 shows porosity/permeability relationships for the chosen core samples, compared to the equations found by Lønøy (2006) for the pore classes in question. S-929 is here considered as M-Ma. The best correlation is found for the IC-UMa samples, while the M-Ma samples are extremely scattered.

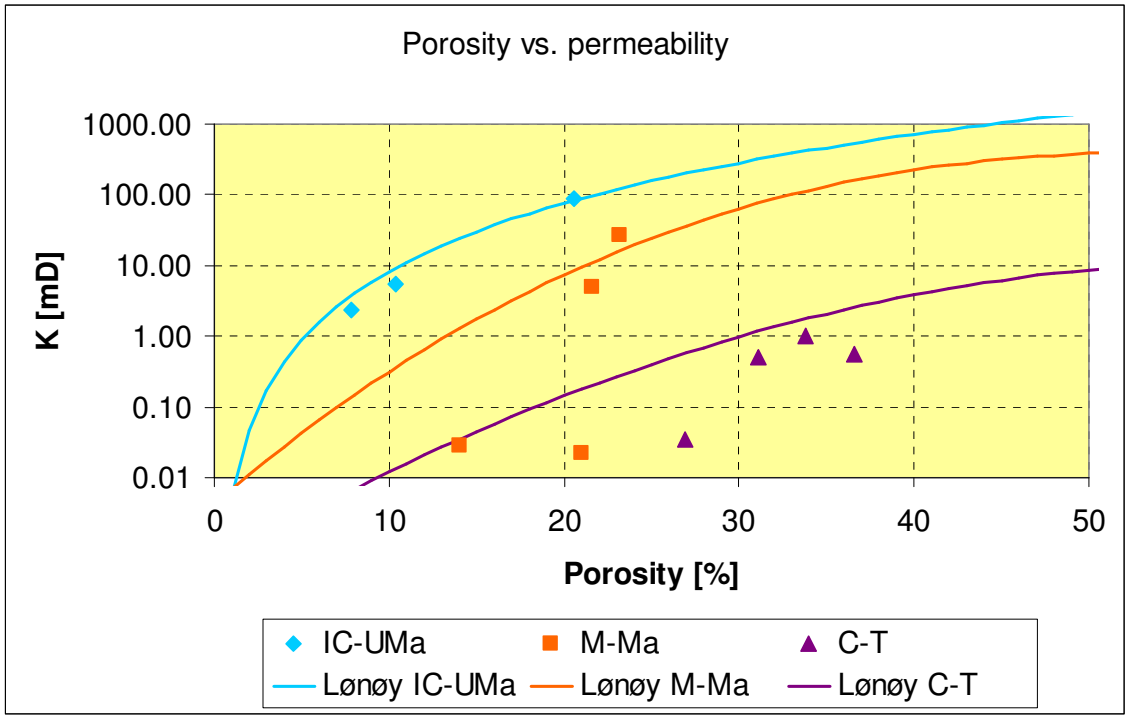

Figure 5.2 – Porosity/permeability relationships for the 11 selected core plugs (S-929 considered as M-Ma). Note that the permeability scale is logarithmic. The three IC-UMa core samples fit Lønøy's (2006) classification very well. The C-T samples all have lower permeability than the average trend found by Lønøy. Data for M-Ma samples are scattered significantly.

The Hydro core samples HE-1 – HE-4 are from the Ekofisk oil field, located in the Norwegian sector of the North Sea; the reservoir rock is tertiary chalk. The final Hydro sample, F-3, is of Iranian origin. All Statoil core samples (starting with a capital S) originate from South Pars, situated in the Iranian sector of the Persian Gulf (see appendix 3). Together with the Qatari North Field, South Pars constitute the world's largest gas condensate field. As seen on the stratigraphic chart shown in appendix 3, the geology of the field is rather complex. The gas-bearing reservoir formations consist of mainly limestones, dolomites and anhydrites. According to Statoil's facies analysis, which is based on pore textures, the following facies can be associated with the core samples relevant for this thesis:

- Macrocrystalline dolomite (S-296 and S-783; IC-UMa). Reservoir properties are good, porosities range from 5 % to 25 % and permeabilities from 5 mD to 1000 mD. Porosity/permeability correlation is also good; this is consistent with Fig. 5.2.
- Limestone grainstones/packstones (S-929; M-Ma and IP-UMa). This facies is related to bioclastic sediments and/or ooids, which are small (< 2 mm in diameter), spherical concretions of calcium carbonate. The grains have not undergone dolomitisation, but instead they have been micritised or recrystallised. Calcite spar cement is common; this can explain the low permeability seen for S-929. The porosity present is both primary (intergranular) and secondary (intragranular, due to dissolution). Reservoir properties are generally good.
- Oomoldic limestone (S-294, S-829 and S-889; M-Ma). This facies is caused by dissolution of ooid grainstones, leaving moldic pores. The moldic porosity is commonly high (20 % – 40 %), however the intergranular porosity is practically non-existing due to calcite cementation. These characteristics lead to moderate reservoir properties. The permeability is often low, averaging around 1 mD. Yet some samples may have high permeability due to fractures or interconnected moldic pores; S-829 and S-889 are examples of this. S-294 on the other hand has very low permeability.

All samples underwent dispersion analysis when saturated with sea water (SSW, see appendix 1), and eight of them also went through dispersion analysis at residual oil saturation (using decane, see appendix 1). All laboratory tests were performed with the setup and method described in chapter 3.2 and the simulation procedure explained in chapter 3.3. The results only apply for core samples in *cleaned state* (except F-3, which was in original state); no ageing has taken place. Note, however, that results from CIPR wettability studies show that not all cores are strongly water-wet. On the contrary, several samples show only weak water-wetness and two samples even show neutral wettability despite being cleaned. This issue re-emerges several times in chapters 5.2.4 and 6.

5.2.2 Water-saturated

Fig. 5.3 shows dispersion profiles for all the core samples, sorted by Lønøy's pore-type classification (2006), in the state of 100 % water-saturated.

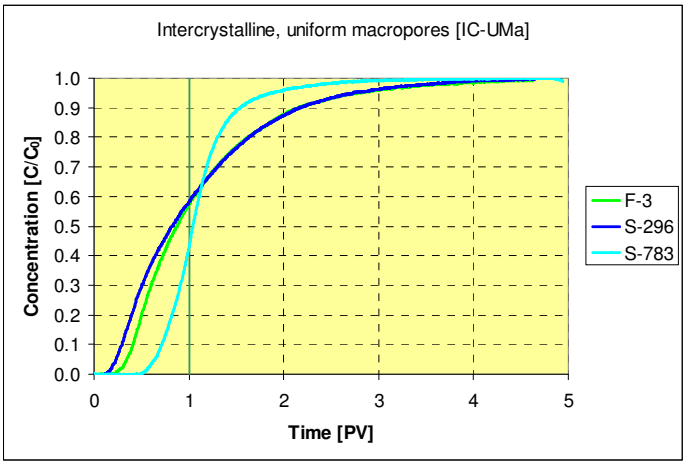

(a) Intercrystalline, uniform macropores (IC-UMa); F-3, S-296 and S-783.

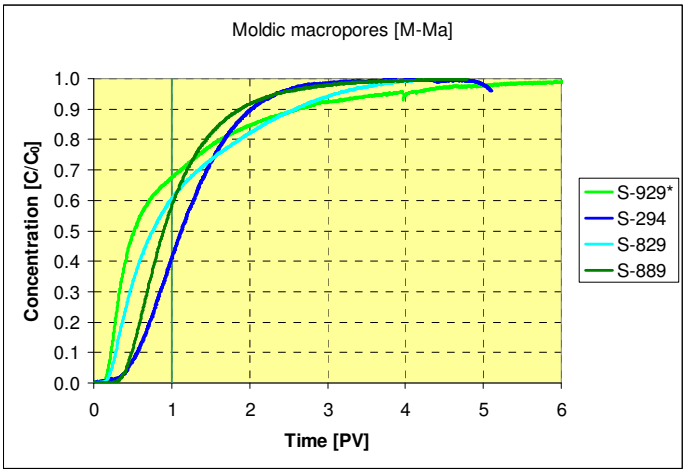

(b) Moldic macropores (M-Ma); S-929, S-294, S-829 and S-889. S-929 also contains interparticle, uniform macropores (IP-UMa).

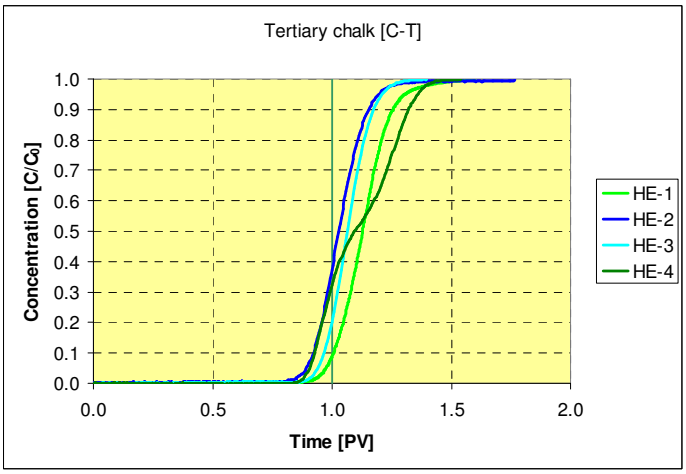

(c) Tertiary chalk (C-T); HE-1, HE-2, HE-3 and HE-4.

Figure 5.3 – Dispersion characteristics at S_w *= 1 for 11 carbonate core samples, sorted by Lønøy's pore-type classification (2006). The tertiary chalk samples (c) are on the whole less dispersive than the other two pore classes, indicating that these samples are more homogeneous. HE-4 stands out from the rest of the C-T samples, showing signs of two separate pore structures. The IC-UMa (a) and M-Ma (b) samples are all characterised by tailing and to some extent early breakthrough, suggesting noticeable heterogeneities. However, these two pore classes are seemingly more difficult to separate from each other, and also the samples within the pore class are less comparable. Several samples (mainly chalk samples) were observed to dissatisfy* $t \leq 1$ *PV for* $C/C_0 = 0.5$.

Tab. 5.2 sums up the simulation results for the dispersion tests presented in Fig. 5.3. Charts, found in Appendix 4, generally show fairly good agreement between experimental dispersion profiles and simulated profiles. However, some of the high-dispersive samples such as S-929 are difficult to model using Coats and Smith's (1964) equations. As can be seen from Fig. 5.3, some samples have the non-physical feature $t > 1$ PV for $C/C_0 = 0.5$. Thus, the fraction of inaccessible pores is often incorrect (see chapter 3.3 for discussion). In fact, change in flowing fraction also (f) shifts the profile somewhat, and so f should be taken with a pinch of

salt. The total porosity, φ_T, is divided into flowing porosity, φ_f, dendritic (dead-end) porosity, φ_D and inaccessible porosity, φ_I, so that

$$\phi_T = \phi_f + \phi_D + \phi_I = f(\phi_T - \phi_I) + (1-f)(\phi_T - \phi_I) + \phi_I . \quad (5.1)$$

The sizes of flowing fraction and dispersivity found in Tab. 5.2 fit in with Fig. 5.3; all the C-T samples have rather low dispersivities and flowing fractions near unity. Thus they contain hardly any dead-end pores. None of the examined core samples contained inaccessible pores. Two samples (S-783 and S-829) had different mass-transfer coefficients, indicating that pore geometry influenced mass transfer in these samples. IC-UMa and M-Ma samples are generally more heterogeneous; however the characteristics within one pore class are seemingly not as consistent with Lønøy's classification. Dispersivities and flowing fractions range over large intervals. In chapter 6 there will be a detailed study of these results.

Table 5.2 – Simulation results at S_w *= 1 for 11 carbonate core samples, sorted by Lønøy's pore-type classification (2006). Note that* f *and (in particular)* φ_I *are uncertain parameters. S-783 and S-829 have lower M values; this may be related to pore geometry. The results are generally in good agreement with the experimental data; higher values for* α *and lower values for* f *are to be expected for the more heterogeneous IC-UMa and M-Ma samples. The behaviour of HE-4 is not possible to simulate using Coats and Smith's model (1964), however it is possible to generate two separate solutions that match the first and last part of the its' dispersion profile (see Appendix 4). The two sets of porosity fractions (see Eq. 5.1 for explanation) for HE-4 should be interpreted as possible solutions, and are not addable.*

Simulation results S_w = 1								
Pore class	**Sample**	**Total porosity φ_T**	**Dispersivity α [cm]**	**Mass transfer coeff. M [s^{-1}]**	**Flowing fraction f**	**Porosity fractions**		
						φ_f	φ_D	φ_I
IC-UMa	F-3	0.104	1.50	$5\cdot10^{-4}$	0.60	0.063	0.041	0.000
	S-296	0.078	2.25	$5\cdot10^{-4}$	0.82	0.064	0.014	0.000
	S-783	0.205	0.18	$1\cdot10^{-5}$	0.86	0.177	0.028	0.000
M-Ma	S-929*	0.140	2.00	$5\cdot10^{-4}$	0.55	0.077	0.063	0.000
	S-294	0.210	0.75	$5\cdot10^{-4}$	0.72	0.151	0.059	0.000
	S-829	0.216	2.50	$8\cdot10^{-5}$	0.70	0.151	0.065	0.000
	S-889	0.232	0.65	$5\cdot10^{-4}$	0.76	0.176	0.056	0.000
C-T	HE-1	0.269	0.025	$5\cdot10^{-4}$	1.00	0.269	0.000	0.000
	HE-2	0.311	0.025	$5\cdot10^{-4}$	1.00	0.311	0.000	0.000
	HE-3	0.366	0.015	$5\cdot10^{-4}$	0.97	0.355	0.011	0.000
	HE-4	0.338	0.025 0.040	$5\cdot10^{-4}$	0.97 1.00	0.327 0.338	0.011 0.000	0.000

5.2.3 Residual oil saturation

As explained in the paragraph "Influence of immobile phase on dispersion" in chapter 2.3.2, dispersion tests at residual oil saturation, S_{or}, can provide information on phase distributions in a two-phase scenario if compared to single-phase (water-saturated) results.

There are a couple of alternatives when it comes to the procedure of comparing results at the two saturations ($S_w = 1$ and $S_w = 1 - S_{or}$). It is really a matter of preference, but in this chapter the results are presented as follows:

1. The time scale is the same for the two saturations; the pore volume is not adjusted due to the pore space occupied by immobile oil.
2. Inaccessible porosity at S_{or} is understood as inaccessible pores *for water*, as fraction of the total pore volume. This is simply the portion occupied by oil, $\phi_I = S_{or} \cdot \phi_T$.
3. Flowing fraction and dendritic fraction at S_{or} are given as fractions of the total *water-filled pore volume*. This definition makes the results more comparable to single-phase dispersion results.

Based on these three definitions, a few trends can be anticipated.

- Due to oil occupying a certain portion of the pore volume at S_{or}, a *leftwards* shift of the dispersion profile can be expected for the S_{or} tests; the larger the oil volume (and as a result φ_I), the more the profile is shifted, presumably.
- The shape of the dispersion profile at S_{or} is influenced by the phase distributions. One might expect that the fraction of dendritic water is likely to increase due to oil globules blocking flow patterns, i.e. increasing tortuosity. This would in turn lead to an increase in dispersivity, and conceivably also to a lower flowing fraction at S_{or}. On the other hand, it is imaginable that oil could block the entrance to dead-end pores or occupy dead-end pores. The effect of this is a more homogeneous pore system, i.e. an increased flowing fraction. The latter may also be caused by water film flow (see chapter 2.3.2).

Fig. 5.4 shows dispersion profiles for two of the IC-UMa samples (a), two of the M-Ma samples (b) and all four C-T samples (c), all at both $S_w = 1$ and S_{or}.

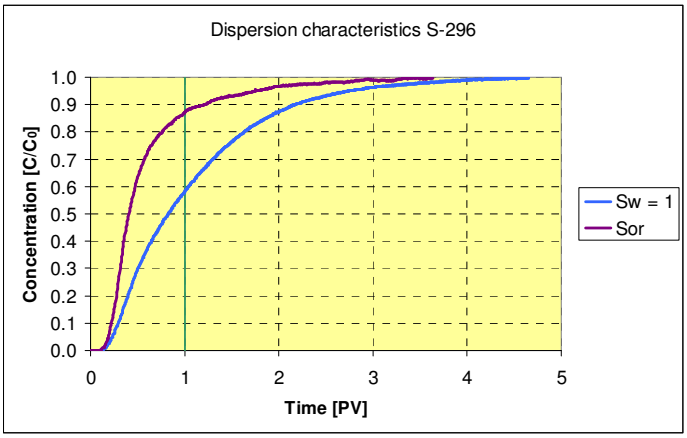

5.2 Dispersion tests

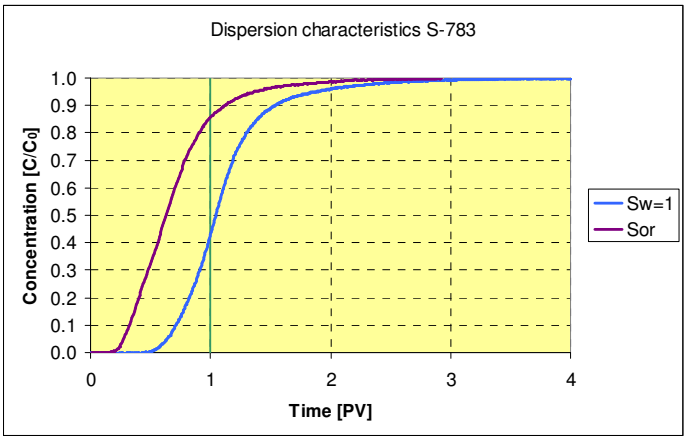

(a) Intercrystalline, uniform macropores (IC-UMa); S-296 and S-783.

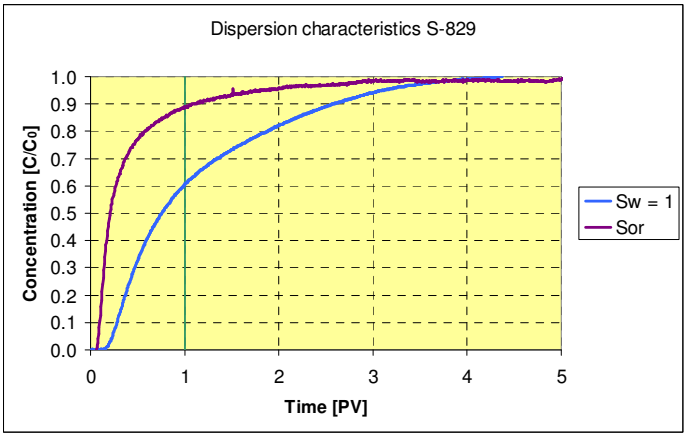

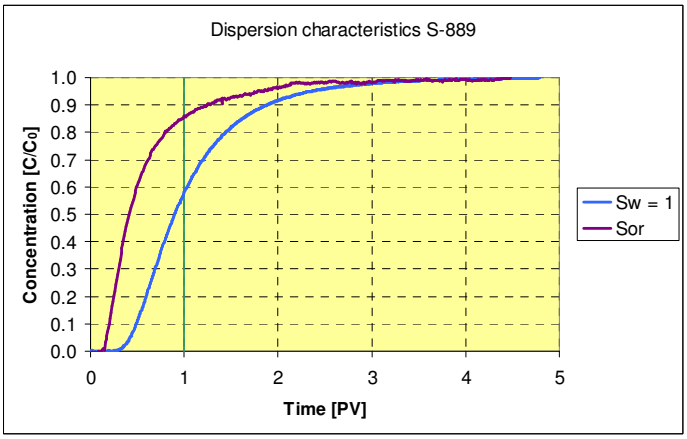

(b) Moldic macropores (M-Ma); S-829 and S-889.

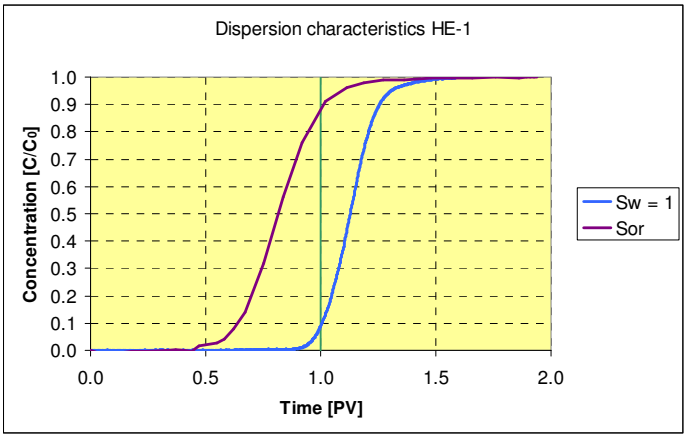
Dispersion characteristics HE-1
Concentration [C/C0]
1.0
0.9
0.8
0.7
0.6
0.5
0.4
0.3
0.2
0.1
0.0
0.0
0.5
1.0
1.5
2.0
Time [PV]
Sw = 1
Sor

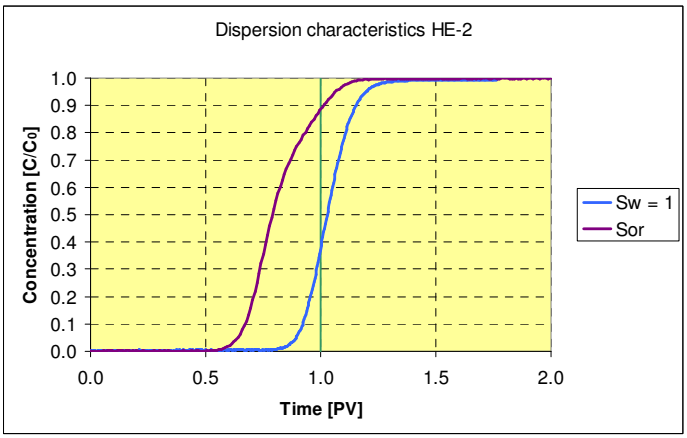
Dispersion characteristics HE-2
Concentration [C/C0]
1.0
0.9
0.8
0.7
0.6
0.5
0.4
0.3
0.2
0.1
0.0
0.0
0.5
1.0
1.5
2.0
Time [PV]
Sw = 1
Sor

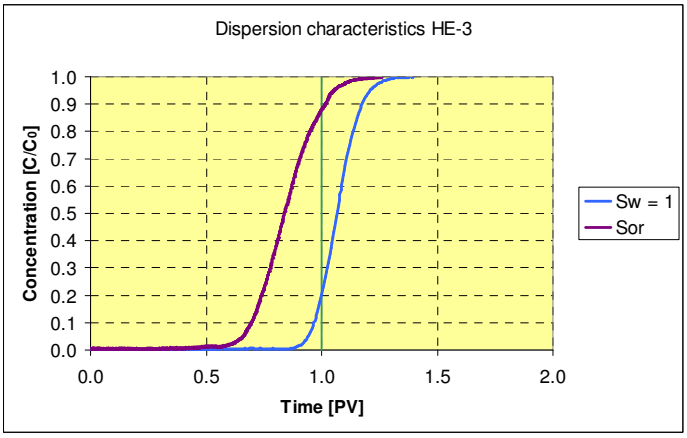
Dispersion characteristics HE-3
Concentration [C/C0]
1.0
0.9
0.8
0.7
0.6
0.5
0.4
0.3
0.2
0.1
0.0
0.0
0.5
1.0
1.5
2.0
Time [PV]
Sw = 1
Sor

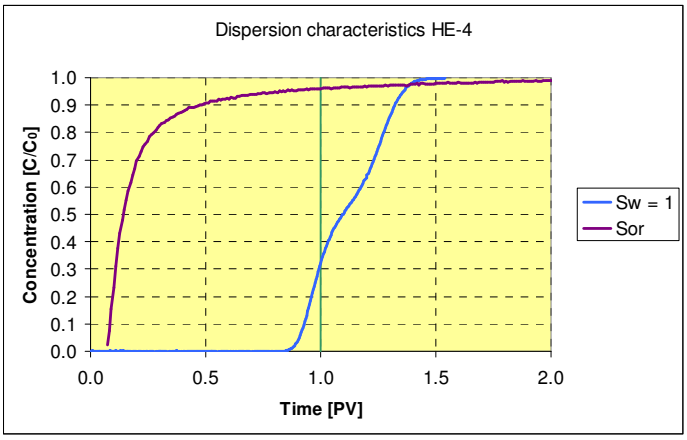

(c) Tertiary chalk (C-T); HE-1, HE-2, HE-3 and HE-4.

Figure 5.4 – Dispersion characteristics at $S_w = 1$ *and* S_{or} *for 8 carbonate core samples, sorted by Lønøy's pore-type classification (2006). As expected, all* S_{or} *profiles are shifted to the left, because oil takes up pore volume and reduces water breakthrough time. More samples are required to see clear trends, but from these data it seems as though the change in dispersive behaviour at* S_{or} *(compared to* $S_w = 1$*) are more easily predictable for the homogeneous C-T samples. The exception is HE-4, which shows inexplicable characteristics at* S_{or}.

Tab. 5.3 shows simulation results for both saturations for the eight core samples. Keep in mind the definitions that apply for inaccessible porosity and flowing fraction. As seen for water-saturated characteristics, trends are easier to spot for C-T samples than for IC-UMa and M-Ma samples. The charts for the simulations are given in Appendix 4. As was seen for the water-saturated samples, samples with asymmetric profiles are more difficult to fit; some of these heterogeneous samples also caused lower mass-transfer coefficients (as was the case for water-saturated samples). In addition, the presence of oil also affects the mass-transfer coefficient for a few core samples. The results will be more thoroughly studied in chapter 6.

Table 5.3 – Simulation results at $S_w = 1$ *and* S_{or} *for 8 carbonate core samples, sorted by Lønøy's pore-type classification (2006). Inaccessible pores arise due to immobile oil, and flowing fraction is defined as fraction of water volume. HE-4 was not possible to simulate using Coats and Smith's model (1964) and the dispersion profile (see Fig. 5.4c) also looks erroneous. For C-T samples, the presence of oil does not affect water dispersion much; however, the flowing fraction is slightly decreased and the dispersivity a little higher due to the increased tortuosity. For the IC-UMa and M-Ma samples, several combinations of dispersivity and flowing fraction are observed; S-296 has a lower dispersivity (i.e. shorter mixing zone) at* S_{or}*, whereas the flowing fraction is practically unaffected. S-783 and S-889 have higher flowing fractions at* S_{or}*, whilst S-829 has a much lower dispersivity and flowing fraction. S-296, S-783 and S-889 have different* M *values at the two saturations.*

Simulation results $S_w = 1$ vs. S_{or}

Pore class	Sample	State	Total porosity φ_T	Dispersivity α [cm]	Mass transfer coeff. M [s^{-1}]	Flowing fraction f	Porosity fractions φ_f	φ_D	φ_I
IC-UMa	S-296	S_w=1	0.078	2.25	$5\cdot10^{-4}$	0.82	0.064	0.014	0.000
		S_{or}	0.080	1.30	$1\cdot10^{-5}$	0.82	0.030	0.007	0.044
	S-783	S_w=1	0.205	0.18	$1\cdot10^{-5}$	0.86	0.177	0.028	0.000
		S_{or}	0.226	0.70	$5\cdot10^{-4}$	0.92	0.132	0.012	0.082
M-Ma	S-829	S_w=1	0.216	2.50	$8\cdot10^{-5}$	0.70	0.151	0.065	0.000
		S_{or}	0.225	0.30	$8\cdot10^{-5}$	0.50	0.050	0.050	0.126
	S-889	S_w=1	0.232	0.65	$5\cdot10^{-4}$	0.76	0.176	0.056	0.000
		S_{or}	0.234	0.60	$5\cdot10^{-5}$	0.83	0.098	0.020	0.116
C-T	HE-1	S_w=1	0.269	0.025	$5\cdot10^{-4}$	1.00	0.269	0.000	0.000
		S_{or}		0.100	$5\cdot10^{-4}$	0.90	0.188	0.021	0.060
	HE-2	S_w=1	0.311	0.025	$5\cdot10^{-4}$	1.00	0.311	0.000	0.000
		S_{or}		0.080	$5\cdot10^{-4}$	0.90	0.203	0.023	0.085
	HE-3	S_w=1	0.366	0.015	$5\cdot10^{-4}$	0.97	0.355	0.011	0.000
		S_{or}		0.060	$5\cdot10^{-4}$	0.95	0.270	0.014	0.082
	HE-4	S_w=1	0.338	0.025	$5\cdot10^{-4}$	0.97	0.327	0.011	0.000
		S_w=1	0.338	0.040	$5\cdot10^{-4}$	1.00	0.338	0.000	0.000
		S_{or}	N.A.	N.A	N.A.	N.A.	N.A.	N.A.	N.A.

5.3 Water floods

Since water injection is such a common recovery technique on the Norwegian continental shelf (see chapter 2.4), it is appealing to perform laboratory water floods on core samples. In this thesis water-flood results are compared to dispersion characteristics and moreover results for samples from different pore classes (as defined by Lønøy, 2006) are compared. Similar to dispersion tests, the objective is to find out whether Lønøy's pore classification is consistent with results obtained through water flooding.

There are many potential aspects to study on the subject of water flooding. In this thesis the simple parameters are emphasised; the development of oil production as a function of time (measured in pore volumes of injected water) and also the production endpoint, which is the final recovery efficiency. It is of course possible to plot *average* water saturation instead of

produced oil; this would result in a similar curve shifted upwards due to the initial water saturation, S_{wi}. The endpoint of such a plot is known as the residual oil saturation after water flooding, S_{orw}. The laboratory tests are performed on the same core samples as the dispersion tests, all which were in *cleaned state*, except F-3 (original ["as is"] state). As pointed out in chapter 5.2.1 however, CIPR studies show that wettabilities still range from neutral to strongly water-wet. Thus not all core samples are expected to produce a sharp water-cut (see Fig. 2.11).

It is evident that pore structure controls both dispersion characteristics and water-flooding properties, even though dispersion occurs during miscible processes while water floods are immiscible displacements. If significant heterogeneities (dead-end pores, etc.) are present in the core sample, it is likely that: (1) the dispersion profile is characterised by tailing, early breakthrough and in general asymmetric behaviour; and (2) permeability contrasts will lead to lower recovery efficiency. This relationship is confirmed by Skauge et al. (2006). Still, there are other parameters that may influence recovery profiles, such as mobility ratio and wettability. To be fully able to compare water-flood results to dispersion profiles, studies of relative permeability and capillary pressure are recommended, as well as repeating the testing series after ageing the core samples (restored state) to observe wettability effects. Nonetheless, comparing oil production profiles to dispersion profiles can provide useful information on the effect of pore structure on oil recovery. Porosity and permeability data are included in tables, making it possible to check whether (for instance) low-permeable samples still can produce oil effectively if they are homogeneous.

Fig. 5.5 shows water-flood results for all core samples that underwent dispersion tests (see Figs. 5.3 and 5.4), except for S-294 (M-Ma). The results are summarised in Tab. 5.4 in terms of endpoint saturations and recovery efficiency (% of original oil in place, *OOIP*). Some petrophysical core data are also included in this table. On the average, the C-T samples produce more oil, presumably due to their homogeneous nature. This backs up the results observed by Skauge et al. (2006); pore structure can be just as important as permeability when it comes to water-flooding recovery efficiency. Indistinct water-cuts are seen for samples that are not strongly water-wet. All these results are further discussed in chapter 6.

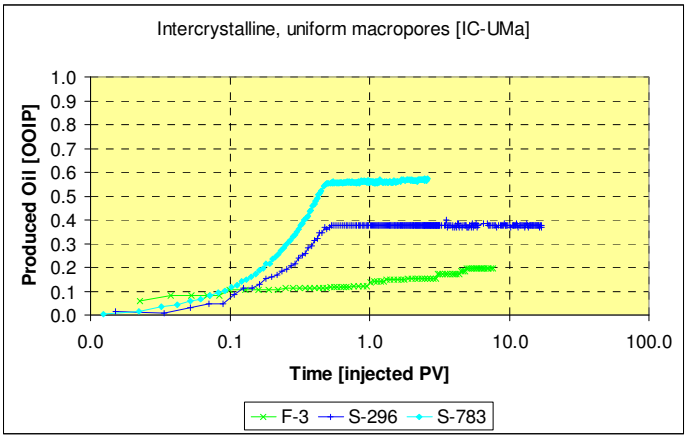

(a) Intercrystalline, uniform macropores (IC-UMa); F-3, S-296 and S-783.

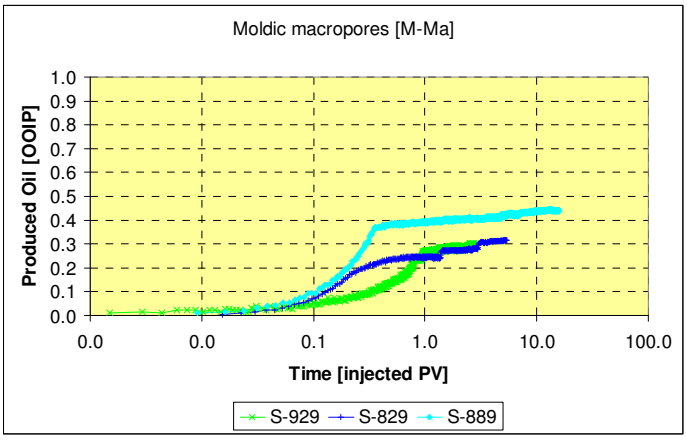

(b) Moldic macropores (M-Ma); S-929, S-829 and S-889.
S-929 also contains interparticle, uniform macropores (IP-UMa).

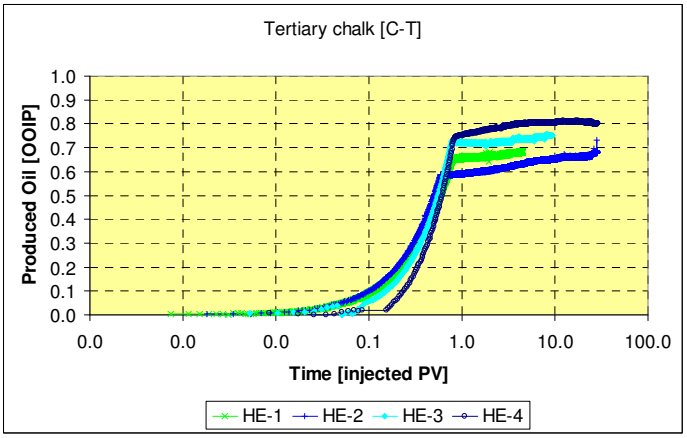

(c) Tertiary chalk (C-T); HE-1, HE-2, HE-3 and HE-4.

Figure 5.5 – Water-flooding results for 10 carbonate core samples, sorted by Lønøy's pore-type classification (2006). Note that the time scale is logarithmic. The more homogeneous C-T samples are seen to produce more oil than IC-UMa and M-Ma samples. Most of the samples (independent of pore class) produce oil after water breakthrough, indicating that they are not strongly water-wet. The final recovery efficiency is known to increase slightly as the degree of oil-wetness increases towards neutral wettability; this is consistent with results seen for S-889 and HE-4, which both have indistinct water-cuts. The low recovery efficiency seen for F-3 is presumably due to the fact that it was not cleaned; this causes high S_{wi} *and low recovery factor. There seems to be no strong link between pore class and final recovery efficiency based on the results for IC-UMa and M-Ma samples.*

Table 5.4 – Summary of water-flood results for the samples presented in Fig. 5.5. No data was available for S-294. It is seen that initial water saturations are low, except for F-3 (0.62) and HE-1 (0.29). Residual oil saturations range from 0.18 to 0.58, and are lower for C-T samples (as observed in Fig. 5.5), even though they generally have lower absolute permeability than several IC-UMa and M-Ma samples.

Results, laboratory water floods							
Pore class	**Sample**	**Total porosity φ_T**	**Absolute permeability K [mD]**	**Initial water saturation S_{wi}**	**Residual oil saturation S_{orw}**	**Recovery efficiency % of PV**	**% of OOIP**
IC-UMa	F-3	0.104	5.55	0.624	0.303	7.3	19.5
	S-296	0.078	2.40	0.118	0.558	32.4	36.8
	S-783	0.205	86.0	0.154	0.363	48.3	57.1
M-Ma	S-929*	0.140	0.028	0.184	0.577	24.0	29.4
	S-294	0.210	0.022	0.147		N.A.	
	S-829	0.216	4.90	0.180	0.562	25.9	31.5
	S-889	0.232	26.8	0.114	0.496	39.0	44.0
C-T	HE-1	0.269	0.034	0.289	0.223	48.8	68.6
	HE-2	0.311	0.498	0.141	0.275	58.5	68.0
	HE-3	0.366	0.548	0.104	0.223	67.3	75.1
	HE-4	0.338	1.00	0.092	0.182	72.6	80.0

Chapter 6: Discussion and conclusions

Salinity vs. permeability in carbonates

The purpose of these laboratory tests was to find out whether absolute permeability is dependent on the content of monovalent and divalent ions present in the brine. The results shown in Figs. 4.1 and 4.2 clearly have limited value, due to the facts that: (1) only two carbonate core samples were considered; (2) the effects here are only valid for injected slugs of approximately 7 – 10 pore volumes (including the pre-flush treatment), and may not be representative for larger volumes (i.e. equilibrium is perhaps not reached); (3) there are no reference series with constant water composition to compare the data with; and (4) the effluent composition was not analysed in order to study dissoluted minerals.

Despite these discouraging facts, the results are still very interesting. The issues addressed in the very last paragraph of chapter 4 are not all easily explained; nonetheless, most results are understandable to some extent.

A reasonable subject to start with would be the dissolution trend seen for O-14; a result that was not observed for D-1. There are several plausible answers to this. Firstly, the amount of injected brine was not equal for the two samples; during the actual measurement series (four flow rates) ca. 5 PV's was injected for both samples, but the pre-flush treatment was ca. 5 PV's for O-14, compared to ca. 2.5 PV's for D-1. The difference was, as stated in chapter 4, caused by the dispersion characteristics for the two samples; D-1 was thought to be more homogeneous. Secondly, the flow rates were totally different (due to different permeabilities), ranging from 40 ml/h to 160 ml/h for O-14, compared to 2 ml/h – 4 ml/h for D-1. As concluded by Ochi and Vernoux (1998), the velocity affects the release of fines from the pore surfaces. Lastly, the magnitude of the permeability itself may conceivably affect the dissolution process; since the original permeability of O-14 was more than 25 times as high as the permeability of D-1, the transport of fines will probably be more effective in O-14. Hence, fines that are transported all the way to the effluent for O-14 might get stuck somewhere on the way for D-1. A flaw in this last theory is that no significant permeability *decrease* is observed for D-1. Even though all these suppositions are *possible* reasons for the trends seen, they are not the most *likely* reason. A study of the two samples' mineralogical composition proves that O-14 is classified as IC-PMe (intercrystalline mesopores, patchy distribution). This is (a translated version of) A. Lønøy's (Pers.com) response to the results for O-14:

> *"The main mineral present is dolomite ($CaCO_3$), but there is a patchy distribution of anhydrite ($CaSO_4$) cements. These cements are responsible for the patchy porosity distribution. Anhydrite is a relatively highly soluble mineral, and would supposedly dissolute during water flood, at least partly. Dolomite is normally quite stable, and should not be significantly affected by the water flood."*

D-1 presumably contains only dolomite ($CaCO_3$), and thus no significant dissolution effect is seen for this core sample.

Having explained the dissolution in O-14, it is time to move on to water composition, and its influence on permeability. This subject is perhaps more easily discussed when introducing figures that show absolute permeability as function of injected pore volumes. In this way it is simpler to analyse the effect of salinity on O-14. Figs. 6.1a and 6.1b show such charts for O-14 and D-1, respectively. The data points are marked halfway through the measurement series; to exemplify the first permeability obtained for O-14 was 6.37 mD. A total amount of 4.63 PV's was injected during the four flow rates, after an initial pre-flush treatment of 5 PV's. The data point is then marked at 7.32 PV's (5 + 4.63/2). All pre-flush treatments are set to 5 PV's for O-14 and 2.5 PV's for D-1.

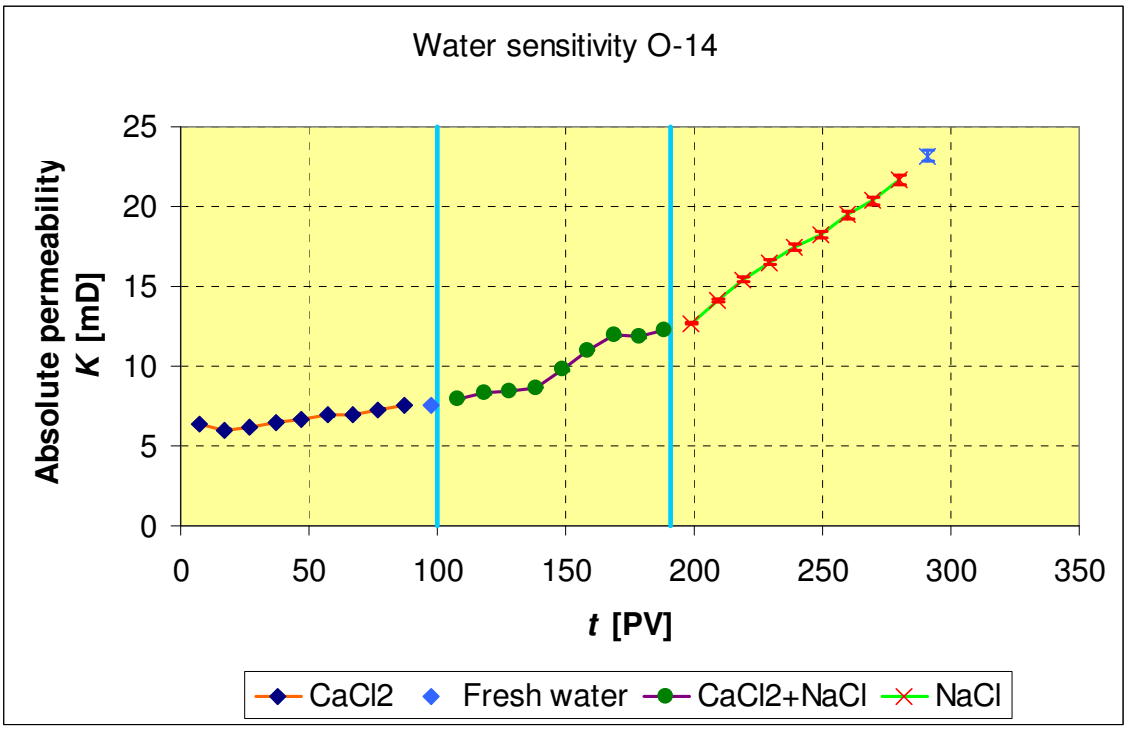

Figure 6.1a – Absolute permeability as function of time (injected pore volumes) for O-14. Even though the dissolution effect is dominating, the increase is more significant when Ca^{2+} is not present. This indicates that ionic composition affects permeability.

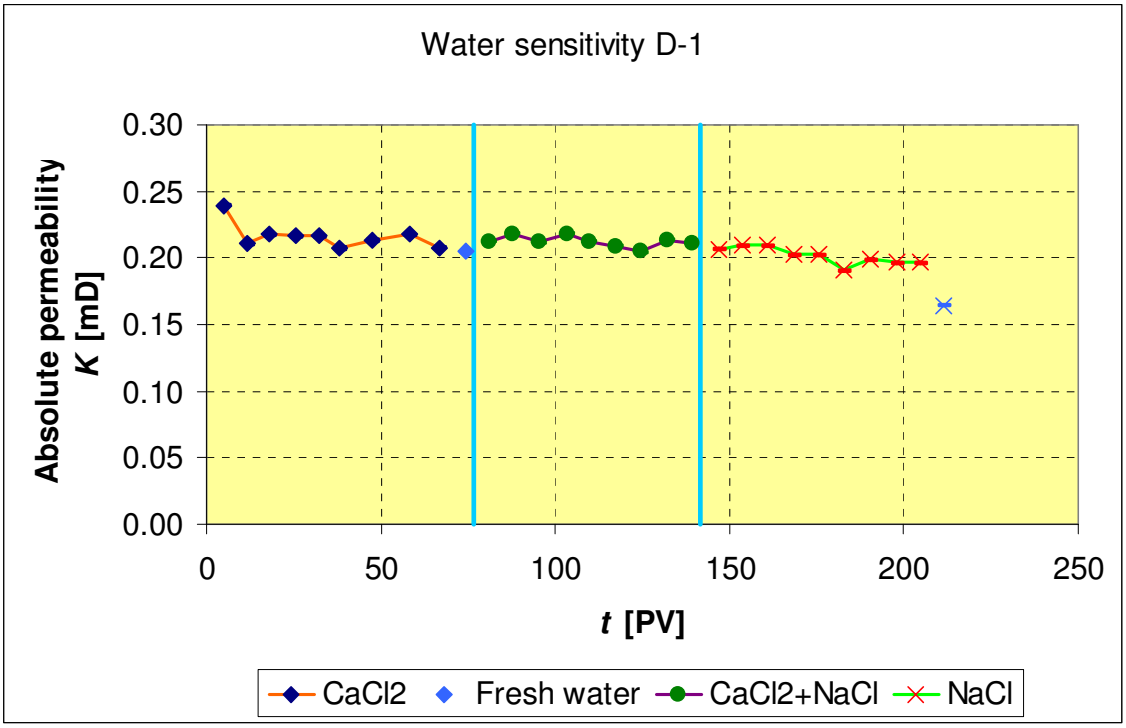

Figure 6.1b – Absolute permeability as function of time (injected pore volumes) for D-1. There is no clear dissolution trend.

Examining Fig. 6.1a, it becomes clear that the permeability increase for O-14 definitely is higher when only Na^+ is present. This fact suggests that soluble minerals on the pore surfaces might be somewhat stabilised by Ca^{2+}-ions.

Another issue that comes up is the fact that lower permeability is observed for increasing concentration than decreasing concentration for D-1. This is also seen for the content of Ca^{2+}-ions at constant total salinity (see Fig. 4.2b). A possible reason for this effect is that low content of Ca^{2+}-ions, or perhaps low salinity in general, causes release of fines, which may migrate and block pore throats. Thus, the permeability is reduced. This theory is supported by the dry weight measurements (see Tab. 4.2); the dry weight is practically unchanged after the measurements, and hence significant amounts of released fines cannot have left the core sample. If this theory is right, the permeability reduction may not be directly reversible; this would explain the long term effects seen on Figs. 4.2b and 4.2c.

The fresh-water measurements were meant to reveal any "shock effects", similar to what has been found for sandstones by Khilar and Fogler (1984) and Kia et al. (1987). Due to the dissolution trend it is difficult to identify this effect for O-14, let alone quantifying it. Also, the uncertainty is estimated as higher for the fresh-water measurement with Na^+ present. Still, it seems a justifiable statement to claim that the permeability increase with Na^+ is higher. Again, this supports the theory that the divalent Ca^{2+}-ions stabilise soluble minerals. The theory is actually further supported by the results for D-1; the permeability drop (presumably caused by fines migration and blocking) with Na^+ present is more than ten times the drop observed with Ca^{2+} present.

The last issue to be discussed is the apparent mismatch between the increase in porosity for D-1 (see Tab. 4.2) and the results, which show little sign of dissolution. The porosity was measured to increase from 0.296 to 0.310 during the measurement series. However, the dry weights are more comparable; 102.81 g (before) and 102.13 g (after). The difference is very small if compared to O-14, where more than 6 g have been dissoluted. The porosity increase is thus more likely to occur due to increased water saturation. This has been observed for some water-flooding measurements at CIPR (S. Hetland, Pers.com); since complete vacuum cannot be obtained, the smallest pores may not saturate completely when water spontaneously floods the sample. However, water is likely to enter even these small pores when flooded sufficiently. The difference in dry weights may be partly due to uncertainty.

On the whole, the results show that salinity and ion valency indeed affect permeability in carbonates. In addition, carbonate cores may contain soluble minerals such as anhydrite, which may cause dissolution and considerable permeability increase when the cores undergo extensive flooding. Even though carbonates generally have low clay content, the results of this study are consistent with previous conclusions from sandstone core samples; the presence of divalent ions (here Ca^{2+}) in all probability stabilises pore-surface minerals. When the content of these ions is sufficiently low, monovalent ions (here Na^{+}) are not able to uphold the equilibrium, and fines are released. In this thesis, this phenomenon is thought to be responsible for both the temporary permeability reductions observed for D-1, and the increase in permeability increase (for Na^{+}) for O-14.

Verification of the new method, the model and the simulation procedure

One of the key objectives in this thesis was to introduce a new approach to dispersion analysis. Essentially there were two new elements (compared to previous methods at CIPR); (1) the use of increased NaCl content to sea water as tracer; and (2) concentration calculation based on measurements of conductivity and temperature.

The calibration resulted in an equation on the form $C(R,T) = a \cdot \left(\frac{1}{R}\right) + b$ (see Eq. 3.1). Overall, linear regression proved adequate and gave good results (see Figs. 3.2 and 3.3). When the new method was tested on some real carbonate core samples, the results were consistent with previous methods (see Fig. 3.5). The injection of tracer was also found reversible (see Fig. 3.4). Compared to the 4-FBA UV spectrometry, there is a massive increase in data points with the new method; this makes it possible to reveal detailed dispersion characteristics even for very heterogeneous samples. Moreover, NaCl is a low-cost, uncomplexed compound that is already present in brine. Because of these properties, the chosen tracer seems ideal. In addition to the nature of the tracer, the laboratory setup (see Fig. 3.1) makes it possible to register the concentration continuously via PC. Hence the method is also time-effective.

Although the results for the new method are promising, there are still a couple of uncertain factors that require consideration. The most important issue is perhaps the delay seen for most dispersion characteristics (see Figs. 3.4, 3.5 and 5.3). As it is unthinkable that adsorption is taking place, there is no physical reason why $t > 1$ PV for $C/C_0 = 0.5$ for so many samples, including homogeneous samples. Hence, the time scale must be incorrect. This is seemingly a weakness of dispersion analysis in general; when trying to match experimental data with simulated data based on Coats and Smith's (1964) model, measurements of pore volumes and other laboratory equipment have to be utterly accurate. If they are not, the dataset must be

shifted leftwards during the simulation procedure, which leads to large uncertainties concerning inaccessible pores fraction and (to some extent) flowing fraction. Fig. 2.7 shows why flowing fraction is sensitive to shifting; lower flowing fractions may cause both increased tailing and earlier breakthrough. The latter is evidently an effect that is influenced by any shifting caused by erroneous pore volume. The problem of pore-volume measurements is unfortunate, because there is no obvious solution to it; measuring pore volume accurately is always going to be a delicate practice.

An additional uncertain factor is the normalisation of concentration. This has not been discussed previously, but the lowest electrical resistance (C/C_0 = 1) was decided based only on individual judgement. When no change was observed for some time, it was assumed that the core sample in question was saturated with tracer. Even though such an assumption is probably not very incorrect, there is still room for improvement on the matter. Since there is already a bypass possibility included in the laboratory setup (see Fig. 3.1), it would not take much effort to measure the resistance of 100 % tracer at specified times. This functions as a reference resistance, and ensures that tracer injection continues until the reference resistance is reached. For very heterogeneous samples, this improvement would lessen uncertainty regarding the concentration.

The uncertainty incorrect pore volumes add to simulation has already been discussed. There is also need to discuss the model itself. The term “inaccessible pores” was defined in chapter 3.3 as pores that are not isolated, but that still do not contribute to fluid flow in the medium. This also leaves out mass transfer through diffusion (and thus distinguishes them from dead-end pores). Such a definition encourages discussions, because the transition from dead-end pores to inaccessible pores is really a matter of opinion. The fact that the pore-type distribution (flowing, dead-end or inaccessible) is dependent on fluid velocity adds to the somewhat vague impression of this definition. However, the model was presumably made this way due to the fact that some dispersion profiles were impossible to match with only flowing pores and dead-end pores. The mass-transfer coefficient’s dependence on velocity and pore geometry also adds uncertainty; should this be kept constant or not? Despite the uncertain elements of the model, carbonate cores are generally heterogeneous and thus mathematical models that perfectly represent the pore structure cannot be expected. After all, Coats and Smith’s model (1964) generally gives results that seem reasonable, at least in this thesis.

Dispersion results, water-flooding results and Lønøy’s pore-type classification

It is a challenging task to discuss the results shown in chapter 5, both because they are hard to interpret and because the issues of interest often overlap; i.e. it is difficult to compare dispersion results and water-flooding results without also discussing pore type, permeability and wettability as well. Nonetheless, relevant subjects will be discussed as separately as possible in the following section.

In order to better understand dispersion simulation results, it is necessary to look into which combinations of dispersivity and flowing fraction that may occur. In theory, there are four different extreme combination scenarios of the two parameters:

1. Low dispersivity and low flowing fraction (such as S-829 at S_{or}); the asymmetry indicates that the pore system is heterogeneous in terms of high-permeable channels which cause even earlier breakthrough. The mixing zone is therefore relatively short.

2. Low dispersivity and high flowing fraction (such as the C-T samples); this is typical for homogeneous material. The amount of dead-end pores is low, and the mixing zone is short.
3. High dispersivity and low flowing fraction (such as F-3 at $S_w = 1$); pore systems with a substantial amount of dead-end pores and a long mixing zone are characterised by this combination. As the dispersivity is high, the dispersion profile is gentle and thus there cannot be significant channels, as this would have accelerated the breakthrough.
4. High dispersivity and high flowing fraction; this indicates a tortuous medium with high connectivity (and symmetry). For single-phase flow, this combination seems unlikely, but the characteristics fit with water film flow in a two-phase scenario.

These considerations are important when interpreting simulation results. However, it is also important to keep in mind that the results not always give the correct representation of the pore structure. After all, this is just a mathematical tool used to try and describe a physically complex system. It is therefore recommended to always verify that simulation results seem reasonable in the physical world.

Wettability studies are not included in this thesis. In view of the results that have been obtained, it is clear that a comprehensive wettability study of the core samples considered may have eased the analysis. The main reason for this is that the initial cleaning did not leave all the core samples strongly water-wet. This causes wettability to become an uncertain factor when discussing the impact of other phenomena such as heterogeneity and permeability. Wettability is thus the likely explanation of two facts; (1) a sharp water-cut is not seen for all samples (see Fig. 5.5) and (2) dispersion simulation results show a decrease in dispersivity in the S_{or} state (compared to water-saturated state) for some samples, indicating that immobile oil makes the medium less tortuous. Consequently, oil must be situated in dead-end pores. A detailed wettability study could reveal to which extent oil-wet pores exist, if the oil preference is influenced by pore size and if oil-wetness is patchily or uniformly distributed.

Another important parameter that may affect both dispersion and two-phase flow is absolute permeability. Intuitively, the flowing fraction is likely to be the main contributor to permeability, and thus a positive correlation between these two parameters should be expected. Furthermore, it can be argued that higher permeability leads to higher recovery efficiency during water floods. However, as upcoming discussions will show, both these theories are left doubtful in view of the results. Concisely, it seems as though pore structure is just as important as permeability when it comes to water-flooding recovery efficiency, and that the interplay between pore-structure properties (such as flowing fraction and dispersivity) and permeability is complex.

Before analysing the results of dispersion tests and water floods, it is necessary to discuss the flow rate effects presented in chapter 5.1. To explain why the results for different core samples apparently are contradictory, the two following facts must be considered;

1. For low velocities, the mass transfer between flowing fraction and dead-end pores takes place almost instantaneously (as explained in chapter 2.3.2), when time is expressed in terms of volume The large value of M leads to nearly symmetrical dispersion profiles.
2. For even lower velocities ($N_{Re} < 10^{-2}$ or 10^{-4}, see chapter 2.3.2), diffusion dominates the dispersion term; this applies for the flowing fraction as well. In this scenario the dispersion profile is in fact approaching a *diffusion* profile, which is adequately described by Fick's laws (see Eq. 2.1). It is however shaped by the tortuosity factor for the porous medium (see Eq. 2.2).

The Reynolds numbers given in Tab. 5.1 indicate that the flow regime still is dominated by convective mixing at the low flow rates. Yet, the transition to diffusion-dominated flow should be considered as gradual. Therefore it is likely that diffusion to a larger extent influences fluid flow for these low flow rates.

The key to understanding flow rate effects is Fig. 2.9. However, it is still difficult to find trends that fully agree with Fig. 2.9 for the three core samples tested in this thesis. On average, it can be argued (see Fig. 5.1) that high rate tests are more similar (than low rate tests) to normal rate tests; a reasonable explanation of this is that the starting (normal) flow rate is closer to the diffusion-dominated regime than the turbulent regime. When studying Fig. 5.1b (S-889) it is still clear that the effect of higher flow rate is dependent on pore structure. This is not really surprising; as HE-3 (Fig. 5.1c) contains virtually no dead-end pores, the capacitance effects will not be significantly different if mass transfer to/from these dead-end pores goes even slower compared to convective mixing. For more heterogeneous core samples, such as S-783 and S-889, higher flow rates may cause a change in dispersion profile in the way that is shown in Fig. 2.9 (case 1). Thus, the conclusion is that higher flow rate does not change dispersion profiles much for homogeneous core samples, unless turbulence occurs.

For low flow rates, the results should be interpreted as a combination of the two mechanisms mentioned above. The effect seen for HE-3 (Fig. 5.1c) differs from the effects seen for the other two core samples, despite the fact that the Reynolds numbers for all three core samples are more or less equal. Since the amount of dead-end pores in HE-3 is low, the profile is nearly perfectly symmetrical at normal flow rate; consequently the effect of more effective mass transfer at low flow rates cannot explain the results seen. Instead, it is likely that the change seen from normal flow rate to low flow rate is due to the flowing fraction flow being more diffusion-dominated. This causes earlier breakthrough. S-783 and S-889, on the other hand, contain a larger amount of dead-end pores, implying that a lower rate would lead to a more efficient dispersion profile due to faster (relative) mass transfer. This effect is seen for S-889 (Fig. 5.1b), but is more difficult to spot for S-783. The reason for this could be the increased influence of diffusion on flowing fraction flow. To summarise, the difference in heterogeneity to some extent explains the differing flow rate effects that are seen in Fig. 5.1. However, the practice of deciding a critical lower flow rate by the Reynolds number *only* does not seem satisfactory, because the interstitial velocity calculated simply considers porosity, and not pore structure and tortuosity. Thus a change in Reynolds number for a homogeneous sample (such as HE-3) may not give the same flow regime as the same change in Reynolds number for a more heterogeneous sample.

Moving on to dispersion tests at intermediate flow rates only, there are a couple of aspects that are of interest. Firstly, it is difficult to correlate permeability to flowing fraction and dispersivity based on the results presented in Tab. 5.2 (dispersion data) and Tab. 5.4 (permeability data). All the chalk samples have very high flowing fractions, even though absolute permeability is low. The opposite is also seen for several samples; for instance, S-889 has a permeability of 26.8 mD, but the flowing fraction is only estimated to 0.76. In similar fashion it is also easy to find both low-permeable core samples that are high-dispersive (S-929) and that have intermediate dispersivity (S-294). Different combinations of flowing fractions and dispersivities are also seen (Tab. 5.2); all core samples with high flowing fractions have low dispersivity, while samples with lower flowing fraction can have either high (S-829) or intermediate (S-294) dispersivity. Comparing dispersion tests at $S_w = 1$ to tests at S_{or}, there are two types of results that are easily explained; (1) the S_{or} profiles are shifted to the left due to the pore volume occupied by oil, and (2) most core plugs have *lower*

estimated flowing fractions at S_{or} due to the increased tortuosity caused by capillary trapped oil drops; such results indicate that film flow is negligible. The low-dispersive C-T samples show more predictable behaviour than IC-UMa and M-Ma samples; the S_{or} dispersion profiles for these core samples are displaced parallel to the water-saturated profiles, with a slight increase in dispersivity and a slight decrease in flowing fraction (typically 0.05 – 0.1 lower at S_{or}). This indicates that the water is located in the centre of the pores, which is characteristic for strong water-wetness. For S-296, S-783 and S-889, the estimated flowing fraction remains constant or increases at S_{or}. As mentioned regarding wettability, local affinities for oil may be the explanation of these results; if dispersivity is lower as well, this theory is strengthened. Fig. 6.2 illustrates the two extreme types of oil distribution that may cause higher or lower flowing fractions and dispersivities at S_{or}, compared to water-saturated conditions. This illustration is merely a schematic representation of the two scenarios, and does not take into account the likely effect of local wettability variations; this may cause oil to break the water film clinging to pore surfaces. Also, the oil distribution in this figure is probably too uniform.

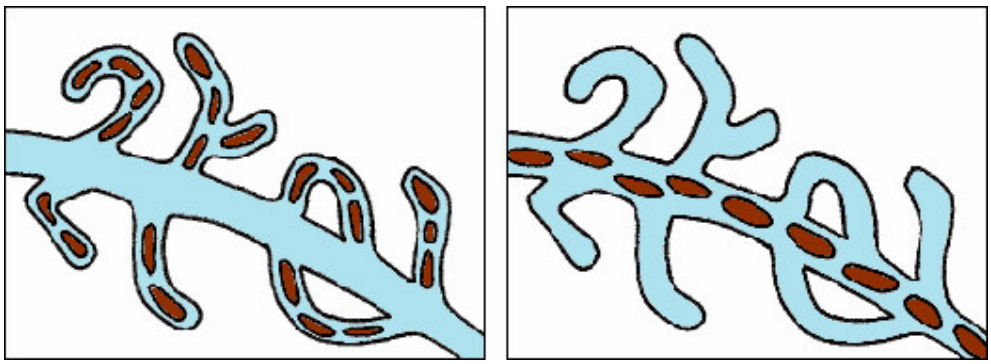

(a) Oil-wetness causing lower dispersivity and higher flowing fraction.

(b) Water-wetness causing higher dispersivity. If film flow is significant, the flowing fraction may still be high. If film flow is negligible, the flowing fraction is reduced.

Figure 6.2 – Two extreme scenarios of oil distribution, leading to lower (a) or (b) higher dispersivities at residual oil saturation, compared to water-saturated state. Local wettability variations are ignored, as are uniformity variations.

Even though Fig. 6.2a motivates an increase in flowing fraction, the same result may be obtained due to film flow. Therefore one should not jump to conclusions naively. Also, the uncertainty of simulation results must not be underestimated; although dispersivity describes the slope of the dispersion profile, while the flowing fraction describes the asymmetry, some core samples show dispersion characteristics where these two properties are difficult to tell apart. For such samples, a mathematical estimation of intermediate flowing fraction and low dispersivity may physically be better described with higher flowing fraction and higher dispersivity. It is important to keep in mind that the simulation procedure's only goal is to match the experimental dispersion profile; there is no better way to check the results than to subjectively consider the results. Adding the simulation results' sensitivity to pore-volume accuracy and flow rate effects (as discussed previously), it is clear that interpreting simulation results is not a straightforward process. It is highly recommended to always study the results with a sceptical point of view; do the results fit in with physical expectations (for instance wettability data) for the sample in question? Which uncertain factors are important?

Having discussed different combinations of dispersivity and flowing fraction, some important single parameters, and also dispersion results independently, it is now time to consider all these elements at the same time. The discussion of water-flooding results and the evaluation of Lønøy's pore classes is a potentially comprehensive matter. However, since only 11 carbonate core samples were investigated in this thesis, the main focus will be on trends that are easily spotted. Such trends are evidently more likely to be consistent with results from a more comprehensive study.

One of the most important aspects for water-flooding analysis is which parameters that affect the final recovery efficiency. Fig. 6.3 shows the influence of permeability on recovery. The different pore classes are marked by different colours.

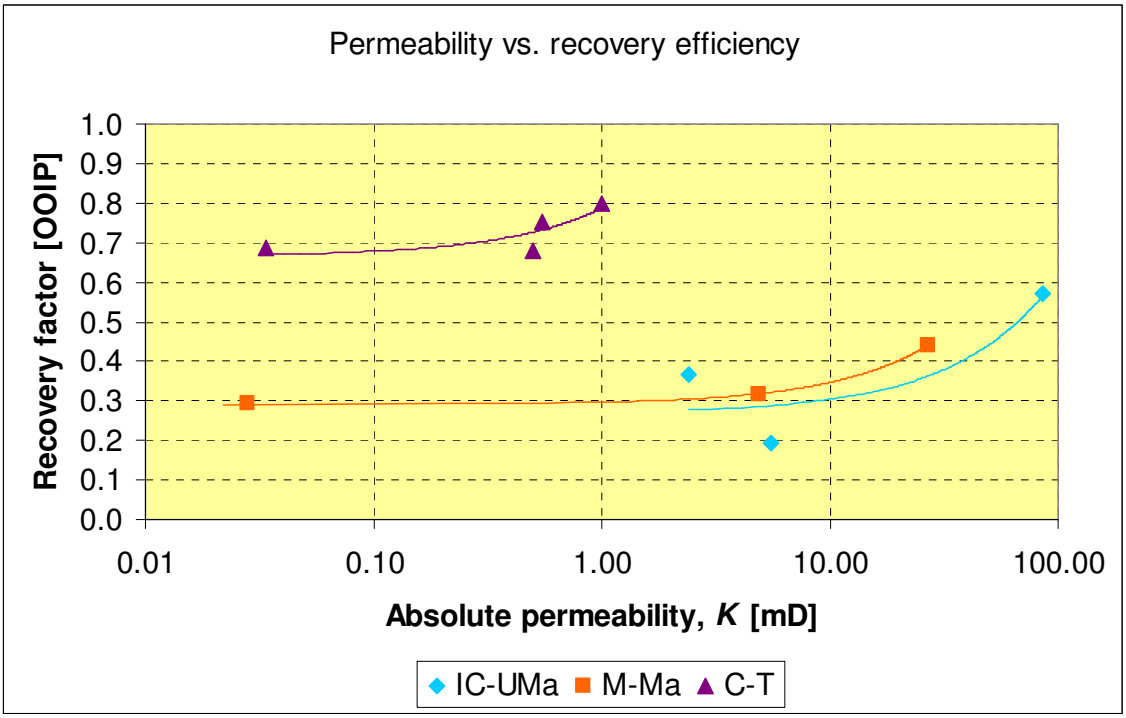

Figure 6.3 – The impact of permeability on recovery efficiency for carbonate core samples from selected pore classes. Note that the permeability scale is logarithmic. S-929 is not included in this chart, due to the fact that it does not consist of exclusively moldic pores. There are two apparent tendencies, even if the number of core samples is very low; (1) within each pore class, the recovery factor increases with increasing permeability, and (2) a very high recovery factor is obtained for the low-permeable Ekofisk chalk samples (C-T).

By studying the results shown in Fig. 6.3, it becomes clear that permeability alone does not control recovery efficiency in water floods. As pointed out at the start of chapter 2.4, permeability *variations* are just as important for recovery efficiency as the magnitude itself. Fig. 6.4 shows recovery efficiency as a function of flowing fraction for the same ten carbonate core samples as in Fig. 6.3. The trend observed is very clear; higher flowing fractions principally lead to higher recovery factors. This result is consistent with results presented by Skauge et al. (2006).

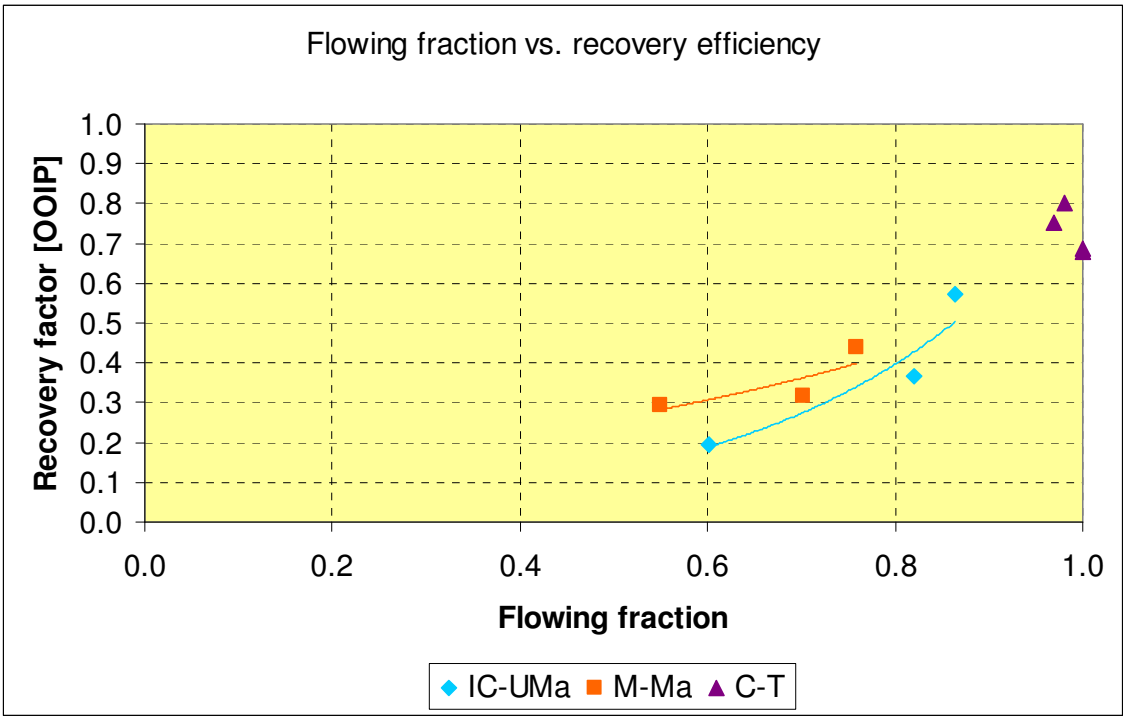

Figure 6.4 – The impact of permeability on recovery efficiency for carbonate core samples from selected pore classes. Independent of pore classes, an increase in recovery factor is observed for increased flowing fractions. The homogeneous C-T samples have very high flowing fractions, and therefore the recovery factors for these samples are high.

From Figs. 6.3 and 6.4 it is clear that both permeability and flowing fraction influences water-flood recovery efficiency. Moreover, it is likely that the low mobility ratio (see Tab. A-2) boosts recovery factor due to piston-like displacement on a microscopic level (see Fig. 2.10); however heterogeneous core samples may have this effect cancelled out due to low volumetric displacement efficiency. As seen from Fig. 5.5 there are also examples of higher recovery efficiency for core samples that have neutral wettability or only weak water-wetness.

None of the factors mentioned above are directly related to pore classes (as defined by Lønøy, 2006). Therefore it is necessary to discuss the effect pore classes themselves have on recovery. The following points sum up the water-flood results compared to Statoil's pore-type facies analysis of the Iranian core samples;

- Moldic macropores (M-Ma) samples show intermediate or low recovery factors (see Tab. 5.4). This is consistent with the facies analysis which estimated moderate reservoir properties. The higher recovery seen for S-889 may be due to the high permeability (26.8 mD). Geologically, the high permeability is presumably caused by interconnected moldic pores (or fractures on a larger scale).
- Uniform, intercrystalline macropores (IC-UMa) samples show intermediate recovery factors (for S-296 and S-783). F-3 is left undiscussed as it was flooded in original state as well as not being of the same origin as the other two samples. Statoil estimated good reservoir properties for this facies. Also, a good correlation between porosity and permeability was suggested; this is consistent with Fig. 5.2. The difference in recovery factor between S-783 and S-296 may be due to difference in permeability.

- The uniform, interparticle macropores and moldic pores (IP-UMa and M-Ma) sample showed low recovery factor. Reservoir properties were suggested to be good by Statoil. However, the permeability for S-929 is very low (0.028 mD), and this may be the reason for the relatively low recovery factor.

The Hydro chalk samples (C-T) from Ekofisk all gave high recovery factors, due to their homogeneous nature. No facies analysis was available for these cores.

Up-scaling and reservoir application

All the matters discussed, based on the results obtained, have neglected uncertain factors that occur when relating laboratory results to real reservoirs. Even though the most important issues already have been addressed in chapters 2.3.2 and 2.4, it seems fitting to bring the subject up again to evaluate the relevance of the results achieved.

Considering the results presented (see chapter 4.2) for the reservoir sample O-14, dissolution effects may increase the permeability drastically when carbonates are exposed to water; there is no doubt that this may cause different flow patterns and alter the recovery properties of core samples compared to reservoir conditions. The best way to avoid this problem is to perform mineralogical studies of core samples that are to undergo water injection in any way, in order to spot any highly water-soluble minerals (such as anhydrite).

Dispersion processes are rarely studied in field-scale displacements. However, it is desirable to obtain pore-structure characteristics at laboratory scale that are relevant for reservoirs. This brings up two issues; (1) the possible exaggeration of capacitance effects due to higher velocities, and (2) the inability to reproduce large-scale heterogeneities such as stratifications and high- or low-permeable zones. As illustrated in Fig. 2.6, the latter leads to laboratory dispersivity being estimated as too *low*, because dispersivity increases with increasing heterogeneity.

For water floods, the mobility ratio may be different in laboratory tests compared to reservoir water floods. This is of course dependent on oil properties for the reservoir in question. In this thesis, the laboratory mobility ratio is low (always less than 1), which is not far off the mark for oil fields on the Norwegian shelf. Still, lower water viscosity at reservoir conditions may lead to a less piston-shaped displacement front in the reservoir compared to laboratory water floods. Mobility ratios in reservoirs with high-viscous oil are much higher than what is achieved using decane, casting doubt on the direct relevancy of laboratory water floods for such reservoirs.

As has been pointed out, wettability affects both dispersion characteristics and water-flooding performance. The cleaning process does not always lead to strongly water-wet cores, and this complicates the analysis of results. Adding to this uncertainty is the possible wettability alteration when bringing the cores from reservoir conditions to atmospheric conditions (see chapter 2.4). Although the effect of wettability is recognised through tests in *restored state*, the ageing process in a reservoir is difficult to reproduce. Restored state studies on topics such as dispersion and water flooding performed by CIPR have shown that the results are even more difficult to interpret and systematise than *cleaned state* studies on the same topics. This is due to the (close to) neutral wettability observed at restored state.

The existence of fractures in carbonate reservoirs was also briefly mentioned in chapter 2.4. They are examples of large-scale heterogeneities that may increase dispersivity, and they also

change the flow pattern to such an extent that both oil distribution and permeability is altered. Thus, the recovery efficiency obtained in laboratory water floods may not be representative for highly fractured reservoirs at all.

Final conclusions and recommendations for further work

On the subject of absolute permeability and salinity in carbonates, the results show that any laboratory experiment conducted with water and carbonate core samples (such as dispersion tests and water floods) should be performed with great care. A mineralogical analysis of the sample(s) in question is recommended, to reveal soluble minerals. To prevent dissolution, it is recommended based on the results of this thesis (even though only performed on two core samples) to always use high-saline water containing a large amount of Ca^{2+}-ions. It would certainly be interesting to see the results of a more comprehensive study of this kind, including more samples (of various pore types and containing different minerals). Effluent compositional analysis would also provide information on which minerals that are dissoluted. Also, long term effects can be studied by enlarging injection slugs; the results might disagree with the results presented here.

The dispersion analysis method presented in this thesis shows good potential for use on carbonate core samples. The large amount of concentration data points, obtained through conductivity and temperature measurements, makes it possible to describe dispersion characteristics accurately. In addition to this advantage, the tracer is uncomplexed and already present in brine, making it simpler to both predict chemical reactions and interpret results. Tracer injection also proved a reversible process; hence it is possible to repeat the dispersion test if needed (taking dissolution possibility into account). Since the measurements are automatically recorded to a computer, the method is less time-consuming than previous methods at CIPR. The main weakness of the method, as was the weakness with previous methods, is the need of precise pore-volume- and laboratory equipment (tubing, valves, etc.) measurements; this adds uncertainty to the simulation procedure. If pore volumes are correct, simulation based on Coats and Smith's (1964) differential capacitance model generally seems to produce reliable values of dispersivity and flowing fraction / dead-end pores. However, it is recommended to verify that simulation results are consistent both with reliable models for phase distributions (including water film flow at S_{or}) and with wettability data.

The main objective of laboratory dispersion tests is to obtain information on pore structure that is representative for the reservoir. Unfortunately, the mathematical model of Coats and Smith (1964) is sensitive to velocity if the Peclet numbers (see Eq. 2.5 and Appendix 2) are not sufficiently low. Thus it becomes an important matter to perform dispersion tests at velocities where the flow regime is not dominated by diffusion (low flow rates) or turbulence (high flow rates). If flow rate effects are ignored, the consequence may well be that the dispersion characteristics obtained are combined results of velocity and pore structure; such results are unwanted because they do not represent the reservoir pore structure only. Moreover, Coats and Smith's (1964) model is not valid for diffusion-dominated flow. Based on the results (see chapter 5.1) in this thesis, it is recommended to (1) keep the Peclet numbers below 100 to avoid velocity-dependence on dead-end-pore mass transfer (Jasti et al., 1988), and (2) to try out various flow rates for each core sample (if dissolution effects are neglectable) in order to find out if the dispersion profile changes significantly. When the velocities are in the correct regime, the flow is dominated by convective mixing (and not diffusion) and only small variations with velocity are to be expected. However, this issue is further complicated by the fact that it is desirable to use similar velocities for all core samples,

in order to better compare them. If a fixed interstitial velocity is to be used for all core samples, heterogeneous samples should be emphasised more than homogeneous samples when deciding this velocity; this is because heterogeneous samples have more dead-end pores (and consequently higher mass transfer through diffusion) making them more susceptible to velocity effects (see Fig. 2.9). Also, a fixed velocity must not surpass a critical lower velocity in order to prevent diffusion from controlling fluid flow in the flowing fraction; based on the results in this thesis, it is recommended that $N_{Re} > 0.2$ for all tests. There is of course a critical higher velocity as well, which if exceeded causes turbulence, but this velocity is so high compared to normal laboratory flow rates that it is of less interest.

The number of carbonate core samples studied in this thesis (11) is arguably too low to draw any unambiguous conclusions regarding Lønøy's (2006) pore-type classification. Still, the results prompt several issues that should be the target of further studies. Apparently pore types are not strongly linked to dispersion characteristics and water-flooding performance. Some might argue that this is incorrect because all the tertiary chalk (C-T) samples showed high recovery and low-dispersive characteristics, but this is in fact an effect of the *homogeneity* of these samples and instead proves the value of dispersion tests. If samples are found low-dispersive and homogeneous (high flowing fraction), a high recovery can be expected (regardless of permeability and pore type). This inverse correlation between amount of dead-end pores and recovery efficiency agrees with the conclusions of Skauge et al. (2006). S_{or} dispersion profiles for homogeneous cores also show a more predictable relation to water-saturated profiles. Based on flowing fractions only, water film flow may be difficult to distinguish from oil located in dead-end pores; wettability studies may assist on this subject.

Even though the recovery factors found for the South Pars carbonate samples agree with Statoil's pore-type facies analysis to some extent, permeability, wettability and the level of heterogeneity probably have a greater impact on recovery. As seen from Fig. 5.2, the core samples included in the thesis mostly fit with Lønøy's classification in terms of porosity/permeability relationships. The apparent lack of correlation between pore type and dispersion/water flooding is not very unexpected. The classification is based on a combination of diagenetic features (rock fabrics) and porosity/permeability and the pore types are determined visually. Since there definitely are other parameters affecting pore structure and oil distribution, it is not surprising that the classification (seemingly) is not directly related to dispersion and water-flooding properties. Nonetheless, it is recommended to further examine Lønøy's (2006) pore-type classification and their relation to flow properties. To perform a more comprehensive study the number of core samples must be increased significantly, both to lessen uncertainty and to cover a wider range of pore classes. Even though the methods used for dispersion analysis and water flooding in this thesis give useful results, it would also be interesting to monitor both processes in situ (using X-ray or similar methods to obtain saturation profiles); this makes it possible to map the macroscopic tracer (or injected water) distribution and thus provides knowledge that may improve the understanding of how dispersion characteristics and water-flooding performance are correlated.

The large-scale heterogeneities (in particular fractures) that are likely to occur in carbonate reservoirs make it difficult to decide the relevance of laboratory tests. Parameters such as mobility ratio and wettability must be considered uncertain factors in this process. In addition, this thesis has proved that velocity effects and dissolution effects might be of great importance. The final sentence in this thesis sums up the concerns on reservoir relevance; *the purpose of laboratory tests, whether it is dispersion tests or water floods, is to obtain data that are relevant for authentic reservoirs' recovery performances.*

References

Aali, J., H. Rahimpour-Bonab and M.R. Kamali, 2005, *Geochemistry and Origin of the World's Largest Gas Field from Persian Gulf, Iran:* Journal of Petroleum Science & Engineering, v. **50** (2006), p. 161-175.

Archie, G.E., 1952, *Classification of Carbonate Reservoir Rocks and Petrophysical Considerations:* AAPG Bulletin, v. **36**, no. 2, p. 278-298.

Aris, R. and N.R. Amundson, 1957, *Some Remarks on Longitudinal Mixing or Diffusion in Fixed Beds:* AIChE Journal, v. **3**, no. 2, p. 280.

Arya, A., T.A. Hewett, R.G. Larson and L.W. Lake, 1988, *Dispersion and Reservoir Heterogeneity:* SPE Reservoir Engineering (February 1988), p. 139-148.

Blackwell, R.J., 1962, *Laboratory Studies of Microscopic Dispersion Phenomena:* SPEJ (March 1962), p. 1-8.

Carberry, J.J., 1976, *Conservation Equations for Reactors* in *Chemical and Catalytic Reaction Engineering:* McGraw Hill Inc., New York, p. 143-193.

Choquette, P.W. and L.C. Pray, 1970, *Geologic Nomenclature and Classification of Porosity in Sedimentary Carbonates:* AAPG Bulletin, v. **54**, no. 2, p. 207-250.

CIPR website, http://cipr.uib.no/, 10 April 2008.

Coats, K.H. and B.D. Smith, 1964, *Dead-End Pore Volume and Dispersion in Porous Media:* SPEJ, v. **4**, no. 1, p. 73-84.

Dahab, A.S., A. Omar, M.H. Sayyouh and A. Hemeida, 1993, *Effects of Clay Content on Permeability Damage, Capillary Pressure and Wettability Characteristics of Saudi Reservoir Rocks:* Journal of The Japan Petroleum Institute, v. **36**, no. 3, p. 197-203.

Deans, H.A., 1963, *A Mathematical Model for Dispersion in the Direction of Flow in Porous Media*: SPEJ, v. **3**, no. 1, p. 49-52.

Fourar, M., G. Konan, C. Fichen, E. Rosenberg, P. Egermann and R. Lenormand, 2005, *Tracer Tests for Various Carbonate Cores Using X-Ray CT:* SCA paper 2005-56, presented in Toronto, Canada, 21-25 August 2005.

Gudmundsson, J.S., 1992, *Molecular Diffusion* in *SPOR Monograph – Recent Advances in Improved Oil Recovery Methods for North Sea Sandstone Reservoirs*, edited by Skjæveland, S.M. and J. Kleppe: Norwegian Petroleum Directorate, Stavanger, p. 20-24.

Holt, T., 1992, *Dispersion* in *SPOR Monograph – Recent Advances in Improved Oil Recovery Methods for North Sea Sandstone Reservoirs*, edited by Skjæveland, S.M. and J. Kleppe: Norwegian Petroleum Directorate, Stavanger, p. 13-20.

Jasti, J.K, R.N. Vaidya and H.S. Fogler, 1988, *Capacitance Effects in Porous Media:* SPE Reservoir Engineering (November 1988), p. 1207-1214.

Khilar, K.C. and H.S. Fogler, 1983, *Water Sensitivity in Sandstones:* SPEJ, v. **23**, no. 1, p. 55-64.

Khilar, K.C. and H.S. Fogler, 1984, *The Existence of a Critical Salt Concentration for Particle Release:* Journal of Colloid and Interface Science, v. **101**, no. 1, p. 214-224.

Kia, S.F., H.S. Fogler, M.G. Reed and R.N. Vaidya, 1987, *Effect of Salt Composition on Clay Release in Berea Sandstones:* SPE Production Engineering (November 1987), p. 277-283.

Klinkenberg, L.J., 1951, *Analogy Between Diffusion and Electrical Conductivity in Porous Rocks:* Bulletin of the Geological Society of America, v. **62**, p. 559-564.

Lager, A., K.J. Webb, C.J.J. Black, M. Singleton and K.S. Sorbie, 2006, *Low Salinity Oil Recovery – An Experimental Investigation:* SCA paper 2006-36, presented in Trondheim, Norway, 12-16 September 2006.

Lake, L.W., 1989, *Dissipation in Miscible Displacements* in *Enhanced Oil Recovery:* Prentice Hall, New Jersey, p. 157-168.

Lien, J.R., 2007, *PTEK212 Reservoarteknikk I:* Institutt for Fysikk og Teknologi, Universitetet i Bergen, 146 pp.

Lucia, F.J., 1983, *Petrophysical Parameters Estimated From Visual Descriptions of Carbonate Rocks: A Field Classification of Carbonate Pore Space:* Journal of Petroleum Technology, v. **216**, p. 221-224.

Lucia, F.J., 1995, *Rock-fabric / Petrophysical Classification of Carbonate Pore Space for Reservoir Characterization:* AAPG Bulletin, v. **79**, no. 9, p. 1275-1300.

Lucia, F.J., 1999, *Carbonate Reservoir Characterization:* Springer-Verlag, Berlin, 226 pp.

Lucia, F.J., C. Kerans and J.W. Jennings Jr., 2003, *Carbonate Reservoir Characterization:* SPE 82071; Journal of Petroleum Technology, v. **55**, no. 6, p. 70-72.

Lønøy, A., 2006, *Making Sense of Carbonate Pore Systems:* AAPG Bulletin, v. **90**, no. 9, p. 1381-1405.

Ochi, J. and J.F. Vernoux, 1998, *Permeability Decrease in Sandstone Reservoirs by Fluid Injection – Hydrodynamic and Chemical Effects:* Journal of Hydrology, v. **208**, p. 237-248.

Perkins, T.K. and O.C. Johnston, 1963, *A Review of Diffusion and Dispersion in Porous Media:* SPEJ (March 1963), p. 70-84.

Pourmohammadi, S., S. Hetland, K. Spildo and A. Skauge, 2007, *Fluid Flow Properties of Different Carbonate Pore Classes:* SPE 111433, presented in Abu Dhabi, the United Arab Emirates, 28-31 October 2007.

Rafaelsen, B. and J.K. Nielsen, 2005, *Introduction to Carbonates:* Online presentation, http://www.ig.uit.no/~bjarne/Rafaelsen&Nielsen_2005_ver_1_01.swf, 15 February 2008.

Salter, S.J. and K.K. Mohanty, 1982, *Multiphase Flow in Porous Media: I. Macroscopic Observations and Modeling:* SPE 11017, presented in New Orleans, USA, 26-29 September 1982.

Skauge, A., K. Spildo, A. Lønøy, G. Njøten and B. Ottesen, 2005, *Waterflood Efficiency for Different Pore Classes in Carbonate Reservoirs:* presented at 13th European Symposium on Improved Oil Recovery, Budapest, Hungary, 25-27 April 2005.

Skauge, A., B. Vik, S. Pourmohammadi and K. Spildo, 2006, *Dispersion Measurements Used in Special Core Analysis of Carbonates:* SCA paper 2006-14, presented in Trondheim, Norway, 12-16 September 2006.

Tang, G.-Q. and N.R. Morrow, 1999, *Influence of Brine Composition and Fines Migration on Crude Oil Brine Rock Interactions and Oil Recovery:* Journal of Petroleum Science & Engineering, v. **24**, p. 99-111.

Taylor, G.I., 1953, *Dispersion of Soluble Matter in Solvent Flowing Slowly Through a Tube:* Proceedings of the Royal Society A, v. **219**, p. 186-203.

Tchistiakov, A.A., 2000, *Physico-Chemical Aspects of Clay Migration and Injectivity Decrease of Geothermal Clastic Reservoirs:* presented at Proceedings World Geothermal Congress, Kyushu – Tohuku, Japan, 28 May – 10 June 2000.

Thomas, G.H., G.R. Countryman and I. Fatt, 1963, *Miscible Displacement in a Multiphase System:* SPEJ (September 1963), p. 189-196.

Turner, G.A., 1959, *The Frequency Response of Some Illustrative Models of Porous Media:* Chemical Engineering Science, v. **10**, p. 80-90.

Appendix 1: Properties of synthetic seawater and decane

Table A-1 – Composition of synthetic seawater (SSW). The recipe is used internally at CIPR, and might be considered simplified compared to what components you would normally find in sea water (even though sea water composition varies all over the world). Many of the minor components are neglected; this makes it easier to interpret flooding results and understanding what chemical reactions that could take place, and also excludes some toxic compounds. In addition, the basic recipe makes it possible to mass produce synthetic sea water. The uncertainties of weighing and molecular weights are negligible.

Composition of SSW			
Component	**Molecular weight [g/mol]**	**Weight-%**	**Mole fraction**
NaCl	58.443	2.4890	0.00793
$CaCl_2 \cdot 2H_2O$	147.014	0.1726	0.00022
$MgCl_2 \cdot 6H_2O$	203.301	1.1124	0.00102
$NaHCO_3$	84.006	0.0192	0.00004
Na_2SO_4	142.041	0.4056	0.00053
KCl	74.551	0.0668	0.00017
Distilled water	18.015	95.7344	0.99009
Sum		100.0000	1.00000

Table A-2 – Flow properties of synthetic seawater (SSW) and n-decane at 20 °C. The decane used is never less than 95 % pure. The mobility ratio is calculated by means of Eq. 2.9 for each of the 11 samples studied in dispersion and waterflooding experiments in this thesis; the range given in this table is based on minimum and maximum mobility ratios. The low mobility ratios can be explained by the combination of low-viscous oil and water-wet samples causing low endpoint water relative permeabilities and high oil endpoint relative permeabilities. Immiscible displacement processes where $M \leq 1$ *are generally classified as piston-like displacements; this is common for the low-viscous oils found in North Sea oil reservoirs.*

Flow properties of SSW and decane [$CH_3(CH_2)8CH_3$]			
Component	**Density** ρ **[g/cm^3]**	**Viscosity** μ **[cP]**	**Endpoint mobility ratio range** M_{wo}
SSW	1.031	1.100	0.05 – 0.88
Decane	0.73	0.92	

Appendix 2: Peclet numbers for tested core samples

Table A-3 – Peclet numbers for all core samples included in dispersion analysis in this thesis. The numbers are calculated by means of Eq. 2.5. Note that only two samples have Peclet numbers below 100; according to Jasti et al. (1988) M *is then dependent of velocity for all the other samples. The diffusion coefficient used is that for pure water,* $D_0 = 2.5 \cdot 10^{-4}$ *cm*^{2}*/s, corrected for a constant tortuosity factor of* $\tau = 1.5$ *(see Eq. 2.2).*

Peclet numbers

Pore class	Core sample	Injection rate v [cm^3/s]	Area A [cm^2]	Porosity φ	Length L [cm]	Peclet number N_{Pe}
IC-UMa	F-03	0.0015	11.10	0.104	4.74	321
	S-296	0.0010	11.10	0.078	5.08	295
	S-783	0.0026	11.16	0.205	4.98	294
IP/M-UMa	S-929	0.0005	11.10	0.140	5.50	92
M-Ma	S-294	0.0005	11.10	0.210	5.15	58
	S-829	0.0026	11.10	0.216	5.37	301
	S-889	0.0028	10.93	0.232	4.42	256
C-T	HE-1	0.0017	11.04	0.269	6.47	189
	HE-2	0.0039	11.22	0.311	6.42	370
	HE-3	0.0046	11.22	0.366	5.97	344
	HE-4	0.0042	11.16	0.338	6.20	358

Appendix 3: The South Pars field

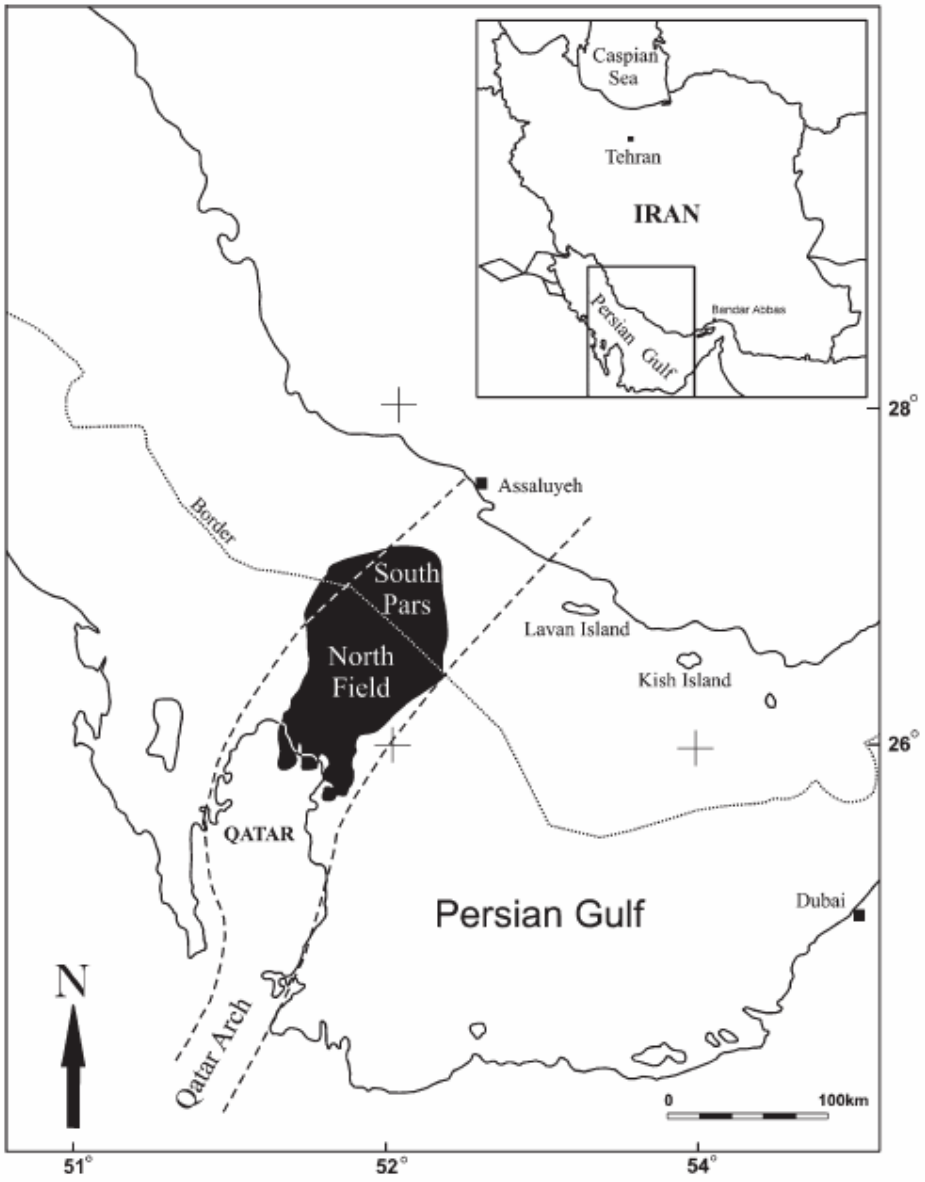

Figure A-1 – Location of the South Pars field within the Persian Gulf (Aali et al., 2005).

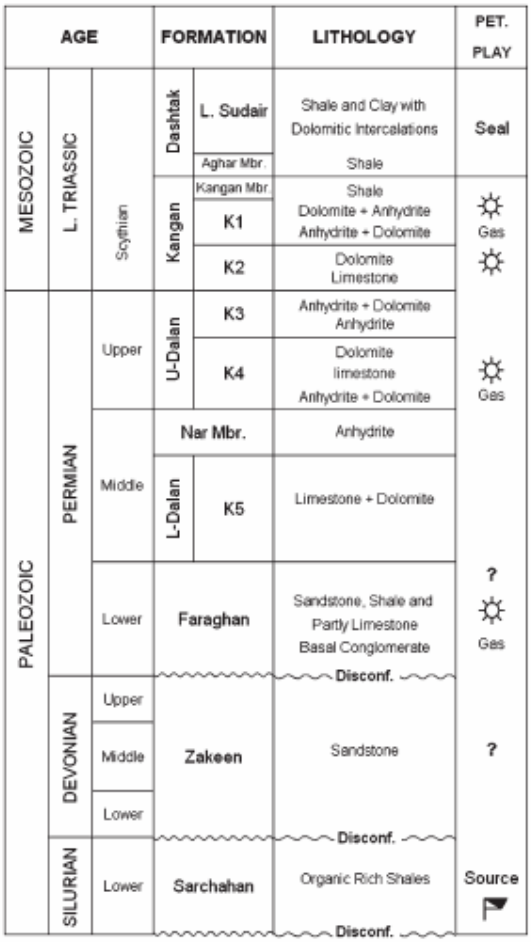

Figure A-2 – Generalised stratigraphic chart for the South Pars Field (Aali et al., 2005).

Appendix 4: Dispersion simulation charts

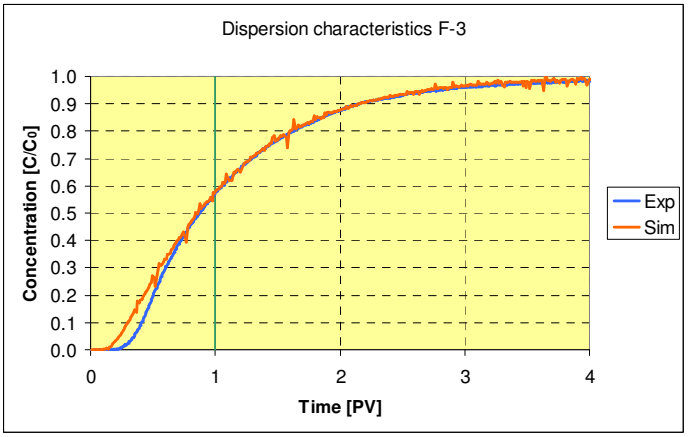

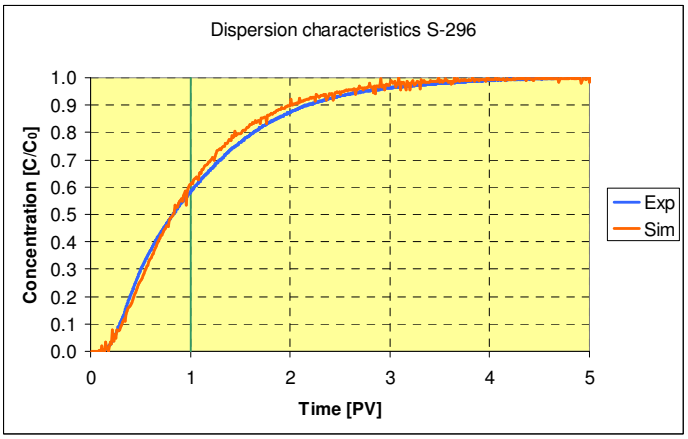

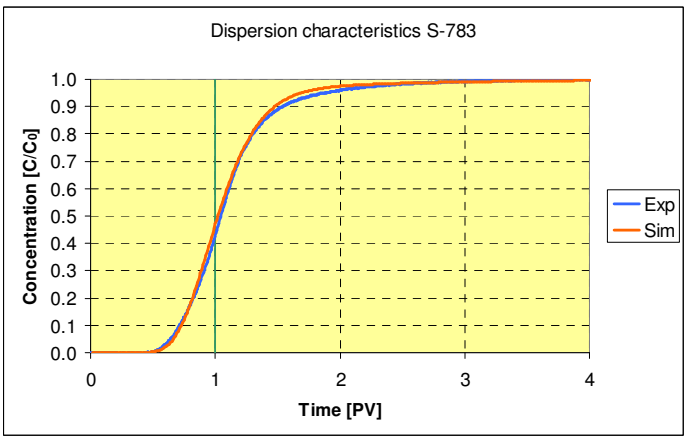

(a) Intercrystalline, uniform macropores (IC-UMa); F-3, S-296 and S-783.

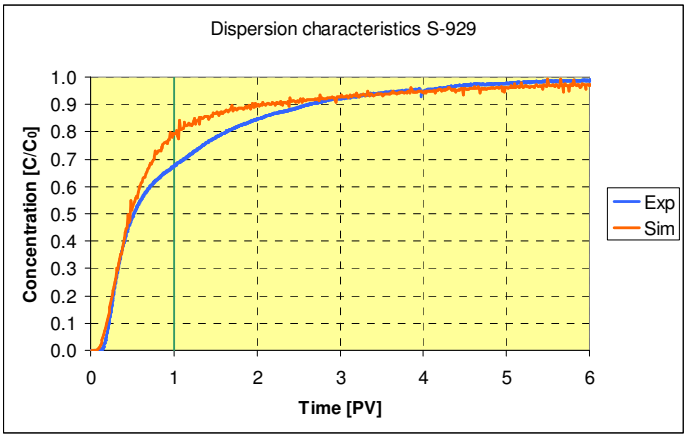
Dispersion characteristics S-929
Concentration [C/C0]
1.0
0.9
0.8
0.7
0.6
0.5
0.4
0.3
0.2
0.1
0.0
0
1
2
3
4
5
6
Time [PV]
Exp
Sim

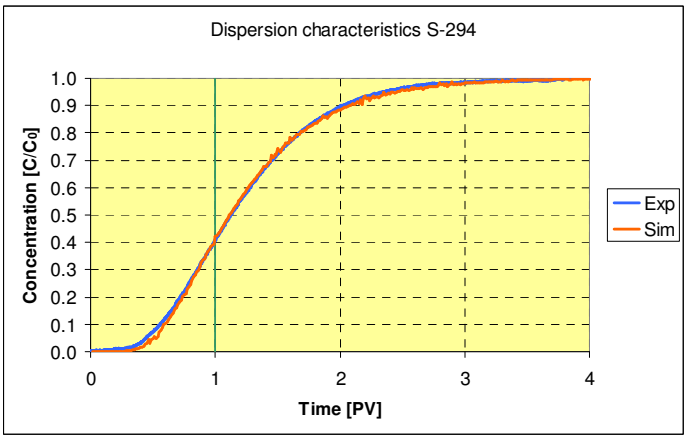
Dispersion characteristics S-294
Concentration [C/C0]
1.0
0.9
0.8
0.7
0.6
0.5
0.4
0.3
0.2
0.1
0.0
0
1
2
3
4
Time [PV]
Exp
Sim

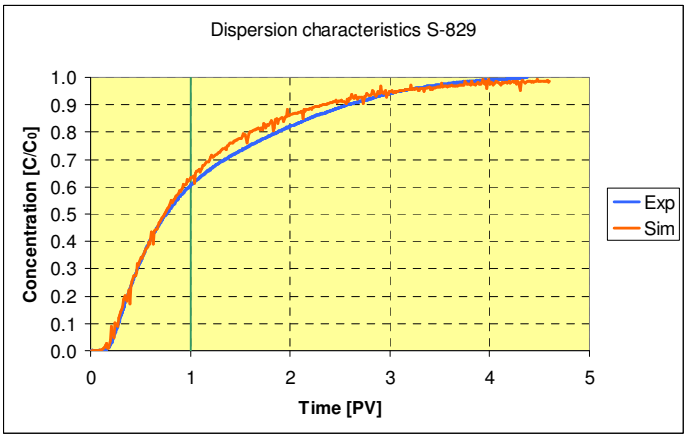
Dispersion characteristics S-829
Concentration [C/C0]
1.0
0.9
0.8
0.7
0.6
0.5
0.4
0.3
0.2
0.1
0.0
0
1
2
3
4
5
Time [PV]
Exp
Sim

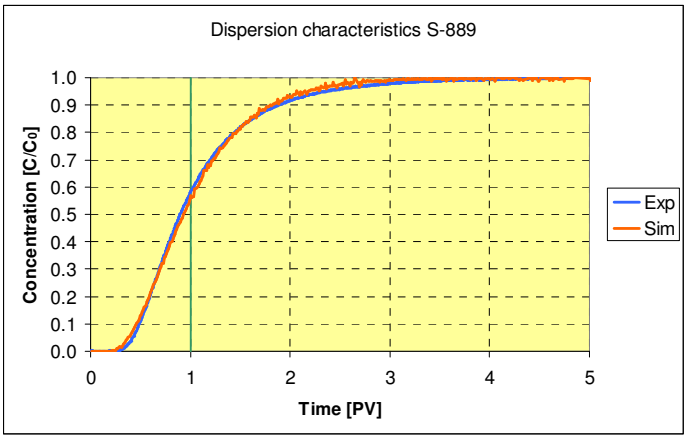

(b) Moldic macropores (M-Ma); S-929, S-294, S-829 and S-889. S-929 also contains interparticle, uniform macropores (IP-UMa).

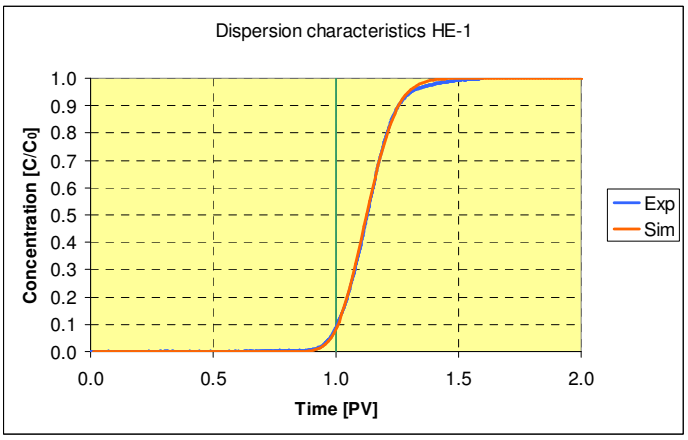

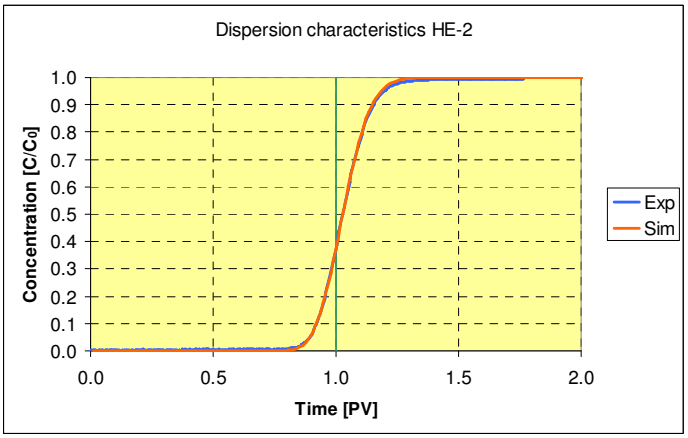

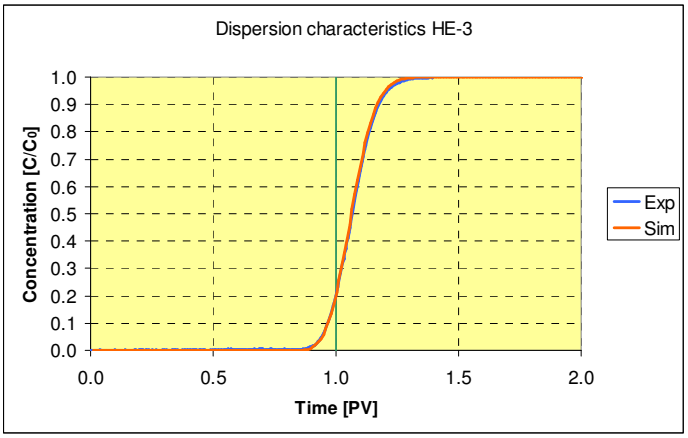

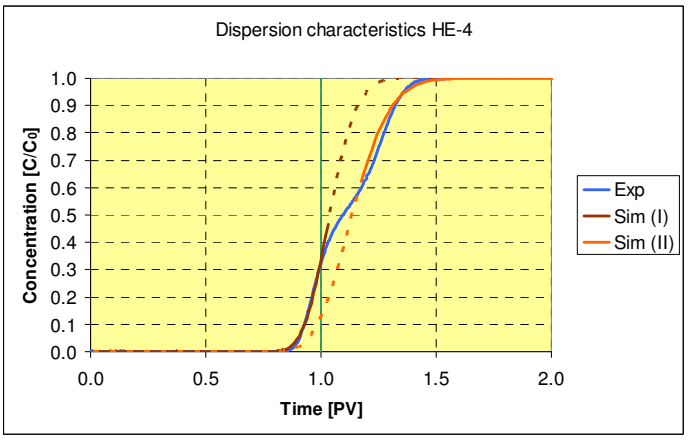

(c) Tertiary chalk (C-T); HE-1, HE-2, HE-3 and HE-4.

Figure A-3 - Experimental- and simulation dispersion profiles at S_w *= 1 for 11 carbonate core samples, sorted by Lønøy's pore-type classification (2006). Simulations for the homogeneous chalk samples fit the experimental profiles better. Take notice of the dual nature of HE-4, solved by using two different sets of simulation parameters.*

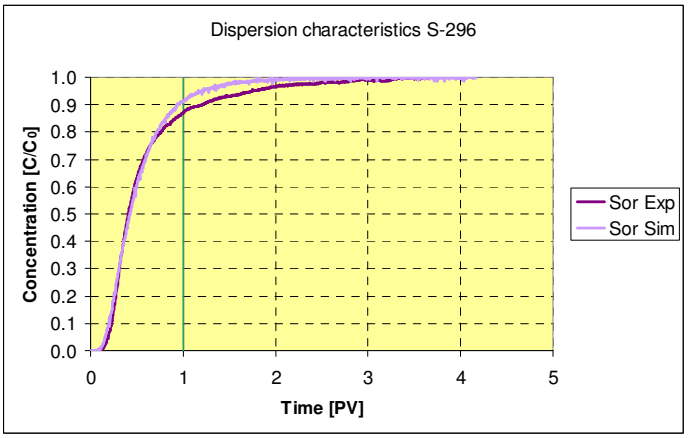

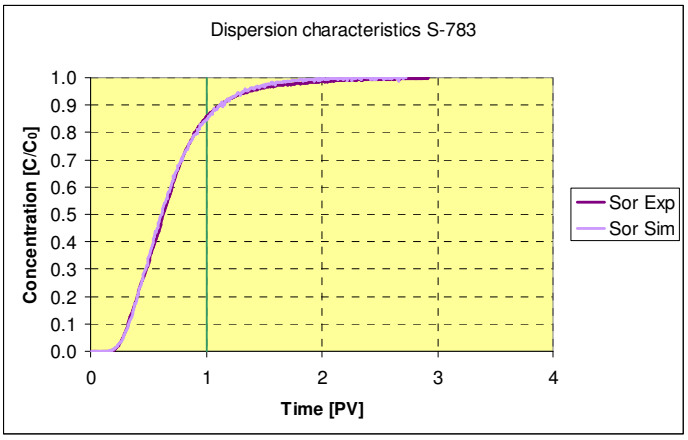

(a) Intercrystalline, uniform macropores (IC-UMa); S-296 and S-783.

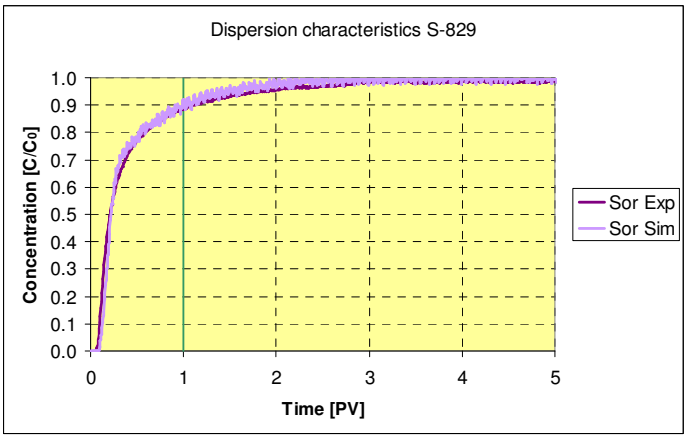

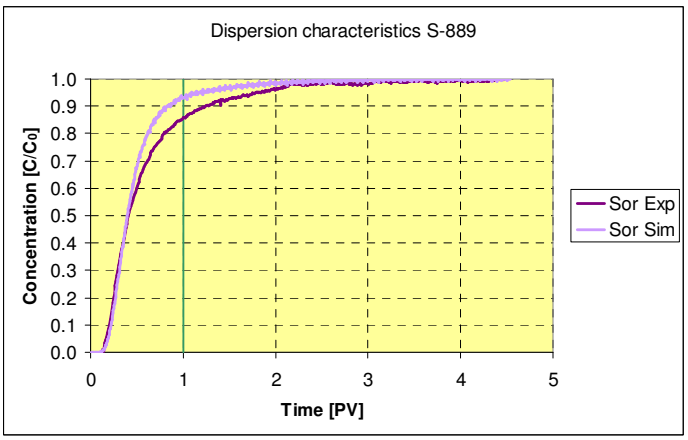

(b) Moldic macropores (M-Ma); S-829 and S-889.

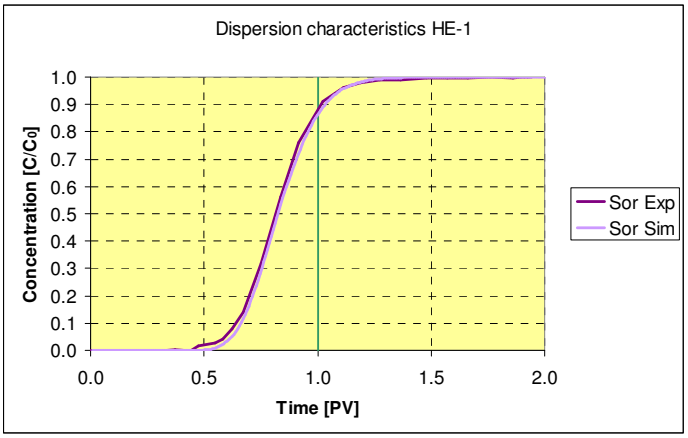

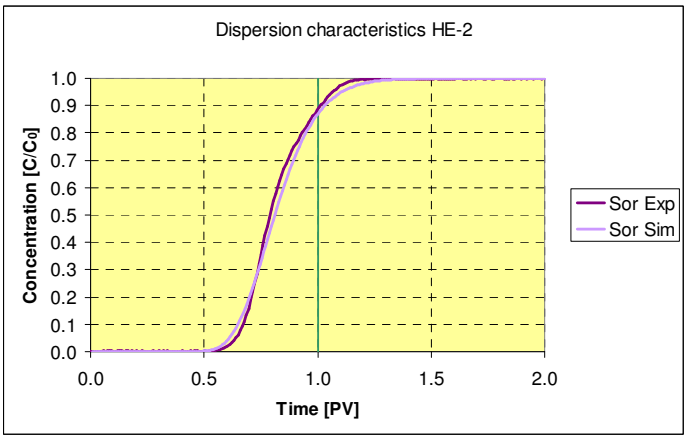

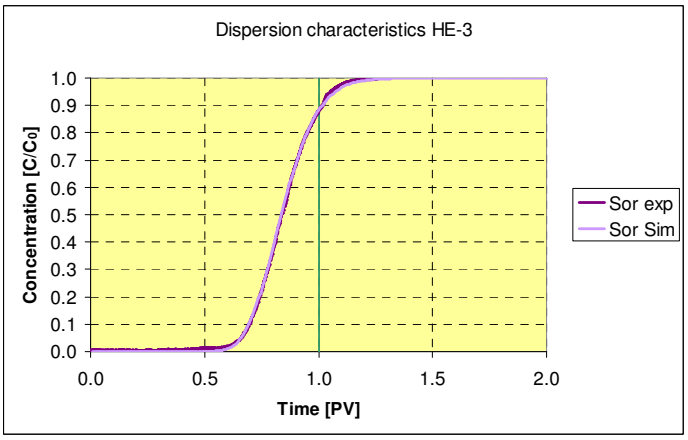

(c) Tertiary chalk (C-T); HE-1, HE-2 and HE-3.

Figure A-4 – Experimental- and simulation dispersion profiles at S_{or} *for 8 carbonate core samples, sorted by Lønøy's pore-type classification (2006). Note that the pore volume is the entire pore volume; thus these curves are shifted rightwards according to* S_{or} *prior to simulation. Dispersivity, flowing fraction etc. are then found for the* water-filled *volume, and the obtained simulation profile is shifted leftwards to overlap the experimental profile. No match was found for the experimental dispersion profile for HE-4. The same trend is seen as for water-saturated samples; a better match is obtained for the low-dispersive chalk samples.*